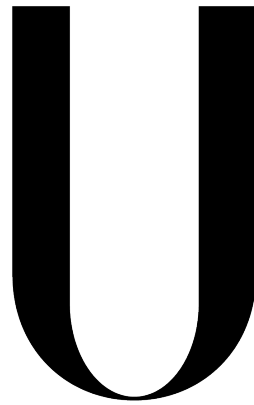Universidade de Lisboa
Faculdade de Ciências
Departamento de Química e Bioquímica

U

LISBOA

UNIVERSIDADE
DE LISBOA

**Effects of metabolism
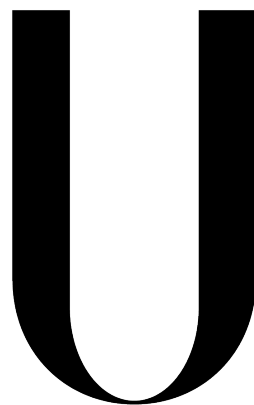upon neuronal activity and synaptic performance**

Clara Cunha Matos Patrício

Dissertação
Mestrado em Bioquímica
Bioquímica

2013

This page was intentionally left blank.

Universidade de Lisboa
Faculdade de Ciências
Departamento de Química e Bioquímica

U

LISBOA

UNIVERSIDADE
DE LISBOA

Effects of metabolism
upon neuronal activity and synaptic performance

Clara Cunha Matos Patrício

Dissertação
Mestrado em Bioquímica
Bioquímica

Orientadores: Doutor Pedro Lima & Doutora Ana Sebastião

2013

This page was intentionally left blank.

AGRADECIMENTOS

Ao meu orientador, Doutor Pedro Lima, pela oportunidade, pelo encorajamento e sobretudo pelas longas horas passadas à distância de um "TOQUEI!" no *setup*, a ensinar-me a entrar no mundo da electrofisiologia e a discutir os resultados.

À minha co-orientadora, Doutora Ana Sebastião, pela oportunidade que me deu e pelo sentido de *joy* em ciência.

Ao Doutor Pedro Costa, por ter posto à minha inteira disposição todos os recursos do laboratório de fisiologia da Faculdade de Ciências Médicas e pelas preciosas dicas, que se revelaram sempre *spot on*.

À Doutora Luísa Lopes, que me aceitou no seu laboratório e grupo sem condicionamentos, e que me ensinou como se fosse uma sua aluna.

À Doutora Ana Isabel Santos e à Gracinda Meneses por, respectivamente, disponibilizar e cuidar dos modelos animais (os famosos ratos!).

Ao André Bastos e ao Bruno Bragança, pelo óptimo ambiente de laboratório e por aceitarem os meus bizarros comportamentos nos "maus dias de patch".

A todo o grupo de neurociências do Instituto de Medicina Molecular, especialmente à Vânia Batalha, à Diana Ferreira e à Sara Carvalho, que me fizeram sentir bem-vinda e parte do grupo. Uma palavra especial à Joana Coelho, que altruistamente me acompanhou e orientou em todo o trabalho feito no IMM – obrigada!

Ao Doutor Luís Marques, pela disponibilidade e tempo despendido.

E finalmente aos meus pais, família, amigos e ao Fábio que sempre tiveram o cuidado de me acompanhar e dar força no percurso da tese, o qual por vezes teve obstáculos, curvas e rectas que pareciam sem fim. Com a vossa ajuda espero estar perante a porta do jardim.

OBRIGADA!

> *The garden of neurology holds out to the investigator captivating spectacles and incomparable artistic emotions. In it, my aesthetic instincts found full satisfaction at last. Like the entomologist in the pursuit of brightly colored butterflies, my attention hunted, in the flower garden of the grey matter, cells with delicate and elegant forms, the mysterious butterflies of the soul, the beating of whose wings may some day – who knows? – clarify the secret of mental life.* - Santiago Ramón y Cajal, from his autobiography "Recollections of my Life"

This page was intentionally left blank.

INDEX

ABBREVIATIONS

The main abbreviations used in this dissertation are listed below.

AD – Alzheimer disease

CA1-3 - *Cornu Ammonis* areas 1-3

CNS – central nervous system

DG – Dentate gyrus

DH – Dorsal hippocampus

DMT1 – type-1 diabetes

DMT2 – type-2 diabetes

FBS – Fetal bovine serum

I_A – A-type current

IGF – Insulin growth factor

I_{DR} - Delayed rectifier current

I_M – M-type K^+ current

InsR (or IR) – Insulin receptor

IRS1 - Insulin receptor substrate 1

GLUT – Glucose carrier

Kv1.3 – voltage-dependent K+ channel 1.3

LZR - Lean Zucker Rat

MgTx – Margatoxin

OZR - Obese Zucker Rat

PBS - Phosphate buffered saline

PCR - Polymerase Chain Reaction

SDS-PAGE - Sodium dodecyl sulfate poly-acrylamide gel electrophoresis

S.E.M. – Standard error of the mean

So - *Stratum oriens*

Sp - *Stratum piramidale*

Sr - *Stratum radiatum*

TMD – Transmembranar domain

VH – Ventral hippocampus

ZDF - Zucker Diabetic fatty

FIGURES

TABLES

RESUMO

O objectivo desta dissertação é avaliar o efeito do metabolismo (ciclo de alimentação) na atividade neuronal. O trabalho centra-se nas correntes de potássio *whole-cell* em neurónios piramidais da região CA1 do hipocampo de ratos *wistar,* particularmente aquelas mediadas pelo canal Kv1.3. Dois objectivos foram estabelecidos: (1) avaliar se a expressão de Kv1.3 e respectiva corrente iónica são afectadas pelo metabolismo e (2) avaliar se o eixo dorsal-ventral do hipocampo é homogéneo no que toca à expressão de Kv1.3 e à sua corrente iónica. Para este efeito, foram usadas abordagens de electrofisiologia e de biologia molecular.

Resultados surpreendentes revelam que os neurónios de ratos em período pós-prandial têm diferentes propriedades biofísicas (dependência da voltagem mais despolarizada e cinética mais lenta) e farmacológicas (maior contribuição de correntes sensíveis à margatoxina, possivelmente com dependência de voltagem alterada) em relação a células de ratos em jejum. Propõe-se a existência de um sistema de regulação complexo, de acordo com o ciclo de alimentação, nos neurónios em estudo. Esse sistema envolveria modificações nas populações de canais iónicos que são expressas na membrana neuronal (nomeadamente do Kv1.3, que a margatoxina inibe seletivamente), bem como vias metabólicas capazes de alterar as propriedades biofísicas destes canais (por exemplo alterando a sua fosforilação constitutiva).

Mais, os resultados apresentados indicam que o hipocampo dorsal é mais afectado pelo condicionamento metabólico do que o polo ventral, sugerindo que as funções associadas às duas porções do hipocampo são afectas de forma diferente com o ciclo de alimentação. Estes resultados podem dar suporte neuronal para a noção intuitiva de que a consolidação da memória é afetada pelo ciclo de alimentação.

Mostra-se ainda que os neurónios piramidais da região CA1 têm características biofísicas e farmacológicas irregulares ao longo do dorso-eixo ventral do hipocampo (as células dorsais têm uma cinética mais lenta, maior densidade de corrente e maior sensibilidade para a margatoxina), associadas a uma expressão diferencial do canal Kv1.3 (maior densidade na parte dorsal). Estes resultados vêm dar mais profundidade a evidências recentes que desafiam a premissa clássica de que os neurónios piramidais de CA1 são uma população electrofisiologicamente homogénea ao longo do eixo longitudinal do hipocampo.

Concluindo, as nossas observações sugerem fortemente que a fisiologia dos canais iónicos, bem como a expressão de proteínas no neurónio, alteram-se durante os ciclos metabólicos de jejum/pós-prandial, inclusive ao longo do eixo dorsal-ventral do hipocampo. Fica assim em causa a ideia do cérebro ser uma entidade insensível a variações metabólicas.

ABSTRACT

This study aims to assess the effect of the feeding cycle onto neuronal performance. The work focused on whole-cell K^+ currents in pyramidal neurons from CA1 region of *wistar* rats' hippocampus, particularly those underlined by Kv1.3 channels. Two goals were established: (1) to assess if Kv1.3 expression and associated ionic currents are affected by metabolism and (2) to evaluate if the dorsal-ventral axis of the hippocampus is homogeneous regarding the Kv1.3 expression patterns and currents. For this purpose, electrophysiology and molecular biology approaches were used.

Striking results reveal that fed rats' neurons have different biophysical (more depolarized voltage-dependence and slower kinetics) and pharmacological (larger margatoxin-sensitive currents, possibly with altered voltage-dependence) properties than fasting rats' cells. It is proposed that a complex regulatory system according to the feeding cycle exists in these neurons. This system would involve modifications in ionic channels populations expressed in the neuronal membrane (namely Kv1.3, that margatoxin selectively inhibits) as well as metabolic pathways capable of altering the biophysical properties of these channels (for example by enhancing their constitutive phosphorylation).

Furthermore, the dorsal hippocampus was more extensively affected by metabolic conditioning than the ventral pole, suggesting that functions associated with the two portions of the hippocampus are differently affected by the feeding cycle. These results may give neuronal backing for the intuitive notion of memory consolidation being affected by the feeding cycle.

Additionally, CA1 pyramidal neurons had uneven biophysical and pharmacological profiles throughout out the length of the hippocampus - dorsal cells have slower kinetics, larger current density and larger sensitivity to margatoxin. Such uneven features are associated with a differential expression of Kv1.3 channel (higher density in the dorsal portion) throughout the dorsal-ventral axis of the hippocampus. These impressive results give further depth to recent evidence challenging the classical assumption that CA1 pyramidal neurones are an electrophysiologically homogenous population along the longitudinal hippocampal axis.

All together, our observations strongly suggest that ion-channel physiology, as well as neural protein expression, change during fast-fed metabolic cycles and within the dorsal-ventral axis of the hippocampus, challenging the idea of a metabolically sealed brain.

1 INTRODUCTION

1.1 NERVOUS SYSTEM

This project focuses on central neurons from a particular brain region – the hippocampus (CA1 pyramidal cells).

1.2 HIPPOCAMPUS

The hippocampus is one of the brains' better-characterized cortical structures. Its name derives from its resemblance with the sea-horse shape (from the greek "hippo" meaning horse and "campus" meaning sea monster). This structure is implicated in learning and memory. A pathological condition affecting this site has serious clinical implications, as it is a target in neurodegenerative disorders (such as Alzheimer disease) and in temporal lobe epilepsy, among others (Jarrard, 1978, Jarrard, 1991).

1.2.1 Localization and structure

The hippocampus (**Figure 1**) is the major brain structure within the hippocampal formation (which it is part of along with the dentate gyrus, the subicular areas and the fimbria-fornix), in the medial temporal lobe of the brain. In the inside of the temporal lobe, it assumes a dorsal position relative to the hypothalamus and its septal-temporal axis has a semi-circular shape around the thalamus. The hippocampus has a cylindrical reniform shape and is duplicated in the two hemispheres.
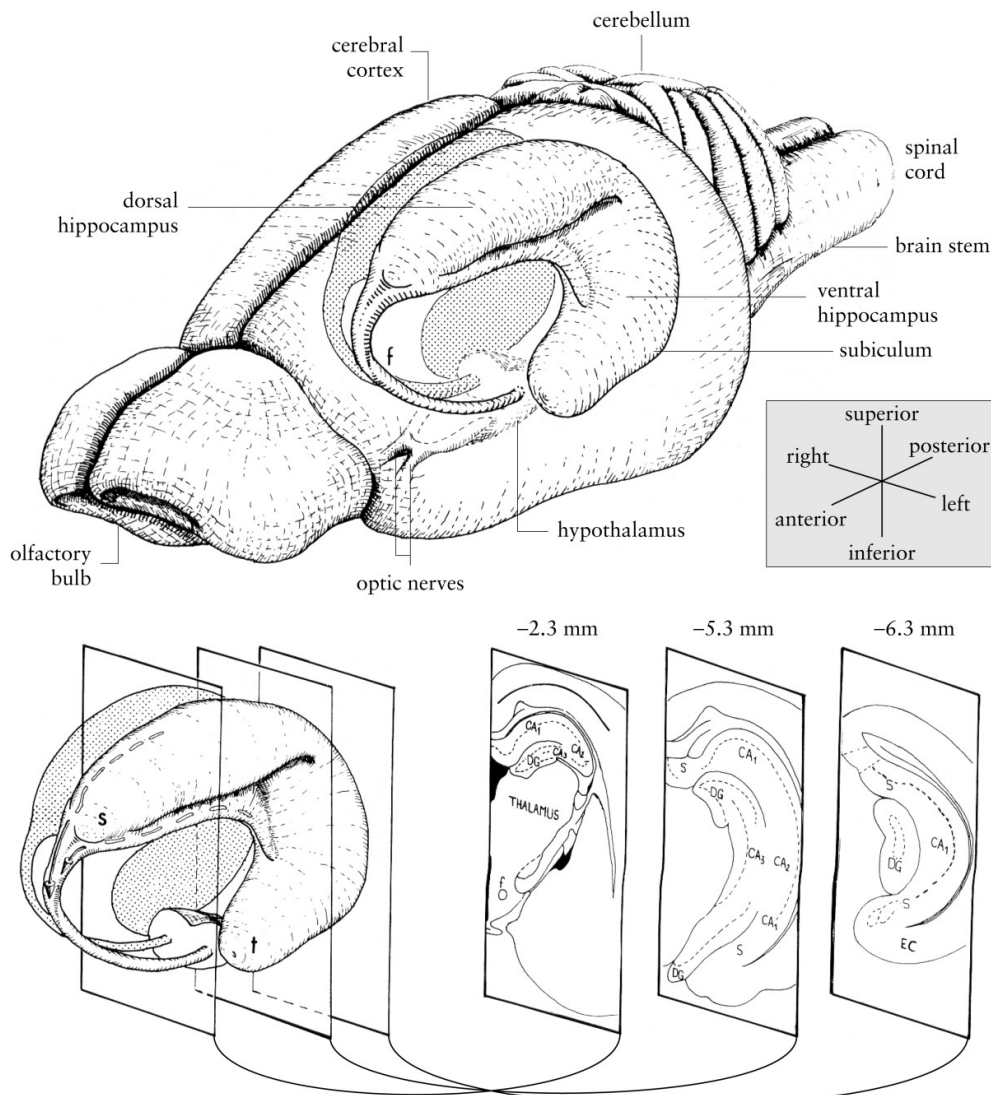
Figure 1: Diagram of the rat's hippocampus. In the upper part, the three-dimensional localization of the hippocampus and surrounding structures; in the bottom panel, three coronal sections of the left hippocampus are presented (with their approximate anteroposterior coordinate relative to bregma). CA1, CA2, CA3 are the cornu ammonis 1-3 fields, DG stands for dentate gyrus, EC for entorhinal cortex; f for fornix; s for septal pole of the hippocampus, S for subiculum and t for temporal pole of the hippocampus. Adapted from (Cheung and Cardinal, 2005).

At the cellular level, the hippocampus is described as having layer histology (**Figure 2**). 3 layers appear more prominently – the polymorphic layer (*stratum oriens*), the pyramidal layer (*stratum pyramidale*) and the molecular one (*stratum radiatum* and *stratum lacunosum-moleculare*).

Pyramidal neurons are the most abundant neurons in the hippocampus and their cytoarchitecture is stratified into the distinct layers. Pyramidal cell's bodies have an inverted conic (pyramidal) shape, with the diameter ranging between 20-40μm to 40-60 μm – the somas are comprised in the pyramidal layer, which forms a curved sheet with variable thickness (2 to 3 body cells). These cells have a fine apical dendrite (Ø 5-10μm) that extends through the entire molecular layer, whereas various basal dendrites stretch for 200-300μm to form the polymorphic layer. These cells' morphology suffers slight modifications from the CA3 to the

CA1 regions (regions are defined in 1.2.3Neuronal circuits) – somas become smaller and the apical dendrites become longer, thinner and more with a more regular formation pattern (Alshuaib et al., 2001).
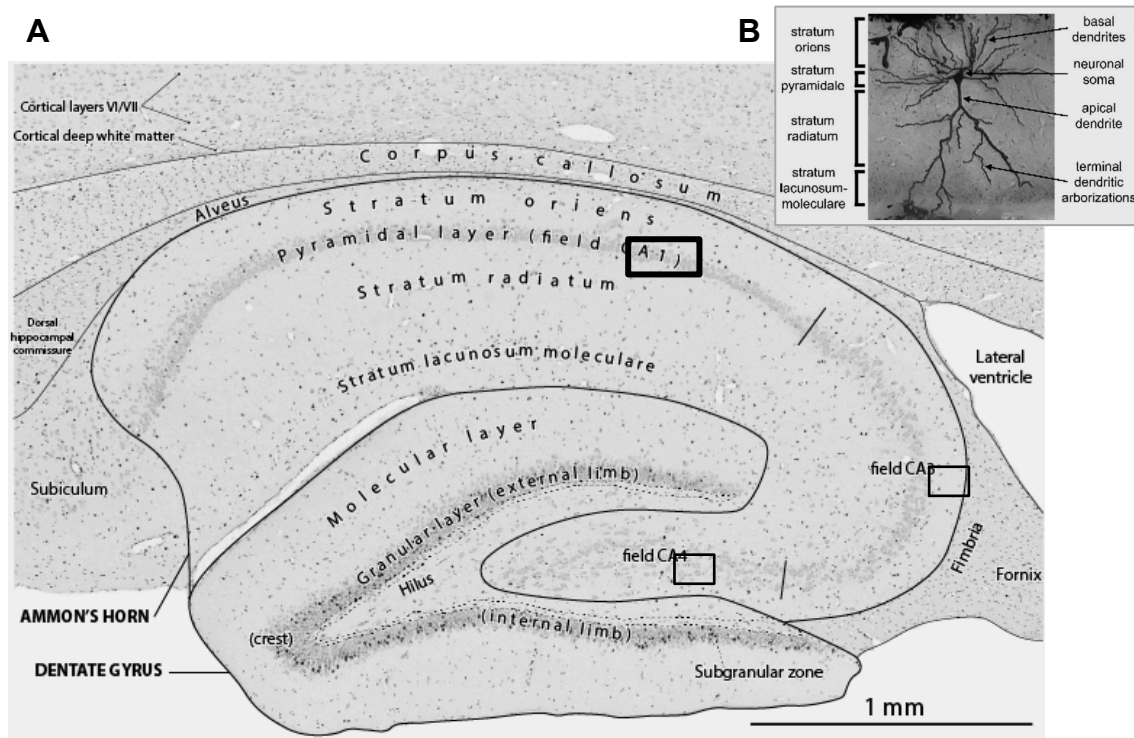
Figure 2: Rat hippocampus histology **A** Section of the dorsal hippocampus, stained by ³H-thymidine. Small black dots mark cell's nucleus. Adapted from Brain Development Maps (Website: ©2013 BrainDevelopmentMaps.org [Internet])**B** Rat hippocampal CA1 pyramidal neuron evidenced by Golgi-stained in section. The neuronal soma is located within the pyramidal layer (*stratum pyramidale*), basal dendrites overlap with the polymorphic layer (*stratum oriens*) and the apical dendrite crosses the molecular layer (*stratum radium* and *stratum lacunosum-moleculare*). Similar cells exist in other regions of the rat hippocampus, such as CA3, the dentate gyrus and subiculum. Adapted from (Shepherd et al., 2006).

The well-known and relatively simple structure of the hippocampus contributes for its utilization as an experimental model in diverse neuroscience scopes, namely the study of memory and learning, synaptic function and neuronal integration. Another advantage of this model is that it is fairly easy to isolate from the brain.

1.2.2 Function(s)

The hippocampus function has been widely studied (Bannerman Dm Fau - Rawlins et al.), as it is involved in memory, learning, information processing and subsequent consolidation and regulation of behaviour (D. Grant and Jarrard, 1968, Pothuizen et al., 2004). It is part of the limbic system, which also includes the parahippocampal gyrus, the fornix and fornix column, the olfactory bulbs, the amygdala, and the limbic cortex, among others.

From the famous "H.M. patient" (as Henry Molaison is usually refered to) (Scoville and Milner, 1957, Milner et al., 1998) onwards, the hippocampus' role on memory formation has been corroborated by a full-hand of studies (Zola-Morgan et al., 1986, Jarrard, 1991, Squire, 1992, Nyberg et al., 1996, Stern et al., 1996, Rempel-Clower et al., 1996, Rombouts et al., 1997, Fernández et al., 1998, Moser and Moser, 1998). It is clear now that the hippocampus plays a critical role in encoding and retrieval of spatial memory (navigation) (O'Keefe and Dostrovsky, 1971, O'keefe and Nadel, 1978, Olton et al., 1978, Morris et al., 1982, O'Keefe and Speakman, 1987, Maguire et al., 1998, Morris et al., 1990, Nadel, 1991, Muller, 1996, Maguire et al., 1997, Alvarado et al., 2002, Jarrard et al., 2012). Moreover, some studies, in both humans (Zola-Morgan et al., 1986, Nyberg et al., 1996, Rempel-Clower et al., 1996, Stern et al., 1996, Rombouts et al., 1997, Vargha-Khadem et al., 1997, Fernández et al., 1998) and rats (Rawlins, 1985, Davidson and Jarrard, 1993, Rudy and Sutherland, 1995, Bunsey and Eichenbaum, 1995, Eichenbaum, 1996, Wallenstein et al., 1998), state that the hippocampus is also involved in the associative learning (mnemonic functions) that is non-relying on spatial strategies (Eichenbaum, 1996, Eichenbaum, 2004). The fact that different hippocampus-dependent memory functions are in place is understood as a consequence of diverse neuronal circuits that are constrained within the hippocampus structure (Moser and Moser, 1998).

1.2.3 Neuronal circuits

The major hippocampal neuronal circuit has been established – it is the one that connects the dentate gyrus, the CA3, the CA1 and the subiculum in an excitatory loop transversal to the hippocampus (**Figure 2**). As far as it is known, it is repeated all the way throughout the longitudinal axis of the hippocampus (Anderson et al., 1971). This circuit is essential for the consolidation of explicit memory, one of the four processes involved in the explicit knowledge formation (encoding, consolidation, storage and retrieval).

Still, neuronal networks within the hippocampus segments also appear to be heterogeneous - different neuronal constitutions have been described in the dorsal and ventral parts of the hippocampus (Gage et al., 1978, Gage and Thompson, 1980, Verney et al., 1985, Blasco−Ibáñez and Freund, 1997, Moser and Moser, 1998), in tandem with diverse excitability features (Racine et al., 1977, Gilbert et al., 1985) and functional correlates (Hughes, 1965, Nadel, 1968, Stevens and Cowey, 1973, Sinnamon et al., 1978, Volpe et al., 1992, Olsen et al., 1994, Kjelstrup et al., 2002, Bast et al., 2009, Fanselow and Dong, 2010, Felice et al., 2012, Tanaka et al., 2012).

1.2.4 Hippocampal subregions & the dorsoventral axis

Customarily, the hippocampus is divided in four subregions (**Figure 2**): CA1-3 and the dentate gyrus (sometimes CA4 is also referenced, and it is called hilus when considered part of

the dentate gyrus). CA1 region is the equivalent of Cajal's hippocampus superior region and extends along almost all the hippocampus' length.

Yet, from as far as the 1960's, evidences in studies using cats started to reveal differences on the dorsal and ventral hippocampus' outputs in the surrounding areas (stimulating either part of the structure) (Elul, 1964, Siegel and Flynn, 1968, Edinger et al., 1973, Kazarian et al., 1995), as well as on pathways with the surrounding brain regions (Siegel and Tassoni, 1971, Pasquier and Reinoso-Suarez, 1977) and some functional corollaries (D. Grant and Jarrard, 1968, Johnson et al., 1977). Studies on serotonin and norepinephrine suggested an uneven distribution of these neurotransmitters (uptake and binding affinities) along the rat hippocampus' dorsal-ventral axis, (as well as the medial-lateral direction in the case of noradrenalin) (Gage et al., 1978, Gage and Thompson, 1980). These early studies have set the ground for the hypothesis that the hippocampus is anatomically, biochemically and functionally diverse throughout its dorsal-ventral axis. While some authors consider two parts (dorsal and ventral), other set three or more portions apart. As reviewed earlier, the intermediate hippocampus may have integrative functions of its own.

By the 2000's, a series of behaviour tests had already been performed to discern the hippocampal functions – the involvement in spatial memory was established (Jarrard et al., 2012) and growing evidence suggested that it was the dorsal hippocampus that played the main role in learning and memory, while the behaviour-regulator roles of ventral hippocampus were beginning to be disclosed. This rose another set of questions regarding its heterogeneity along the longitudinal axis, namely regarding its neural substrates. Molecular and physiological differences provide the basis for the specific properties of dorsal and ventral hippocampus (Marcelin et al., 2012).

1.3 LATELY THE NUMBER OF ESSAYS FOCUSING ON DORSAL-VENTRAL ASYMMETRIES HAS ESCALATED RAPIDLY. SOME OF THE MOST RELEVANT RESULTS FOR THIS STUDY ARE SUMMARIZED IN DORSAL-VENTRAL ASYMMETRIES

Table 1b (Supplementary material: 8.1 Dorsal-ventral asymmetries), but more extensive reviews can be found (7. Moser and Moser, 1998, Bannerman, Dm, and Rawlins et al., Eichenbaum, 2004, Van Strien et al., 2009, Fanselow and Dong, 2010, Poppenk et al., 2013).

1.4 CENTRAL NERVOUS SYSTEM METABOLISM

Although not all the nervous system's metabolic pathways have been disclosed, a major part of the energy metabolism is now known. It is an intricate highly regulated system involving various cell types, namely neurons, astrocytes and endothelial cells, as well as their interactions, giving reason to it sometimes being named as "neurovascular unit" (Byrne and Roberts, 2009).

1.4.1 Metabolism and insulin

This study will focus on the neuronal effects of carbohydrates metabolism rather than on the slower fatty acids one (the diet used for the animals of the present study contained 75.1% carbohydrates of total Atwater Fuel Energy of the rat's diet).

Carbohydrates obtained in food are the organism's provider of energy, apart from its own reserve. The organism is capable of storing carbohydrates, as glycogen, within the muscle and liver, and, as lipids, in fat cells. As availability of glucose reduces, the muscle resorts to glycogen to produce energy (for example during major effort such as intense exercise), whereas fat cells constitute a longer-term reserve. Glucose, which is the monosaccharide that results from the degradation of the ingested complex carbohydrates, is the main fuel of the brain.

There are two protein families involved in glucose's transport through cell membranes:

- Transporters – responsible for glucose's absorption at the small intestines' lumen and reabsorption at the renal tubule; they are Na^+/glucose symporters, promoting glucose's transport against its concentration gradient (driven by high extracellular concentrations of sodium);

- Carriers – known as the "GLUT" (facilitative glucose transporters) family, they exist in every cell's membrane and are classified accordingly, from GLUT1 to GLUT14, in three classes (**Table 1**).

Glucose homeostasis is controlled hormonally, by insulin and counter regulatory (or opposing) hormones. Insulin is an anabolic hormone, produced by β cells of the islets of Langerhans of the pancreas. It is released in a pulsatile manner according to the feeding cycle, since glucose stimulates its release and lack of glucose stimulates its storage. After eating, there is an abundance of glucose in the blood stream ("fed condition"). Under these circumstances, the insulin role is to prevent an abnormal rise of blood glucose levels. To accomplish this, insulin: 1) inhibits glucose's release by the liver - the liver has the capacity to arrest the glucose on his cells by enzymatic (hexokinase or glucokinase) phosphorylation of the glucose molecule and possible storage as glycogen; 2) activates glucose uptake in the skeletal muscle cells (among others) and glycogenesis within it (conversion of glucose to glycogen); and 3)

stimulates storage of glucose in fat cells (conversion of glucose to triglycerides) once glycogen reserves are restored. Mechanisms 2 and 3 are mediated by a translocation of GLUT4 to the respective cell's membrane, as in other circumstances the transporters are mainly trapped in the intracellular space and are therefore inactive.

This hormone also plays a critical role in protein and fat metabolism as, for example, it induces the amino acid transfer into the muscle and other cells, promoting their absorption and inhibiting their catabolism inside the cells (Fulks et al., 1975, Mayer et al., 2007). Insulin is also involved in the activation of cellular cascades and in synaptic facilitation (Craft and Stennis Watson, 2004).Numerous pathological conditions have been described as consequences of insulin's malfunctions, namely diabetes, hypertension and obesity (Henquin, 2000).

Table 1: Glucose carriers (GLUT) family. Class, name, tissue distribution and function are defined for each GLUT protein (gene SLC2). CNS Central Nervous system, Cb cerebellum, CTX cortex, Hp hippocampus, Hypo hypothalamus, LH lateral hypothalamus, PVN paraventricular hypothalamic nucleus, VMH ventromedial hypothalamus, n.d. not determined or not reported (grey). Adapted from (Olson and Pessin, 1996, Joost and Thorens, 2001, Wood and Trayhurn, 2003, McEwen and Reagan, 2004, Thorens and Mueckler, 2010)

GLUT class	GLUT	Tissue expression		Function	
		Main	In the CNS	Transport	Insulin sensitive?
I	GLUT1	Erythrocytes, brain, ubiquitous	45kDa isoform: Astrocytes, neurons widespread 55kDa isoform: Endothelial cells widespread	Glucose	No
I	GLUT2	Liver, pancreas, intestine, kidney	Astrocytes, tanycytesin PVN, LH, VMH and Arcuate	Glucose (low affinity), fructose	No
I	GLUT3	Brain (neuronal)	Neurons and neutrophil widespread	Glucose (high affinity)	No
I	GLUT4	Heart, muscle, fat, brain	Neurons (somatodendritic) in Cb, CTX, Hp, Hypo	Glucose (high affinity)	Yes
II	GLUT5	Intestine, testis, kidney	Microglia widespread	Glucose (very low affinity), fructose	No
III	GLUT6	Brain, spleen, leucocytes	n.d.	Glucose	No
II	GLUT7	n.d.	n.d.	n.d.	n.d.
III	GLUT8	Testis, brain, other	Neurons (somatodendritic) widespread	Glucose	No (yes in blastocysts)
II	GLUT9	Liver, kidney	n.d.	n.d.	n.d.

III	**GLUT10**	Liver, pancreas	n.d.	Glucose	No
II	**GLUT11**	Heart, muscle	n.d.	Glucose (low affinity), fructose	No
III	**GLUT12**	Heart, prostate, muscle, small intestine, fat	n.d.	n.d.	Yes
III	**GLUT13 (HMIT)**	Brain	n.d.	H^+-myo-inositol	n.d.
I	**GLUT14**	Testes	n.d.	n.d.	n.d.

1.4.1.1 Into the nervous system

The main energy substrate for the brain is glucose, which is metabolized by glycolysis and oxidative breakdown in both astrocytes and neurons.

There are only small pool-reserves of glucose in the brain (along with the also not extensive reserve glucose stored as glycogen). So that so that other substrates cannot substitute the continuous supply of glucose from blood to sustain brain function in the normal adult (Clarke and Sokoloff, 1999).

GLUT1 protein (55kDa isoform) is responsible for glucose's transport across the blood–brain barrier. This transportation is not usually a rate-limiting step, instead it is thought that what adapts energy delivery to demand is a process known as neurovascular and neurometabolic coupling; i.e., neuronal activation triggers increased glucose consumption and glucose demand, stimulating blood flow and glucose transport over the blood–brain barrier (Leybaert, 2005, Leybaert et al., 2007).

Neurons take up glucose mainly via GLUT3 and perform aerobic cellular respiration to meet their energetic demands. However, great debate stands on whether it is the glucose directly uptaken or lactate supplied by astrocytes that is the major energy substrate (Chih et al., 2001, Schurr, 2005). Astrocytes enable a metabolic shuttle for energy supply to neurons, through uptake of glutamate in the tripartite synapse cleft (Magistretti and Pellerin, 1999).

In the rat's hippocampus, the extracellular glucose concentration is reported in between 1,00–1,24 mmol/L (microdialysis, food available *ad libitum* (McNay and Gold, 1999)) and 2,6 mmol/L (glucose-sensitive micro-electrodes, food available *ad libitum* (Hu and Wilson, 1997)).On its turn, insulin is transported into the central nervous system by crossing the blood brain barrier under a saturable and highly regulated transport mechanism (capable of altering insulin flow during development and by fasting, obesity, hibernation, diabetes mellitus, Alzheimer's disease, among other, and it is not evenly distributed in the central nervous system (Banks, 2004, Banks et al., 2012). This goes in accordance with insulin's unique functions in

the central nervous system, which resort to mechanisms somehow independent to role of insulin in the periphery (Banks et al., 2012).

1.4.2 Insulin

The present work focuses in a K^+ channel (Kv1.3), which is insulin sensitive. Hence, some considerations about insulin and its receptor are due in the context of this introduction.

1.4.2.1 Receptor's activation and signal transduction (Kv1.3)

Insulin runs promptly in the blood stream until it reaches the target tissues (liver, muscle, fat, brain), where it interacts with InsR, its cell surface receptor (**Figure 3**).
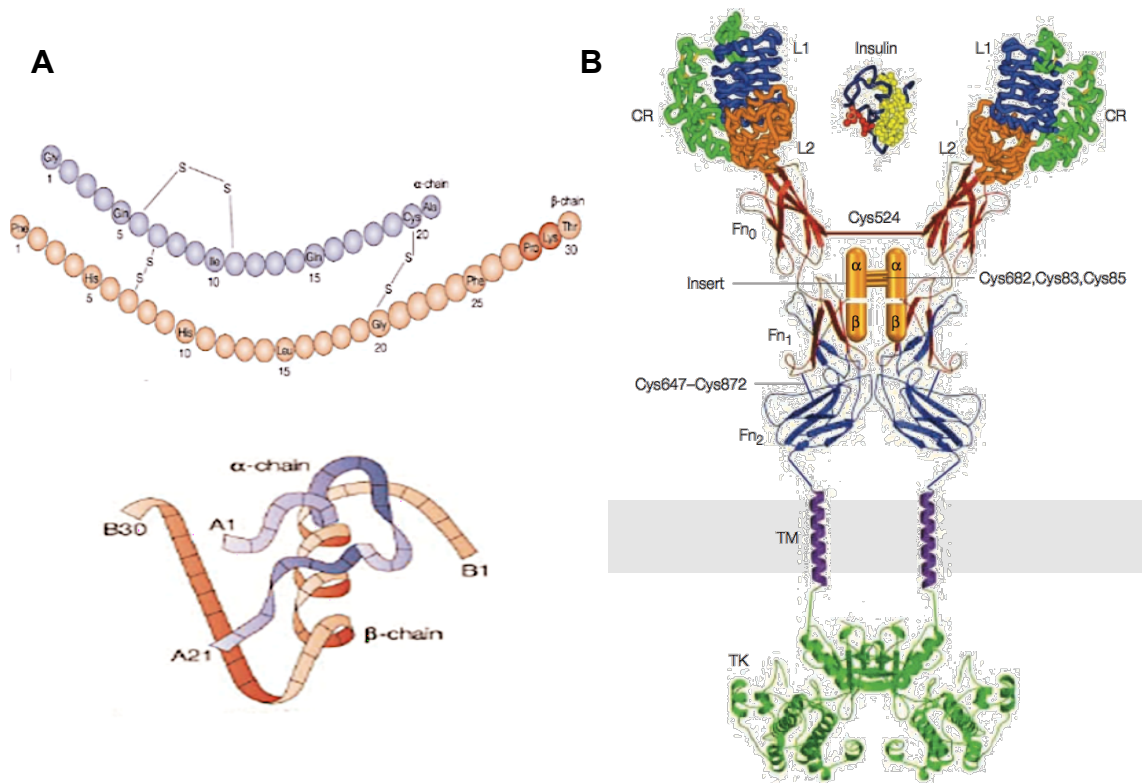
Figure 3: Insulin and its receptor. **A** Primary (upper part) and tertiary (lower part) insulin structures' diagrams. Insulin is a 6kDa protein composed by two chains: chain A has 21 amino acids and has an intrachain disulphide bridge, while chain B has 30 amino acids. The two chains are connected by two disulphide bridges(Marchetti et al., 2008). Insulin's active form is a monomer, but it also dimerizes or associates in hexamers (De Meyts, 2004, Dunn, 2005). Adapted from (Elsayed, 2012). **B** Insulin and its receptor's supra-domain organization model. Insulin backbone is shown in blue, the membrane is represented as a grey band and TK is the Tyrosine kinase domain. The insulin receptor is produced and stored as a single-stranded high-weight precursor (210 kDa) with 3h half-life (Olson et al., 1988, De Meyts, 2004) The mature receptor is a tetramer composed by two α subunits (135kDa) and two β subunits (95kDa). Its tertiary structure is dominated by α helices and a strong structural stability (Chang et al., 1997). Adapted from (Marino-Buslje et al., 1999) and (De Meyts and Whittaker, 2002).

The insulin molecule binds to the extracellular α subunit (despite the presence of two binding sites, only one insulin molecule seems to fit the receptor dimer), inducing a conformational change that leads to the fast autophosphorylation of the receptor's β subunit (that contains the tyrosine kinase enzymatic function). This is followed by the phosphorylation

of the insulin receptor substrate 1 (IRS1), a docking protein that induces the activation of down-stream pathways by binding to SH2 domains of various effector proteins (Gual et al., 2003). The IRS1-PI3K interaction activates the insulin signalling pathway (among others) that leads to increased glucose transportation into the cell by recruiting GLUT4 from an intracellular pool to the membrane (Kahn and White, 1988, Cheatham et al., 1994, Saltiel and Kahn, 2001), The insulin signalling pathway through MAPK drives to gene transcription, cell division and differentiation, as well as various others, as a growth promoter (Saltiel and Kahn, 2001).

Figure 4 is a representation of some insulin-activated pathways, through InsR.
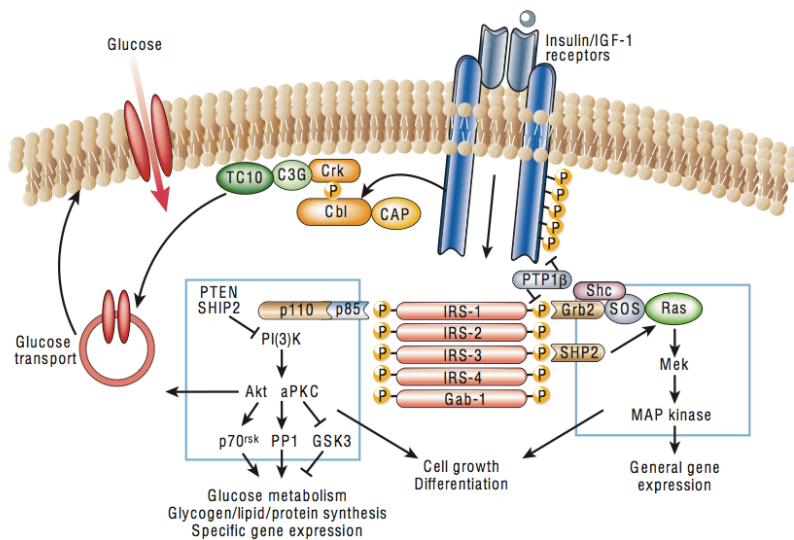
Figure 4:Signal transduction pathways induced by insulin receptor (InsR) activation. Upon activation by an insulin molecule, the tyrosine kinase domain of the receptor induces its own phosphorylation, along with other cellular proteins, such as members of the IRS family, Shc and Cbl. These bind to SH2 domains of various effector proteins, such as PI3K, PKB and MAPK, leading to a broad range of signalling pathways. Consequently, glucose regulates the transport of specific vesicles trafficking, protein synthesis, enzyme activation and inactivation, and gene expression, which results in the regulation of glucose its, lipid and protein metabolism. Adapted from (Saltiel and Kahn, 2001).

1.4.2.2 Insulin, diabetes mellitus and Alzheimer disease

Diabetes is defined as a group of metabolic diseases characterized by hyperglycaemia as a consequence of malfunctions in insulin production, function or both. Chronic hyperglycaemia is associated with long-term damage and various organs dysfunction, namely eyes, kidneys, nerves, heart and blood vessels.

In type-1 diabetes (DMT1), insulin is absolutely absent due to autoimmune destruction of pancreatic β cells (auto-reactive T-lymphocytes produce antibodies anti-β cells). Classically, type-2 diabetes (DMT2) is defined as a metabolic disorder characterized by relative insulin deficits resulting of inadequate secretion of the hormone *or* of tissues reduced sensitivity to the molecule. However, nowadays, it is regarded as a 2 hit disease, meaning that insulin resistance has to be accompanied by a deficit in its secretion (Bergman et al., 2002, Kahn, 2003); it is not

known which starts and which follows but it is established that insulin resistance followed by compensatory hyperglycaemia is one of the earlier onsets of the disease (Gungor et al., 2005).

Alzheimer disease (AD) is characterized by a subtle decline in memory abilities extending to a generalized deterioration of adaptive and cognitive capacities (Watson and Craft, 2004), along with behaviour changes (apathy, agitation and psychosis) and physiological alterations (presence of neurofibrillary tangles and senile plaques, reduction of cerebral volume and alterations in the cholinergic system) in the central nervous system (Duff et al., 2000).

Diverse studies suggest that dysfunctions in glucose or insulin metabolism associate with cognitive impairment in AD. In fact, the inhibition of the insulin's receptor in neurons has been suggested as an *in vivo* model for AD (Frölich et al., 1998, Hoyer and Lannert, 1999, Hoyer, 2002). AD patients revealed low InsR labelling and low tyrosine kinase activity (Frölich et al., 1998). This comes in accordance with the preposition that a decrease of the insulin levels and of the InsR expression result in lower levels of acetylcholine and decreased blood flow in the brain, since in AD's initial stages glucose consumption is cutback by 45% (a AD sign before the first symptoms) and ATP production is reduced (Hoyer and Nitsch, 1989). *Post-mortem* analysis of AD patients' brains also reveals a significant and increasing reduction of Ins/IGF trophic factors and their receptors (Rivera et al., 2005, Steen et al., 2005). Consistently, clinical research demonstrates that hyperinsulinemia (in euglycemia) facilitates memory formation in AD patients (Craft et al., 1996, Craft et al., 1999, Craft et al., 2003). Also, several lines of studies suggest that a lower insulin concentration might reduce the Aβ release from the intracellular compartment to the external one and therefore decelerate the disease's progression.

All in all, there is supporting evidence to say that AD is related with insulin resistance. This idea has been proposed in the late 80's (Hoyer and Nitsch, 1989) and now we have a clearer picture on how various aspects of AD can be explained in light of insulin's signalling malfunctions (Schubert et al., 2003, de la Monte and Wands, 2005, Craft, 2007, Suzanne and Wands, 2008). Evidences on how insulin resistance conditions, such as obesity and DMT2, contribute to cognitive defects and neurodegeneration are several (de la Monte et al., 2009). Those include: DMT2 or obese patients have a higher risk of developing cognitive defects, dementia or AD (Pasquier et al., 2006); AD is accompanied by a progressive increase in resistance to insulin (Steen et al., 2005, Rivera et al., 2005, Craft, 2007); in experimental models, DMT2 causes cognitive deficiencies (Winocur et al., 2005).

Abnormal molecular, biochemical and mechanic characteristics are shared by AD and DMT2 (Nicolls, 2004) (de la Monte et al., 2006, Landreth, 2007, Reger et al., 2008) (Lester-Coll et al., 2006).

1.4.2.3 Insulin in neurophysiology

Insulin's role in the periphery of the central nervous system (CNS) is well known, which is not the case of its role in the brain. Until recently, it was even a generalized belief that the brain was insensible to insulin. Lately however, contrary evidence has sprung up.

Multiple studies identified insulin receptor distributed in specific brain regions, such as the olfactory bulb, the hypothalamus, the hippocampus and the cerebellum (Unger et al., 1991, Schulingkamp et al., 2000). Plus, a minor portion of the insulin present in the brain is produced locally (Woods et al., 2003, Banks, 2004). In either case, the hormone had various functions through mechanisms diverse from its classical glucose-regulator role described for periphery (Banks et al., 2012). The studies advocate that insulin controls central nervous system mechanism such as the regulation of ingestion in the hypothalamus (Woods et al., 1979, Spanswick et al., 2000, Plum et al., 2005) and the olfaction in the olfactory bulb (Fadool et al., 2004, Das et al., 2005, Plum et al., 2005). In addition, insulin has also been described as a memory and learning potentiator – intracerebroventricular injections improve learning tasks performance in rats (Fehm et al., 2000) and intravenous injections improve story recall abilities(Craft et al., 1999). Interestingly, animal that had been subjected to water maze training also revealed more hippocampal expression of InsR mRNA ad protein, namely in CA1 pyramidal neurons (Zhao et al., 1999).

1.4.2.3.1 Insulin as a neuroprotector

Insulin has well-known neuroprotective properties (Venters et al., 2001), as it promotes neurogenesis (Åberg et al., 2000) and synapses formation, as well as potentiating the most effective glucose utilization in the brain (Carro et al., 2001). Moreover, it is documented that insulin protects the neurons from the Aβ aggregates in AD (Klein, 2002, Nelson et al., 2008) and from the oxidative stress that they cause (Moreira et al., 2005, Duarte et al., 2008). Still, the mechanism by which insulin acts as a protector is not yet clarified, even though some evidence suggests that it is via the PKB-akt pathway (Bayascas, 2008).

1.4.2.3.2 Insulin as a neuromodulator

A possible explanation for the insulin's and its receptor's role in learning an memory is that it acts as a neuromodulator in events related to synaptic plasticity (Zhao and Alkon, 2001) (**Figure 5**). Among these events, LTP (long term potentiation) and LTD (long term depression) stand out. Besides, it seems to be involved in neuronal survivor (Zhao and Alkon, 2001) (Gasparini et al., 2002). Results described previously in 1.4.2.2 (Insulin, diabetes mellitus and Alzheimer disease) that advocated the insulin resistance as related to AD fit in this insulin role model (Gasparini et al., 2002, Craft and Stennis Watson, 2004).
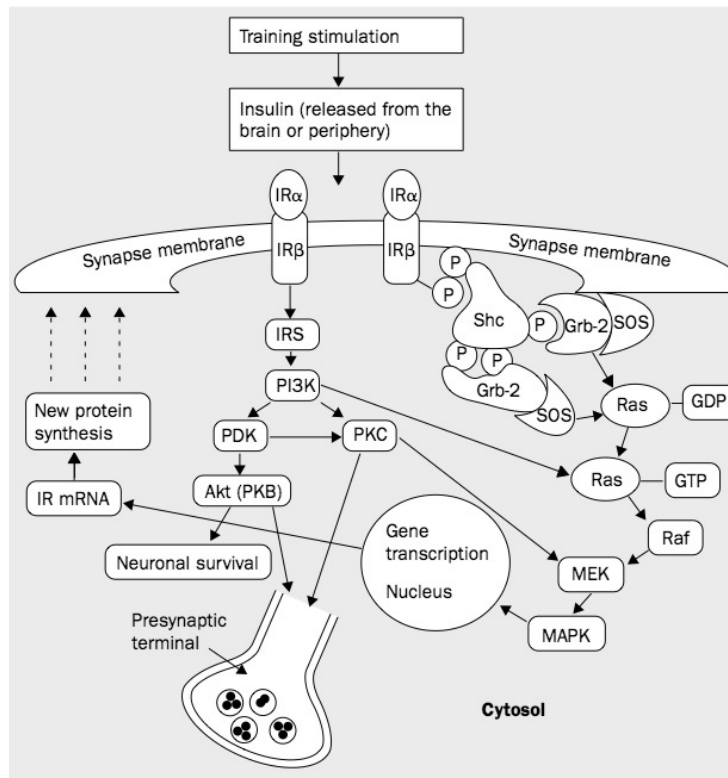
Figure 5: Insulin receptor (represented as IR) modulated pathways in neurons, which are involved in learning and LTP formation. Insulin activates the downstream pathways, through the catalytical function of its receptor, reviewed previously for periphery cells (**Figure 4**). InsR activation induces the activation of a signalling cascade involving Shc, Grb-2/SOS and Ras/ MAPK shortly after memory training, a pathway involved in long-term memory formation through activation of gene expression leading to new protein synthesis. By activating a cross talk with other protein tyrosine kinases, such as pp60c-src, InsR also regulates short-term memory formation. Insulin (and other InsR agonists) may also modulate other memory formation processes and neuronal survival through PI3K, PKC, Akt/PKB and Ras/MEK/MAPK. Adapted from (Zhao and Alkon, 2001).

Results in rats that postulate that InsR absence (InsR knock-out animals) resulted in impaired learning and memory capacity. Heterozygotic animals (InsR$^{+/-}$) revealed problems in short term (1h) and long term (24h) memory when faced with known-objects recognition tasks. Also, cultured neurons from InsR$^{+/-}$ and homozygotic animals (InsR$^{-/-}$) olfactory bulb had lower current peak amplitude than wild type (wt) cultured neurons. Summing up, these results suggest that the loss of one or both InsR alleles modifies the electric performance phenotype in olfactory bulb neurons underlying learning and memory deficits, an event probably related to diminished Kv1.3 protein expression (Fadool et al., 2000).

Insulin is then proposed as a neuroexcitability modulator. Further evidence for this thesis is that insulin's actions upon specific neuronal mechanisms related to K$^+$ conductance alter the neuron's neuroexcitability profile. Contrary to what happens in peripheral tissues, fasting increases insulin's levels in the olfactory bulb, which results in an inhibition of Kv1.3 currents that is translated to increased excitability and a more refined olfactory sense (Das et al., 2005). Kv1.3's inhibition by insulin is mediated by Kv1.3 channel phosphorylation. Kv1.3 and InsR were co-transfected in cultured cells, and a major outward current was observed (due to

increased K^+ currents). This current was then significantly decreased by insulin application onto the superfusing medium. In parallel, Kv1.3 had been phosphorylated in various residues. However, cells co-transfected with Kv1.3 and truncated InsR (without the tyrosine kinase domain) showed no K^+ current inhibition by insulin superfusion neither Kv1.3 phosphorylation (Fadool et al., 2000).

In fact, Kv1.3 knockdown mice neurons also have altered neuroexcitability, are not sensible to insulin and the animals have an above-average olfactory sensibility ("super-smellers") (Fadool et al., 2004), giving further support to the previous assumption of Kv1.3 mediated insulin action.

Insulin's effect upon Kv channels was also verified in differentiated neuroblastoma cells (N1E-115) and results show a clear reduction of two current components, in a concentration-dependent manner (Lima et al., 2008).

Furthermore, in the hypothalamus, insulin has been described as a K_{ATP} activator that causes a neuronal hyperpolarization that is translated as a decrease in glucose consumption (Woods et al., 1979, Spanswick et al., 2000). In the hippocampus, however, the effect of insulin and IGF (insulin growth factor) seems to be more complex than in cell lines or in the hypothalamus. Results showing an upregulation of BK mediated currents' conductance and reduced neuroexcitability by insulin (O'Malley et al., 2003, O'Malley and Harvey, 2004)contrast with results exhibiting a dowregulation of Kv currents and increased neuroexcitability by IGF-1 (O'Malley et al., 2003, O'Malley and Harvey, 2004). Further support is given to the insulin-sensitive Kv current by recent results that reveal that insulin inhibit specifically the slow component of Kv currents in rats' CA1 isolated cells, whereas the fast component (corresponding to the A-current) is not affected (Lima et al., 2008). These results are further developed in 1.8 (Framework of the Project), as they give support for this project's thesis.

1.5 NEURONAL EXCITABILITY & IONIC CHANNELS

In the basis of neuroexcitability are ion channels, receptors (ionotropic and metaboltropic), transporters and pumps. Electrical signals result from temporary local changes that drive the resting potential away from it's resting value and are propagated throughout a neuron or nervous fibre. Ion channels mediate those alterations.

Since over 100 types of ion channels have been described so far, and new ones are being described: a systematic classification is in place. Ion channels are divided into families

depending on amino acid structure and function (ion selectivity, gating). Regarding function, channels are divided in:

- **Voltage-gated channels**: a change in the voltage across membrane is the trigger. Usually they are subdivided according to the ion selectivity (voltage-gated Na^+/K^+/Ca^{2+} channels - many subtypes within each category);

- **Ligand-gated channels**: the binding of a chemical ligand (either extracellular, for instance a neurotransmitter, or intracellular, for example an ion or a nucleotide) is the stimuli. Often these channels are subdivided according to the type of ligand;

- **Mechanically-gated channels:** a mechanical stress (for example the stretch of the membrane itself) is the stimuli. Gap-junction channels are an example of this kind of channel.

This family classification is not sealed however, since channels can be gated by more than one stimulus (often voltage and ligand).

Here, we will focus on voltage-activated channels, namely voltage activated K^+ channels.

1.6 POTASSIUM CURRENTS AND CHANNELS

K^+ selective ion channels is the larger and most diverse group of ionic channels, considering that 70 loci have been identified in the mammalian's genome coding for its principal subunits (Gutman et al., 2005), and that they can undergo alternative splicing, RNA editing, post-translational modifications and heteromeric assembly. Since 1987, when the first gene codifying for a K^+ channel has been cloned (Papazian et al., 1987), dozens of genes have been identified that share the selectivity pore signature sequence (Gutman et al., 2005).

In excitable cells, K^+ channels are involved in the stabilization of the membrane potential, since they converge the resting membrane potential to the K^+ equilibrium potential, lowering it, and therefore keeping it away from the action potential firing threshold (Hille, 1992). Hence, they are critical to neuroexcitability. Not only they establish the resting potential but also keep the depolarization in the action potential short, are involved in shortening periods of high activity, keep a time separation between repetitive spikes and tend to diminish the excitatory inputs efficacy in the cell (Hille, 1992). Hence, as K^+ has a negative reversal potential, these cells tend to dampen excitation (Hille, 1992).

1.6.1 Potassium channel structure and groups

The K^+ channel was the first natural membrane channel for which crystallization and high-resolution real structure analysis was done (Doyle et al., 1998). This speaks of its biological relevance.
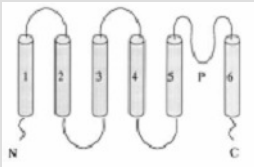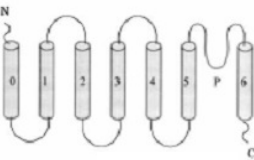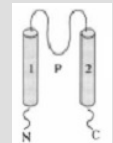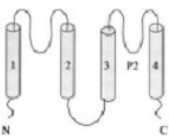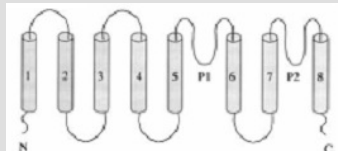
Concerning the function, their structure reveals a hydrophilic conducting pore, lined by a pore-loop responsible for the K^+ selectivity and a gating mechanism that supports the open/close/inactive/desensitized states (Hille, 1992). It is the selectivity pore segment – TXXTXGYG (Heginbotham et al., 1994) – which is homologous in all the genes codifying for potassium channels that defines them as belonging to this category.

More particularly, four α subunits (also named pore-forming or principal subunits) assemble as a homotetramer or a heterotetramer of one or two subunits with fourfold symmetry around the central pore, determining the infrastructure of the channel. Other subunits, with similar structure to the α ones, are often necessary for functional channel formation – these are called coassembly principal subunits. β subunits (or auxiliary proteins), with distinct sequences, also often interact with the principal subunits complex, usually altering their electrophysiological or biophysical properties, expression levels or expression patterns (Coetzee et al., 1999). Associated proteins, such as regulatory proteins or elements of the cytoskeleton, are also sometimes in play. Due to the possible combinations, the number of possible distinct K^+ channels is by the hundreds, if not thousands (Coetzee et al., 1999).

The customary classification system of K^+ channels is based upon structural properties of the main protein that composes the channel. Groups are structural classes established according to the α subunit's number of transmembranar domains (TMD's) and porous loops (P-loops). They then comprise families, classified by the amino acid sequence homology, which are further divided into subfamilies. **Table 2** frames the five known groups of potassium channels.

Different potassium channel subpopulations have different operating profiles and therefore assume different functions in the cell. A fair representation of the variability of these channels and supposed function is the age-dependent axonal expression of some of these proteins described in (Pruss et al., 2010).

Table 2: Potassium channels groups, their schematic information (TMD's are represented by grey cylinders; P stands for the P-loops numbers; N and C represent the protein's amine and carboxyl terminals), families and other relevant information. Adapted from (Robbins, 2001)

Group	Schematic representation	Families	Other relevant information
6DTM-1P		Kv (voltage-activated K^+ channels; subfamilies Kv1-6,Kv8-9) SK_{Ca} (small conductance Ca^{2+}-sensitive K^+ channels) IK_{Ca}(intermediate conductance Ca^{2+}-sensitive K^+ channels)	TMD S4 is the voltage sensor; the P-loop has the selectivity signature Differently from BK_{Ca}, SK_{Ca} and IK_{Ca} channels are activated by low concentrations of intracellular Ca^{2+}(<1µM) and are not sensible to voltage. SK_{Ca} differ from IK_{Ca} by being sensible to apamine (100pM-10nM).
7DTM-1P		BK_{Ca} (big conductance Ca^{2+}-sensitive K^+ channels)	Formerly covered in 6DTM-1P group, these channels have been ungrouped for having an extra TMD in the N-terminal, named S0, making 7 of them. BK_{Ca} channels are activated by intracellular Ca^{2+}(1-10µM, as it binds to the divalent cation sensor in each C-terminal of the α subunit) or by voltage (voltage sensor in S4).
2TMD-1P		K_{ir} (inward rectifier K^+ channels; subfamilies K_{ir}1-7)	Unlike other K^+ channels, inward rectifiers' conductance is bigger when there is a hyperpolarization and decreases when a depolarization occurs (the pore is blocked by cytoplasmic cations, as Mg^{2+} and polyamines, at S2). Their main function seems to be keeping the membrane's potential close to E_{K+}.
4DTM-2P		TWIK (two-pore weak inward rectifier) TREK (TWIK-related K^+ channel) TASK (TWIK-related acid-sensitive K^+ channel) TRAAK (TWIK-related arachidonic acid- stimulated K^+ channel)	This group comprises the channels responsible for the leak (or background) currents. These currents stabilize the membrane's potential below the threshold and are involved in the repolarization. Two α subunits have to form the protein to make it functional. This allows for distinct P-loop sequences, which may supress the channel's activity.
8DTM-2P		TOK	Only found in yeast, these channels are outward rectifiers. Their gating is sensible to extracellular potassium and they are very little inactivated.

1.6.2 Voltage-dependent potassium channels

Voltage-gated channels are found in main cell types such as neuronal, skeletal and cardiac cells. They open and close in response to voltage change across the plasma membrane and as a result an action potential can arise.

In the brain, potassium voltage-gated potassium channels (Kv's) are highly relevant for flow and processing of information, given that they complete the action potential, repolarize the membrane, determine the resting potential and regulate the neurotransmitters' release in the pre-synaptic terminal (Gutman et al., 2005). In addition, each cell has its own unique set of Kv's (different in terms of voltage-dependence, activation and inactivation rates and pharmacology), which supports the impressive diversity and large number of Kv's in the brain(Robbins, 2001).

1.6.2.1 Structure, activation and selectivity

All voltage-dependent ion channels share the same basic structural themes (for instance the $K_v\alpha$ subunit is similar to the motif that is repeated 4 times in Na_v and $Ca_v\alpha$ subunits). The major functional domains are the following:

- *Ion selectivity filter* (selective for Na^+ or K^+ or Ca^{2+});
- Gate opens and closes, controlled by a *voltage sensor* (positively charged amino acids), which responds to the level of the membrane potential;
- *Inactivation gate*, which limits the period of time the channel remains open, despite steady stimulation.

Regarding potassium voltage-gated channels (**Figure 6**), typically they are composed by four identical (or similar) transmembranar α subunits surrounding a central pore. Both N- and C-termini of the protein in the intracellular part of the membrane (the N-terminus has a role as the inactivation gate and the C-terminus as the determinant for channel localization within the membrane, with a PDZ-binding motif). Each αsub-unit is composed by six transmembranar segments (S1-6) and loops. Amino acid domains are the ones that dictate each segment length and function (usually related to the amino acid charge or other properties).

The selectivity filter is in the narrowest part of the pore and is formed by the smaller loop, between S5 and S6.S4 transmembranar domain is the voltage sensor, acquiring its cationic properties from arginine and lysine amino acids. At rest, this positively charged domain (which exists four times due to the existence of 4 αsub-units) is attracted to the inner residues of S2 and S3. When a depolarization occurs, this domain is electrostatically repelled and rotates from slanted to a more upright position, which permits ion conductance through the channel.

It is the N-terminus of the protein (green in **Figure 6A and C**) that acts as the inactivation gate.

Exception is made to this structure in voltage-gated KCNQ and eag/erg channels, as well as channels gated coordinately by voltage and ligand binding (BK Ca^{2+}-activated channels and HCN hyperpolarization and nucleotide-gated channels), and channels gated exclusively by intracellular ligands (CNG channels and SK channels).
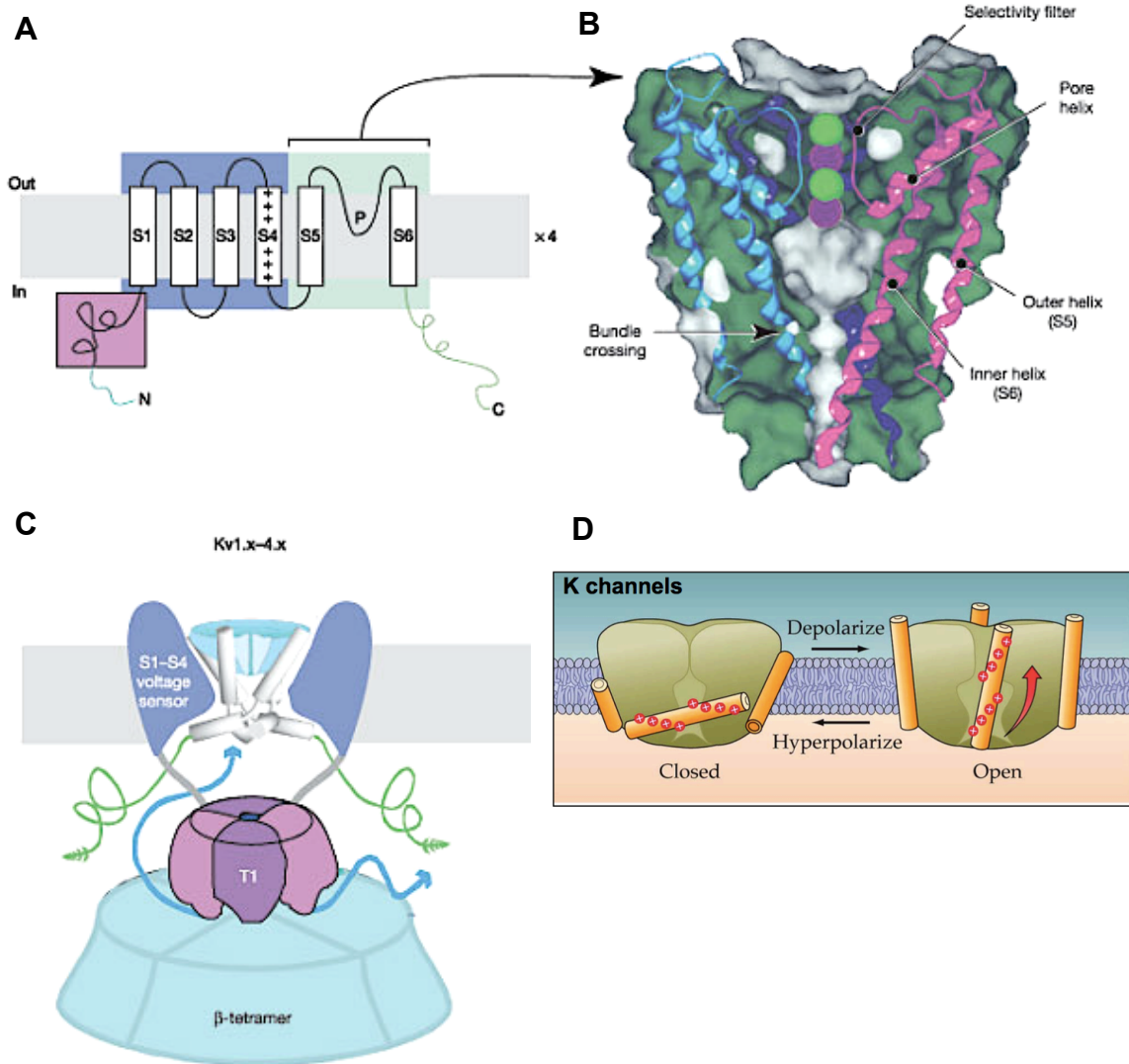
Figure 6: Schematic diagram of a voltage-activated potassium channel. **A** Composition of a typical voltage-gated K^+ channel α subunit, displaying the six transmembranar domains (S1-6) and the selectivity filter (P); the membrane is represented as a grey band. **B** The bacterial KcsA K^+ channel as a prototype for the pore-forming domain of the channel: the interior of the protein is dark green, with secondary structure shown as ribbons for three of the four subunits, and the water-exposed surface of the protein is grey; the selectivity filter is highlighted, with the extended selectivity filter loop supported by the pore helices. The four spheres mark the four K^+ ion binding sites: these are typically occupied by alternating K^+ ions and water molecules. **C** Kv1.x–Kv4.x subfamily's protein complex; the tetramerization domain' (T1, purple)determines the specificity of subunit assembly and interacts with possible β sub-units as well as with other proteins; the inactivation gate is in green; the membrane is represented by the grey band. **ABC** Adapted from (Yellen, 2002). **D** Voltage-gating mechanism shows the four S4 transmembranar domains making a rotary movement enabling the channel's aperture.

1.6.2.2 Voltage-dependent potassium channels groups

The Kv channel family is a very diverse and abundant group of ion channels, due to their importance, versatility and specificity.

Table 3 frames the known Kv subfamilies – it presents the subfamily name (according to the International Union of Pharmacology, IUPHAR), the gene locus, its functional correlates and tissue distribution.

These channels are much more diverse than one could predict from the gene loci that codify them. The diversity arises from several factors(Gutman et al., 2005):

i. Heteromultimerization enables the channel to be formed from either four identical subunits or from four different ones (from the same family – Kv1, K7, Kv10);

ii. "Modifier" subunits, which are not functional by themselves but form heterotetramers with Kv2 family subunits, enlarging its diversity;

iii. Accessory proteins (including β-subunits) may alter channel's properties;

iv. Alternate mRNA splicing (mainly in Kv3,4,6,7,9,10,11 subfamilies);

v. Post-translation modifications (primarily phosphorylation, but also ubiquitinylation and palmitoylation).

From **Table 3**, one can also infer that voltage-activated potassium channels are the molecular basis for mainly three types of currents – delayed rectifier current (I_{DR}), A-type current (I_A) and M-type K^+ current (I_M). **Table 4** states their main electrophysiological and pharmacological properties. More comprehensive information can be found in (Coetzee et al., 1999), (Gutman et al., 2005) and in (Shieh et al., 2000).

Table 3: Potassium voltage-dependent channels subfamilies (α-subunit, channel names, gene locus, functional correlates and tissue distribution). Kv states for voltage-dependent K$^+$ channel, EAG ether-a-go-go K$^+$ channel, ELK ether-a-go-go-like K$^+$ channel, (h)ERG (human) ether-a-go-go-related K$^+$ channel, I$_{DR(S)}$ (slow) delayed rectifier current, I$_{DR(R)}$ rapid component of delayed rectifier current (heart), I$_A$ A-type current, I$_{ur}$ ultrarapid delayed rectifier current, I$_{cAMP}$ cAMP-activated K$^+$ current, I$_M$ M-type K$^+$ current. Adapted from (Coetzee et al., 1999, Robbins, 2001, Gutman et al., 2005, Shieh et al., 2000).

Subfamily (α-subunit)	Channel name IUPHAR / Other names	Gene Locus	Functional correlates (associated current)	Tissue distribution
Kv1 (Shaker)	Kv1.1	KCNA1	I$_{DR}$	Brain, heart, skeletal muscle
	Kv1.2	KCNA2	I$_{DR}$	Brain, heart, smooth muscle
	Kv1.3	KCNA3	I$_{DR}$	Brain, lung, retina, spleen, lymphocytes, kidney
	Kv1.4	KCNA4	I$_A$	Brain, heart, skeletal muscle
	Kv1.5	KCNA5	I$_{DR}$ /I$_{ur}$	Heart, kidney, smooth muscle, skeletal muscle, brain, lung, pituitary, aorta and lungwort
	Kv1.6	KCNA6	I$_{DR}$	Brain, heart, lung
	Kv1.7	KCNA7	I$_{DR}$ /I$_{ur}$ component	Placenta, skeletal muscle, heart, lung, kidney, brain
	Kv1.8	KCNA10	I$_{DR}$ /I$_{ur}$ component	Kidney, brain, heart, skeletal muscle
Kv2 (Shab)	Kv2.1	KCNB1	I$_{DR}$	Brain, heart, skeletal muscle
	Kv2.2	KCNB2	I$_{DR}$	Brain, heart
	Kv2.3 / Kv8.1	KCNV1	Modifier/silencer	Brain, kidney
Kv3 (Shaw)	Kv3.1	KCNC1	I$_{DR}$	Brain, skeletal muscle, heart, T lymphocytes, lung
	Kv3.2	KCNC2	I$_{DR}$	Brain, heart
	Kv3.3	KCNC3	I$_A$	Brain, heart, thyme
	Kv3.4	KCNC4	I$_A$ (fast inactivation)	Parathyroid, prostate, brain, skeletal muscle, heart
Kv4 (Shal)	Kv4.1	KCND1	I$_A$	Brain, heart, lung, liver, kidney
	Kv4.2	KCND2	I$_A$	Brain, heart
	Kv4.3	KCND3	I$_A$	Heart, brain, smooth muscle
Kv5	Kv5.1	KCNF1	Kv2 modifier	Brain, heart, skeletal muscle, liver, kidney, pancreas

Kv6	Kv6.1	KCNG1	Kv2	Skeletal muscle, brain, uterus, ovary, liver, kidney, lung
	Kv6.2	KCNG2	Kv2 modifier/silencer	Heart, brain
	Kv6.3	KCNG3	Modifier/silencer	Brain
	Kv6.4	KCNG4	Modifier/silencer	Brain, liver, small intestine, colon
Kv7	Kv7.1 / KVLQT1	KCNQ1	$I_{DR(S)}$ (with KCNE1) I_{cAMP} (with KCN3)	Heart, kidney, lung, pancreas, placenta
	Kv7.2 / KQT2	KCNQ2	I_M	Brain, heart, neuroblastoma cells
	Kv7.3 / KQT3	KCNQ3	I_M	Brain
	Kv7.4 / KQT4	KCNQ4	I_L	Cochlea, placenta
Kv8	Kv8.1 / Kv2.3	KCNV1	Modifier/silencer	Brain, kidney
	Kv8.2	KCNV2	Modifier/silencer	Lung, liver, kidney, pancreas, spleen, thyme
Kv9	Kv9.1	KCNS1	Modifier/silencer	Brain
	Kv9.2	KCNS2	Modifier/silencer	Brain
	Kv9.3	KCNS3	Modifier/silencer	Brain, heart, kidney, lung
Kv10	Kv10.1 / eag1	KCNH1	I_{DR}	Brain, skeletal muscle, tumours
	Kv10.2 / eag2	KCNH5	I_{DR} (non inactivating)	Brain
Kv11	Kv11.1 / erg1 / HERG	KCNH2	$I_{DR(R)}$ (inwardly rectifying properties)	Heart, brain, neuroblastoma cells
	Kv11.2 / erg2	KCNH6	---	Brain, neuroblastoma cells
	Kv11.3 / erg3	KCNH7	---	Brain
Kv12	Kv12.1 / elk1, elk3	KCNH8	(slow activation and inactivation)	Sympathetic ganglia, brain
	Kv12.2 / elk2	KCNH3	---	Brain, tumours
	Kv12.3 / elk1	KCNH4	(slow activation)	Brain, neuroblastoma cells

Table 4: K$^+$ voltage-dependent currents - main electrophysiological and pharmacological properties. Ach states for acetylcholine, TEA for tetraethylammonium, 4-AP for 4-aminopyridine, 3,4-DAP for 3,4-diaminopyridine. Adapted from (Hille, 1992).

Current type	Electrophysiological properties	Pharmacological properties (blocked by)
Delayed rectifier current (I$_{DR}$)	- Activated by a membrane depolarization - Delayed activation - Slow inactivation - Conductance: <1-20 pS - Responsible for the membrane potential repolarization	TEA, 4-AP, 3,4-DAP, Cs$^+$, Ba^{2+}, dendrotoxins, quinidine
A-type current (I$_A$)	- Activated by a membrane depolarization - Fast activation and inactivation - Conductance: <1-20 pS	TEA, 4-AP, 3,4-DAP, quinidine
M-type K$^+$ current (I$_M$)	- Activated by a membrane depolarization - Slow activation - Non-inactivating (except by messengers: Ach, which act upon muscarinic receptors, and peptides) - Slow deactivation - Conductance: 5-18 pS - Supports resting K$^+$ conductance - Increases action potential and synaptic potential repolarization rates	Muscarine, linopyrdine, bradykinin, substance P, XE-911, Ba^{2+}

1.6.3 Kv1.3 channel

1.6.3.1 Kv1.3's structure

Kv1.3, also known as n-channel or KCNA3 (which is actually the human gene locus name), is a 523 amino acid protein with ~58.4 kDa[1](Gutman et al., 2005) formed by tetramers of approximately 65 X 65 Å (Spencer et al., 1997). **Figure 7** presents a diagram showing major functional domains and phosphorylation sites, among other functionally relevant structures.

Post-transcriptional modifications play a regulatory function on this channel as it does in other Kv channels (discussed previously) - there is a continual phosphorylation and dephosphorylation of Kvl.3 by endogenous kinases and phosphatases that modulate its functional properties(Holmes et al., 1996) and N-glycosylation promotes Kv1.3 cell surface expression(Zhu et al., 2012).

---

[1]523 amino acid protein in human, 528 aa protein in mouse, 525 in rat. ~55 kDa when translated in vitro, ~150 kDa could be the heterotetramer and ~ 23kDa band could be a truncate fragment of Kv1.3 truncate fragment.

Apart from the α-subunit, this channel is also often associated with the other subunits (Kvβ, hDlg, β1 integrin, KChaP). It can ensemble in heteromultimers with other Kv1 subunits too, but not with other Kv family proteins (Gutman et al., 2005), namely Kv1.1 and Kv1.5 (Gribkoff and Kaczmarek, 2008).Other from the traditional cytoplasmic NH_2 terminus (T1 domain), which is undoubtedly the tetramerization site, sites in the central core of Kv1.3 have been described facilitating intersubunit association(Tu et al., 1996).

As its correct functioning depends not only on the regulation of their biophysical properties but also on the fine-tuning of their subcellular localization and number of cell surface copies, a focus has been shed on the Kv channels cell trafficking. Kv1.3 proteins' folding and oligomerization studies (Kosolapov and Deutsch, 2003)have revealed pertinent information for axonal targeting of Kv channels (Gu et al., 2003)andfor uncovering a precise physiological role of Kvβ subunits in channel trafficking (beyond their ability to increase cell surface numbers) in neurons(Heusser and Schwappach, 2005).
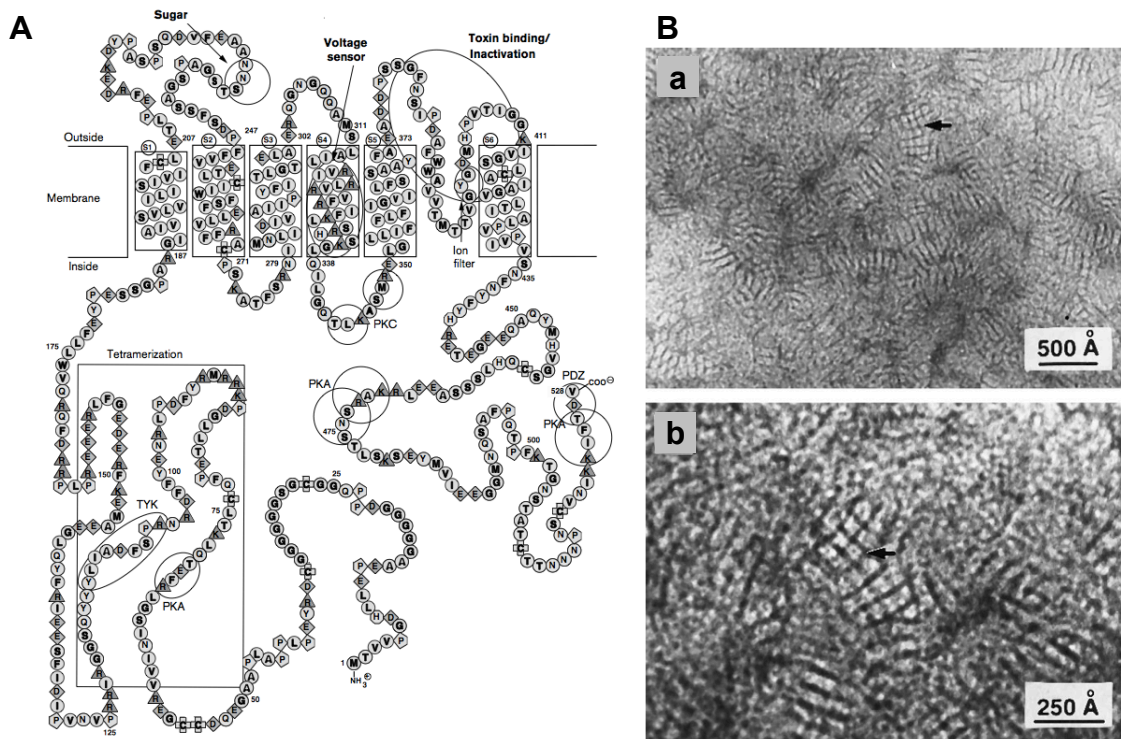
Figure 7: Kv1.3 structure **A** Diagram showing major functional domains within the amino acid sequence. The rectangle with 'tetramerization' shows the site of monomer–monomer interaction. The circles show sites that are functionally associated with various properties. Sx denote transmembrane segments. PKA, protein kinase A; TYK, tyrosine kinase. Adapted from (Cahalan and Chandy, 1997)**B** Kv1.3 tetramers visualized by electron microscopy. Small crystalline domains of Kv1.3 protein are stained with uranyl acetate at a low lipid-to-protein ratio. In **b** a higher magnification was used and well defined square-shaped objects appear to represent tetramers of Kv1.3.A centrally located stain-filled depression can be seen in many tetramers and is presumed to represent the location of the ion conduction pathway. Scale bars are shown for each image. Adapted from (Spencer et al., 1997).

1.6.3.2 Kv1.3's electrophysiological and pharmacological properties

Kv1.3 is a voltage-activated delayed rectifier potassium channel (Gutman et al., 2005). Most of its electrophysiological and pharmacological properties are now identified and they go as follows.

The channel ion selectivity is mostly for K^+ (1), but other ions are also able to flow through it, namely Rb^+ (0.77), $NH4^+$ (0.1), Cs^+ (0.02), Na^+ (<0.01) (Gutman et al., 2005). However, these are not as relevant physiologically as potassium is, for either being very scarce in the cellular environment, or for having a very low selectivity. The single channel conductance is 9,6 to 14pS (Coetzee et al., 1999).

Kv1.3 gating kinetics is diverse from other Kv channels – when a membrane depolarization occurs, a fast Kv1.3 current is activated within few milliseconds (τ_{activ}= 3ms-20ms, at 40mV; V_{on}= -50mV; $V_{1/2}$=-30mV; k= 5-7mV (Coetzee et al., 1999, Gutman et al., 2005)), but the inactivation is slower, taking up to some seconds ($\tau_{inactiv}$= 250-600ms; $V_{1/2}$=-44,7mV (Coetzee et al., 1999, Gutman et al., 2005)), which is an inactivation rate in between classically defined A-currents ($\tau_{inactiv}$< 100ms) and delayed rectifiers ($\tau_{inactiv}$>1s)(Brammar, 1998). Deactivation may occur with an intermediate kinetics (τ= 38ms, at -60mV(Coetzee et al., 1999)).

Pharmacologically, it does not have activators nor gating inhibitors, but it has various blockers 4-AP (195 μM; IC_{50}=0,2-1,5mM), TEA_O (10-50 mM), DTX (250 nM), CTX (0,5-2,6 nM), HgTx (86 pM with cumulative inactivation), TTA (10 mM), charybdotoxin (3 nM), naltrexone (1 nM), MgTx (110pM; IC_{50}=230 pM), kaliotoxin (650 pM), AgTx2 (200 pM), Pi1 (11 nM), Pi2 (50 pM), Pi3 (500nM), HsTx1 (12 pM), ShK (11pM), BgK (39pM), ShK-Dap22 (52 pM), quinine (14 μM), diltiazem (60 μM), verapamil (6 μM), CP339818 (150 nM), UK78282 (200nM), correolide (5μM), sulfamidbenzamidoindane (100nM), capsaicin (26 μM), resiniferatoxin (3 μM), nifedipine (5 μM) and H37 (23 μM)(Coetzee et al., 1999, Gutman et al., 2005).

In this study, margatoxin (MgTx) will be used. MgTx is a 39 amino acid peptide extracted from scorpion venom (*Centruroides margaritatus*)(Garcia-Calvo et al., 1993) that acts as a selective blocker of the Kv1.3 (IC_{50}~30-100pM in lymphocytes (Garcia-Calvo et al., 1993), IC_{50}~30 in *Xenopus* oocytes(Garcia-Calvo et al., 1993), ~230pM in mammalian cells (Coetzee et al., 1999) and ~125pM in CA1 pyramidal cells (Mondragão, 2010) - **Figure 8**) but also blocks Kv1.6 (IC_{50}~5 nM in *Xenopus* oocytes (Garcia-Calvo et al., 1993)).
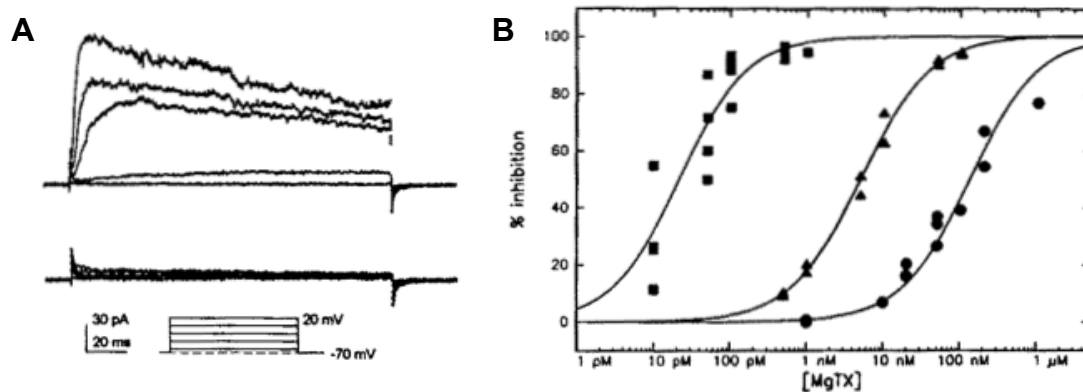
Figure 8: Kv1.3 current inhibition by margatoxin (MgTx). **A** Whole cell current recording from a human peripheral T-lymphocyte – upper traces obtained with control saline bath and lower ones obtained during addition of MgTx (1 nM) to the bath. Voltage protocol showed in inset – holding potential at -70mV and depolarizing voltage steps (-60 mV to +20 mV in 20 mV increments; 180ms duration, 45 ms apart) were given 45 s apart. **B** Dose inhibition curves for MgTx block of three cloned potassium channels expressed in Xenopus oocytes (■ Kv1.3). Eachcurvecontainsdatafrom2 to 4cells to which voltage pulses to 0 mV (100 ms duration) from a holding potential of -80 mV were applied, at the same time of the application of increasing concentrations of MgTx. Adapted from (Garcia-Calvo et al., 1993).

1.6.3.3 Kv1.3's localization and function

Regarding Kv1.3 localization, one can notice from **Table 4** that it expressed in various cell types (T and B lymphocytes, pre-B cells, platelets, fibroblasts, macrophages, osteoclasts, microglia, and oligodendrocytes) and tissues (lungs, islets, lymph node, retina, thymus, spleen, kidney and brain) (Gutman et al., 2005). Its role in the immunological synapse has been widely studied and is now accepted(Lewis and Cahalan, 1995, Cahalan and Chandy, 1997, Spencer et al., 1997, Wulff et al., 2003, Xu et al., 2004, Beeton et al., 2005, Rus et al., 2005, Beeton et al., 2006, Wulff and Pennington, 2007, Wang et al., 2012, Upadhyay et al., 2013). A n-type potassium current in lymphocytes exists in both humans and animal models (Gutman et al., 2005).

As to the brain, Kv1.3 is expressed in the inferior colliculus, olfactory bulb, pons/medulla, midbrain, superior colliculus, corpus striatum, cerebellum and hippocampus (Coetzee et al., 1999, Gutman et al., 2005).

In the olfactory bulb, its relevance is, above all, validated by Kv1.3 knock-down mice turning out to be "super-smellers" (1,000- to 10,000-fold lower threshold for detection of odors and an increased ability to discriminate between odorants), implying that Kv1.3 subunit has a role in signal transduction (being in a node where various signalling cascades converge), development, and in olfactory coding (Kv1.3 ion channel may regulate the kinetics and timing of neuronal responses to repetitive stimulation, and its absence changes the structure of OB glomeruli and modifies the capacity to detect odorant molecules), in addition to its role in the control of excitability (olfactory neurons from Kv1.3 null mice have modified action potentials and altered potassium currents that fail to be modulated by activators of receptor tyrosine

kinases, insulin and brain-derived neurotrophic factor) (Fadool et al., 2004). The physiological support for this effect has been further discussed in 1.4.2.3.1Insulin as a neuroprotector.

Kv1.3 has also been described in the hippocampus. There, Kv α-subunits have a complex subcellular distribution, differing between different types of neurons and within the neurons – subunits are targeted either to presynaptic or to postsynaptic domains, depending on neuronal cell type. So much so that distinct combinations of Kv1 α-subunits are co-localized in different neurons – and this has consequences at the membrane excitability level (Veh et al., 1995). In cultured cells, the transfection of Kv1.3 recombinant channel is translated into a faster repolarization of the action potential (due to addition outward K^+ current) and into the stabilization of tonic firing (in contrast to non-transfected cells or to cells treated with MgTx, which fire few action potentials, with decreasing amplitude before entering a stationary depolarized state, a result corroborated by computational simulation for the most part)(Kupper et al., 2002). This unique Kv1.3 effect is possibly due to the slow deactivation of Kv1.3 upon repolarization, which is behind a form of cellular short-term memory that is independent of any changes in the synaptic efficacy (Turrigiano et al., 1996).

All in all, and since the hippocampus is one of the most affected areas in Alzheimer disease, it is urgent to study Kv1.3 biophysically and biochemically.

Apart from neurons, other cells in the brain express Kv1.3, namely microglia. Both Kv1.3 and Kv1.5 proteins are present in cultured microglia, however their relative membrane expression and current changes with time in culture. This suggests that Kv1.5 is most important for "resting" cells and Kv1.3 is necessary for activated microglia functions, resembling its role in lymphocytes T.

Table 5 Kv1.3 expression. Tissue distribution, determined by Northern (RNA) analysis; brain regions are indicated as – absent, ± moderately present, + present. Adapted from (Coetzee et al., 1999). Hippocampal regions follow - absent; +, weak; ++, moderate; +++, strong and references are available. Adapted from (Kim et al., 2007). n.d. stands for not determined or not reported (grey) and IN for interneurons.

		Species				
		Rat	**Mousse**	**Gerbil**	**Seizure resistant gerbil**	**Seizure sensitive gerbils**
Tissue distribution	**Heart**	−	n.d.	n.d.	n.d.	n.d.
	Kidney	±	n.d.	n.d.	n.d.	n.d.
	Skeletal muscle	−	n.d.	n.d.	n.d.	n.d.
	Lung	+	n.d.	n.d.	n.d.	n.d.
	Brain	+	n.d.	n.d.	n.d.	n.d.
	Other	Retina, Spleen, Lymphocytes	n.d.	n.d.	n.d.	n.d.
Brain regions	**Cerebral cortex**	n.d.	n.d.	n.d.	n.d.	n.d.
	Dorsal thalamus	n.d.	n.d.	n.d.	n.d.	n.d.
	Cerebrum	+	n.d.	n.d.	n.d.	n.d.
	Olfactory bulb	+	n.d.	n.d.	n.d.	n.d.
	Hippocampus	+	n.d.	n.d.	n.d.	n.d.
Hippocampal regions	*Stratum pyramidale*	n.d.	+++ (Grosse et al., 2000)	− (Park et al., 2001)	+++ ++, IN (Kim et al., 2007)	+++, IN (Kim et al., 2007)
	Stratum radiatum	n.d.	+ (Grosse et al., 2000)	n.d.	− (Kim et al., 2007)	− (Kim et al., 2007)
	Stratum oriens	n.d.	− (Grosse et al., 2000)	n.d.	− (Kim et al., 2007)	− (Kim et al., 2007)
	Stratum lucidum	+++ (Veh et al., 1995)	− (Grosse et al., 2000)	n.d.	− (Kim et al., 2007)	− (Kim et al., 2007)
	Stratum lacunosum-moleculare	n.d.	n.d.	n.d.	− (Kim et al., 2007)	− (Kim et al., 2007)
	Granule cell layer	n.d.	+++ (Grosse et al., 2000)	− (Park et al., 2001)	− (Kim et al., 2007)	− (Kim et al., 2007)
	Molecular layer	n.d.	n.d.	− (Park et al., 2001)	− (Kim et al., 2007)	− (Kim et al., 2007)
	Hilar region	+++ (Veh et al., 1995)	n.d.	n.d.	+++, IN (Kim et al., 2007)	++ (Kim et al., 2007)
	Protein distribution	Somatodendritic	n.d.	n.d.	n.d.	n.d.
	Specification	CA3 pyramidal cells' dendrites and/or mossy fiber terminals Cerebellar purkinje cells Type I and II hypothalamic paraventricular nucleus cells	CA1-3 and dentate gyrus pyramidal and granule cells		(pre-seizure:)CA2–3 pyramidal cells, hilar PV+ neurons, and astrocytes within the stratum radiatum of the CA1 region (after seizure:) CA1–3 pyramidal neurons, PV neurons (CA2–3), astrocytes	
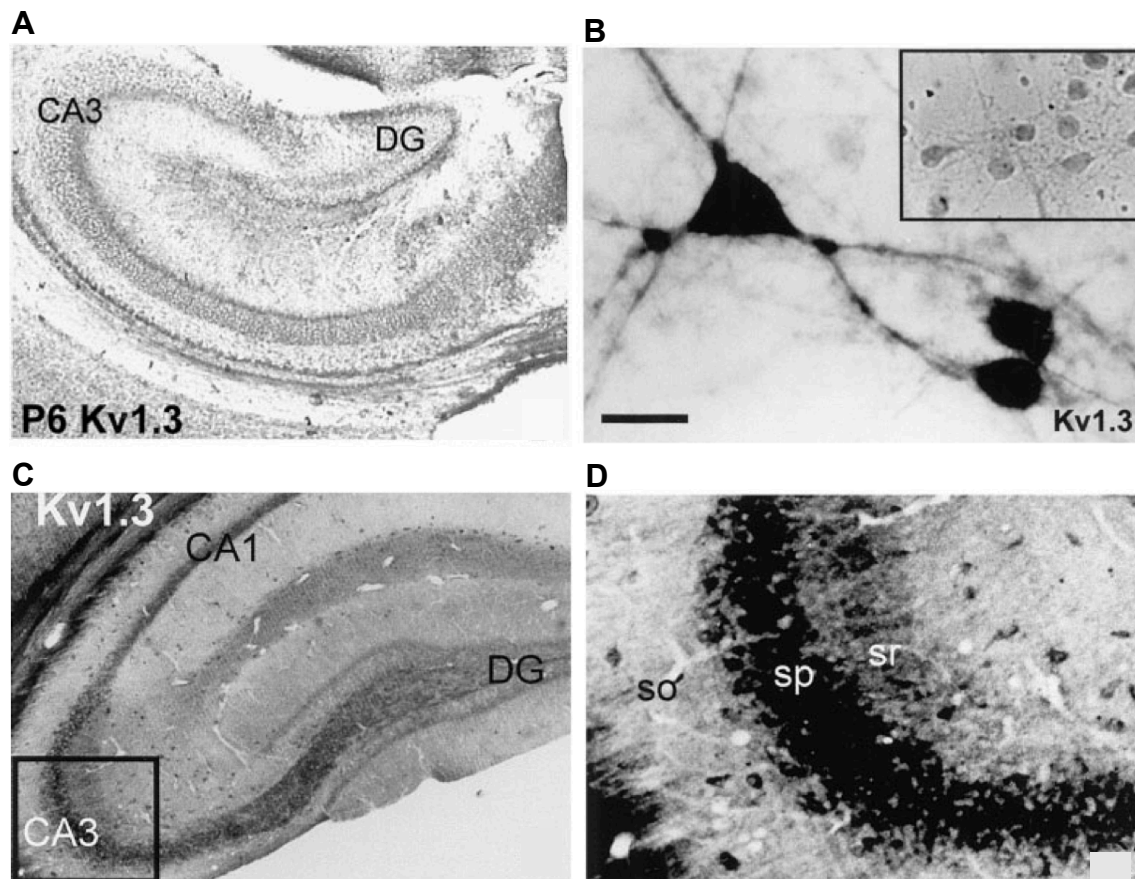
Figure 9: Kv1.3 expression in mousse hippocampus and hippocampal primary culture. Coronal slices of adult mousse (50 μm sections, panel **A**) and 6 days mice pups (70 μm sections, panel **C**) hippocampus reveal Kv1.3 staining increasing with age. **D** is a detail of CA3 region (marked in panel C) where it is clear that Kv1.3 occurs in high amounts in stratum pyramidale (*sp*), whereas lesser amounts are present in stratum radiatum (*sr*), and almost no channel protein is found in stratum oriens (*so*). **B** Expression of Kv1.3 in hippocampal pyramidal neurons (cultivated for 18 days) reveals a somatodendritic distribution. Scale bars, 20 μm. Inset shows neuronal cultures at 6 days analysed by phase contrast. Adapted from (Grosse et al., 2000).

1.7 EXPERIMENTAL MODEL

1.7.1 Voltage-gated potassium currents in hippocampal CA1 pyramidal cells

To the study of voltage-activated events, space clamp is mandatory. Here, it is compulsory the use of isolated neurons, rather than their use within the brain slice preparation. Diverse voltage-dependent K^+ currents have been identified in hippocampal CA1 cells by whole-cell voltage clamp. Delayed rectifier current (I_{DR}) and A-type current (I_A) take part in the total current of these cells and perform major functions in excitability control (Wong and Traub, 1983). I_{DR} is responsible for the action potential's repolarization and I_A for the stabilization of the membrane potential in-between action potentials (Alshuaib et al., 2001). To discriminate each current various strategies can be applied, namely based upon different voltage dependence or pharmacological agents.

The effect of a hyperpolarization before a depolarizing pulse is significant due to the recruitment of A-currents. These have short activation times and a fast inactivation profiles.

1.8 FRAMEWORK OF THE PROJECT

This project emerged from open questions arising from recent results obtained by our group.

It was previously shown that the feeding-cycle affected insulin-mediated regulation of neuronal activity and excitability, in rat hippocampal neurons. In fact, insulin reduces the activity of slow-voltage-activated K^+ channels (Kv1.3 in hippocampal neurons and ERG in N1E-115 neuroblastoma) in neurons from fed but not fasted animals (voltage-clamp recordings, **Figure 10A** (Lima et al., 2008)). Consequentially, it increases neuroexcitability by reducing the interspike interval in neurons from fed but not fasted animals, as shown by current-clamp recordings (**Figure 10B**). Moreover, this change is correlated with a marked decrease in the protein expression of the neural insulin receptor (InsR) in fasted animals as well as in obese and diabetic rat models (Zucker) but not in fed rats (**Figure 10C**).

Since the assumption that the brain being hermetic to physiological and metabolic oscillations was challenged, it was seen as pivotal to identify what is changing and consequently to characterize the implications for neuronal activity.

Kv1.3 was a suitable candidate to be differentially expressed along the feeding cycle, as a tight association with InsR had been shown in the olfactory bulb and Kv1.3 has been implicated in insulin resistance (Xu et al., 2004).

Besides, the dissociated study of the metabolic effects in the two hippocampal portions (dorsal and ventral hippocampus) filled some gaps in the explanation of evidences. In this regard, recent results had shown surprising evidences of nonuniformity in CA1 pyramidal neurons intrinsic excitability (ventral cells were more excitable than dorsal cells) (Dougherty et al., 2012). Therefore, it was reasonable to question if Kv1.3 was evenly expressed and functionally intact throughout the dorsal-ventral axis of the hippocampus.
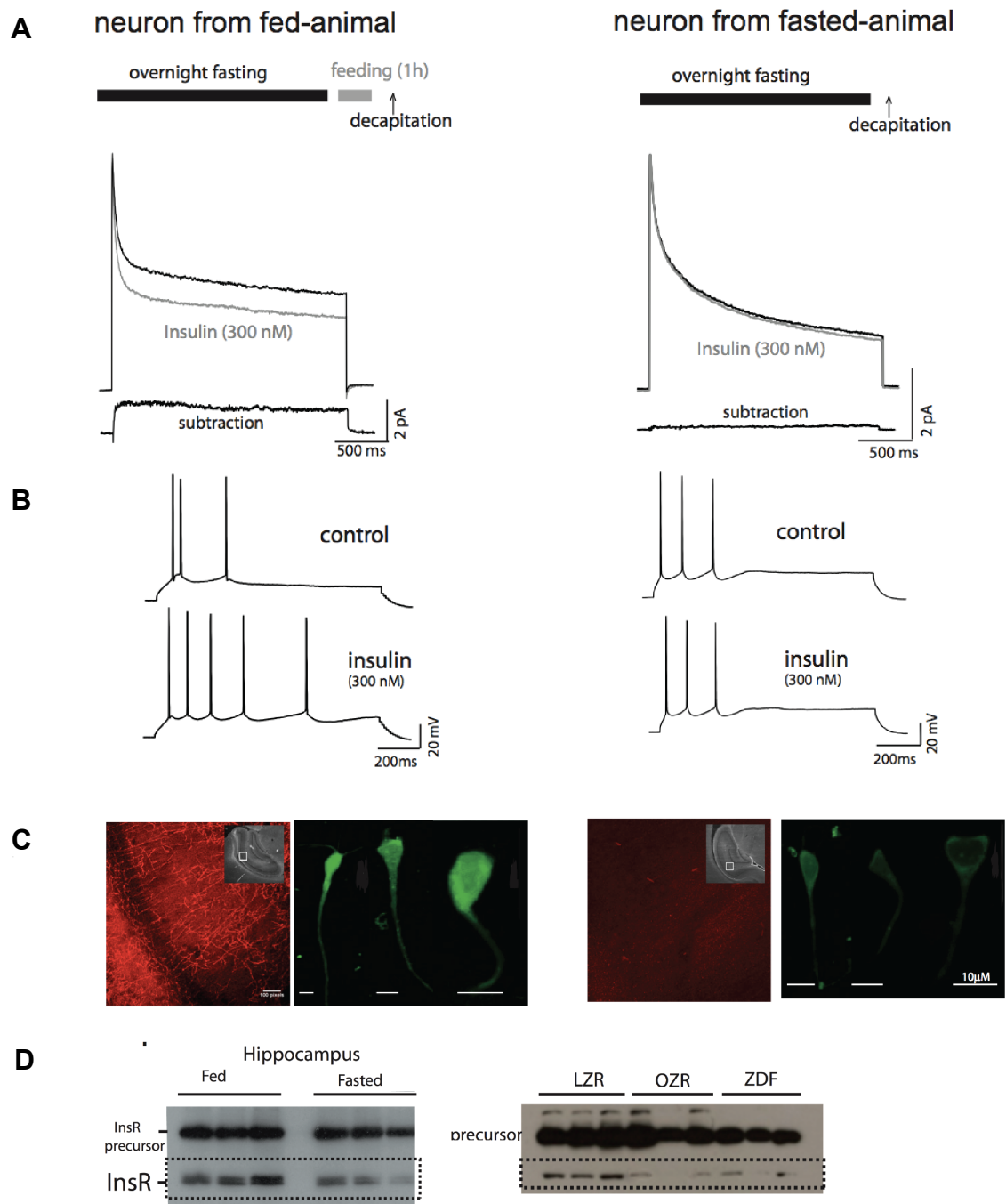
Figure 10: Framework of the project. (**A**) Whole-cell voltage-clamp recordings from CA1 pyramidal neurons from *wistar* rats (P21-29) which were subjected to overnight fasting and subsequently fed for 1 hour (left traces) or not fed (right traces). Currents were elicited by a depolarisation pulse to +40mV with a pre-pulse to -120mV.In neurons obtained from fed animals, application of 300 nM insulin decreases I_{slow} only, whereas in fasting animals that current inhibition did not occur. (**B**) Current -clamp recordings from pyramidal neurons from the CA1 region of the hippocampus within brain slices sampled from the same conditioned rats. Train of 3 action potentials elicited by a 1 sec current injection showing typical adaptation. Application of 300 nM insulin increases the number of spikes in preparations obtained from fed animals (left side) but not those from fasted animals (right side). (**C**) Immunohistochemistry (InsR marked in red) and immunocytochemistry (InsR marked in green) showed a higher expression of InsR in fed rats (left images) than in fasted ones (right images). (**D**) Western blot analysis of protein extracts from hippocampal preparations from fed and fasted rats illustrating the expression of proteins detected by the antibody to rat insulin receptor (InsR) and its precursor. Expression levels of InsR but not the precursor are markedly higher in hippocampal preparations from rats that were fed. Western blot analysis of protein extracts from whole-brain preparations of diabetic-model rats (LZR- control, Lean Zucker Rats; OZR-

Obese Zucker rats; ZDF- Zucker diabetic Fatty) illustrating the expression of proteins detected by the antibody to rat Insulin receptor (InsR) and its precursor. Expression levels of InsR but not the precursor are markedly decreased in the brains of the diabetic models in relation to control. Margatoxin (MgTx) sensitive current's time constants

2 GOALS

This project is focused on Kv1.3 channel in CA1 pyramidal cells from wistar rat hippocampus. It aims to investigate:

☐ If and how **Kv1.3 mediated current and KV1.3 expression patterns are affected by the feeding cycle**.

☐ If and how the Kv1.3 mediated current and the Kv1.3 expression patterns vary in the **dorsal-ventral axis of the hippocampus.**

Hence, two conditions have to be studied simultaneously – the metabolic condition (feeding cycle) and the anatomical condition (dorsal-ventral axis of the hippocampus CA1 region). In order to do this, differences between these groups will be evaluated by two main approaches.

1. To study K^+ currents, namely the one mediated by Kv1.3, whole-cell voltage-clamp was used. Here the goals were:

   - Assess possible differences in terms of the biophysical properties, particularly K^+ currents voltage dependence (of activation) and current density.

   - Assess possible differences in the pharmacological properties, particularly the margatoxin-sensitive current (margatoxin is a selective Kv1.3 inhibitor).

2. To study the Kv1.3 protein expression. Here, the goals were:

   - Qualitatively and semi-quantitatively evaluate Kv1.3 protein expression through immunohistochemistry.

   - Quantitatively evaluate Kv1.3 protein expression through western blot analysis.

This page was intentionally left blank.

3 MATERIALS & METHODS

3.1 ANIMALS

Throughout this project *wistar* rats were used to address all trails. The animals were mostly female (unless stated otherwise) and their ages were comprehended between 21 and 38 days (P_{21-38}). Two metabolic states have been studied – *fasting animals*, who did not have access to food for at least 12h preceding sacrifice, and *fed animals*, who ate for 1 hour preceding sacrifice, previous to that period being either on fasting (12 hour fasting) or fed conditions (food *ad libitum*). All animals had water available *ad libitum* and light/darkness cycles were kept at all times. Brain preparations were obtained following the recommendations of the European commission to be used with the Directive 86/609/EEC, with procedures approved by the Ethical Committee of the *Faculdade de Ciências Médicas da Universidade Nova de Lisboa*. 52 animals were used.

3.2 ELECTROPHYSIOLOGY

The effects of the metabolic state (fed or fasting) upon cellular excitability were investigated in dorsal and ventral CA1 pyramidal neurons. Particularly, our focus was upon potassium currents.

3.2.1 Animals

The day before sacrifice, P21-35 rats were moved from the animal house to a recovery room, where they fasted overnight, with water available *ad libitum*. Late morning, those, which will hereinafter be named "fed animals", received a portion (RMI (E) Expanded, 801002 SDS), whereas the ones named "fasting animals" did not receive it. Fed animals ate for 1 hour. In total, twenty-nine animals under the condition "fed" and seven animals under the condition "fasting" were used.

3.2.2 Hippocampal CA1 pyramidal neurons preparation

Dorsal and ventral hippocampal pyramidal cells from the mid-third CA1 region of P21-35 fasting and fed *wistar* rats were isolated with an adapted protocol described before (Costa et al., 1994).

After pre-conditioning (12h fating or 12h fasting + 1h feeding or 12h food *ad libitum* + 1h feeding), each animal would be sacrificed by cervical dislocation, immediately decapitated and rapidly the brain would be removed from the skull and placed in dissection solution (**Table**

6) at 4°C. After 30 seconds to lower the brain's temperature, a precise cut was performed along the longitudinal fissure, separating the two hemispheres. Both hippocampi were then cautiously removed, complying with the dorsal-ventral orientation.

One mm coronal slices were obtained and dorsal and ventral ones were selected to subsequent procedures (selection criteria was strictly based upon the anatomical features, arising from the oriented hippocampus removal). The mid-third CA1 region was then detached. These sub-slices of the CA1 region were incubated at 32-36 °C for 30-50 min (depending on the rat's age) in an oxygen saturated dissociation solution (**Table 6**), to which trypsin (0.6 mg/mL) had been added. This enabled an enzymatic dissociation of the sub-slices relevant for following procedures. Sub-slices were transferred to an oxygen saturated enzyme-free dissociation solution (same as before) after a brief wash with this solution and kept at room temperature. This preparation remained viable for about 5–6 h. Immediately before usage, a single sub-slice were selected and cells were mechanically dissociated by gentle trituration of the sub-slices using fire polished Pasteur pipettes (1.5–2 mm bore). Petri dishes were used as recording chambers since isolated cells would be planted in them with an external bathing solution (**Table 6**).

Presented results reflect a total of 55 cells, from 19 animals (n for each experiment/study groups are stated in results).

3.2.3 Recording *Setup and perfusion*

Membrane currents were recorded in *whole-cell voltage-clamp configuration* in uncoupled differentiated pyramidal cells, at room temperature (20-24°C[2]), using an electrometer (*Axon Instruments*, Axopatch 200B), an analogue/digital signal converter (*Axon Instruments*, DigiData 1200) and Clampex 6.0.3 (*Axon Instruments*) software.

The microelectrodes (1.2 - 3.0MΩ) used were produced by a horizontal pipette stretcher (Science Products GmbH, GB150T-8P) from borosilicate glass tubes (Science Products GMBH) were filled with internal solution (**Table 6**). External bathing solution (**Table 6**) was constantly superfused, by gravity, at a 2–3mL/min rate.

The estimated junction potential (Junction potential tool in Clampex 10.3.02, former JPCalc) for the present pairs of solutions was 9.2 mV. Currents were measured with capacitance compensation and series resistance compensation (80-95%), filtered at 10 kHz, sampled at 5 kHz, using a Digidata 1200 AC converter. Still, current amplitude and seal conditions were monitored throughout all experiments.

---

[2] Temperature was maintained thoroughly, as channel gating involves conformational changes, whose rates are temperature-sensitive HILLE, B. 1992. *Ion channels of excitable membranes*.

Previous studies have shown that tetrodozin (TTX; 30nM) superfusion had no difference in studied parameters (Mondragão, 2010) as the currents of interest had much slower kinetics than the TTX Na+ sensitive current. Hence, TTX was not added to the external bathing solution.

3.2.4 Voltage protocols

Experimental conditions enabled us to evoke K^+ currents by application of depolarizing pulses through the whole-cell membrane with minimal disruption of other ions equilibrium (intramembranar and extramembranar solution compositions, as a result of ionic substitution experiments performed in our group (Nascimento, 2009) and voltage protocol particularities (Costa et al., 1994)).

Time was allowed for the stabilization of the recording, before the beginning of the actual experiments could take place (parameters monitored: run-down rate and seal quality – series resistance and holding current, typically at -60mV). The effects of superfusing Margatoxin (MgTx) were taken after current stabilization, customarily > 5 min after addition; this time period took into consideration the perfusing rate of the system and the time course of the MgTx effect.

Currents were elicited by the following voltage protocols (represented in **Figure 14** the inset of figures with current traces), applied in *whole-cell voltage-clamp configuration* to dorsal and ventral cells from either fasting or fed animals:

  i. **To evaluate potassium currents and MgTx (selective Kv1.3 inhibitor) effect:** currents were recorded every 30 or 60s with a set of two depolarizing command pulses to 0 and +40 mV lasting 1.3-2.6s, from a holding potential of -60 mV; only currents evoked by the depolarization to +40 mV were used consequentially (see figure insets). The command pulses were preceded by a hyperpolarizing prepulse (-110mV, 120-240ms) in order to remove channels' inactivation (particularly those responsible for the current's fast-component, formerly know as A-D type currents).

 ii. **To characterize the activation profile:** From a holding potential of -60mV, currents were evoked by a set of 14 command pulses from -80 to +50mV, in 10mV increments, lasting 1040 ms and 30000ms (30s) intervals, so that the total protocol lasted 19 5000ms (3min15s). Each pulse was preceded by a hyperpolarizing pre-pulse (-120mV, 120ms) for the same purposes described in **i**.

iii. **To evaluate the *leak* current:** previous to the pre-pulse described in **ii,** a set of "pre-pre-pulses" was used, from -65 to -52mV in 2mV steps, lasting 120ms. These pulses aimed to assess the leak current present in the trails. The range of applied voltages did not activate any channel evoked current. Data shown in **Figure 16** and **Figure 17** are corrected to the subsequently calculated leak current value.

Table 6: Solutions used in 3.2.2Hippocampal CA1 pyramidal neurons preparation and 3.2.3Recording *Setup and perfusion*

Solutions	Constitution
Dissection solution	NaCl 124mM; KCl 3,5mM; NaH_2PO_4 1,25 mM; $CaCl_2$ 2mM; $MgSO_4$ 2mM; Glucose 10mM and $NaHCO_3$ 24 mM
Dissociation solution	NaCl 120mM; KCl 5mM; $CaCl_2$ 1mM; $MgCl_2$ 1mM; 1,4-Piperazinediethanesulfonic acid (PIPES) 20mM;D(+)-Glucose 25mM; adjusted to pH 7,4 with 1 mM NaOH
Bathing external solution	NaCl 135mM; KCl 5.4mM; $CaCl_2$ 2mM; $MgCl_2$ 2mM; HEPES 10mM; D(+)-glucose 25mM; pH 7.4 titrated with NaOH; 310mOsm
Internal solution	KF 140mM; $MgCl_2$ 1mM; $Na_{1/2}$-HEPES 10mM; EGTA 10mM; $CaCl_2$ 1mM; Na_2ATP 2mM; Na-GTP 0.4mM; pH 7.2–7.3 titrated with KOH; calculated free $[Ca^{2+}]$ 1⁄4 60 nm (Webmaxclite v1.15, MaxChelator); 300mOsm

3.2.5 Data analysis and statistics

For exponential fitting, current measurements and current subtraction Clampfit Clampfit 10.3.0.2 (*Axon Instruments*) was used; for plotting currents against time and voltage Microsoft Excel 14.3.8 (Mac 2011) was used; for Boltzmann fitting OriginPro 5.0 (*OriginLab Corporation*) was used, statistical analysis was performed with GraphPad Prism 6.01(Windows, *GraphPad Software*, San Diego California USA, www.graphpad.com) and Adobe Illustrator 15.0.2 (CS5) was used to compose final images and graphics.

3.2.5.1 Exponential fitting

For each experiment, one or more exponential functions were fitted to the data recorded (K^+ current repolarizing phase), according to the following equation:

$$i_t = \sum_{i=1}^{m} a_i e^{-t/\tau_i} + c$$

where τ_i and a_i are, respectively, the time constant and the exponential amplitude coefficient, c is a constant (derived from the constant component and the leak current) and m is the number of exponential functions that are necessary to describe the K^+ current downfall.

The most common case what the one where m=2, meaning that the current decay (K^+ current repolarizing phase) was best fit by a sum of two exponentials; therefore having two components, a fast one (I_{fast}) and a slow one (I_{slow}) (**Figure 11**).
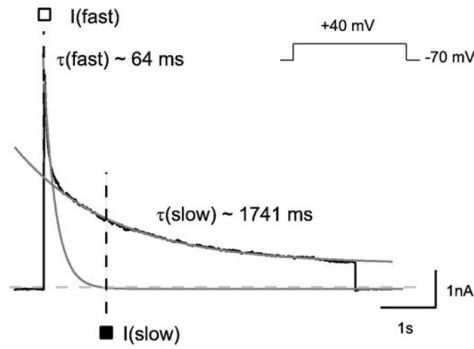
Figure 11:K$^+$ (voltage-dependent) current components evoked in CA1 pyramidal neurons from *wistar* rat hippocampus (voltage protocol as shown in the inset: depolarizing pulse to +40 mV, 5.6 s in duration, from holding potential of −70 mV, preceded by pre-pulse to − 120 mV, 200 ms in duration). Grey lines represent two exponential functions which describe the current record (black line). The peak current was used as a measurement of I$_{fast}$; measure of I$_{slow}$ was taken as the amplitude at time 5*I$_{fast}$, after the start of command pulse (dashed lines). Adapted from(Vicente et al., 2010).

I$_{fast}$ and I$_{slow}$ were then measured as follows for each current sweep. The peak current was used as a measurement of I$_{fast}$. I$_{slow}$'s amplitude was measured at t > 5xτ_{fast}(**Figure 11**) (time-courses analysis) or by fitting an exponential function fitted to the 5xτ_{fast}< t < end-of-pulse current and extrapolating it to the same time as I$_{fast}$ had been measured (peak), I$_{slow}$ assuming the extrapolated current value at that time (activation profiles analysis). Either way it was assured that there was no I$_{fast}$ contamination when measuring I$_{slow}$. I$_{ss}$ was measured at the end of the command pulse, where there was a stabilization of the elicited current. This process is illustrated for activation profile analysis in **Figure 15**.

The control of leak current was done by either measuring it at the beginning of the current record (before the prepulse) and plotting it against time alongside the more relevant I$_{fast}$ and I$_{slow}$, to check for major changes that might be influencing the results (time-courses analysis); or by measuring the current values obtained during the corresponding 'leak-current voltage protocol' (3.2.4 Voltage protocols iii). The calculated value was subsequently subtracted from the current parameters recorded with the command pulses (I$_{fast}$, I$_{slow}$ and I$_{ss}$) (by extrapolating a linear regression fitted to the I$_{leak}$ data (activation profiles analysis)).

Each current component's kinetics was evaluated by the time constant of the fitted exponential function. Representative traces were selected for the illustrations according to the criteria of closest τ_{fast} and τ_{slow} to the mean ones for each condition, and were normalized to the inner maximum.

3.2.5.2 Voltage dependence of activation – "Activation profiles"

Activation profiles are a representation of current as a function of voltage, which have proper features when dealing with voltage-gated channels. Therefore, it can be plotted directly by attributing the elicited current values (measured as described in 3.2.5.1Exponential fitting) to the y-axis and the respective command pulse to the x-axis. Activation profiles were plotted in the form of ionic conductance as a function of voltage.

Hence, conductance was calculated from the I_{fast}, I_{slow} and I_{ss} values (corrected to I_{leak}), according to the following equation:

$$G = I/(V_m - E_K)$$

where V_m is standing for pulse voltage and E_K is the K^+ equilibrium potential, calculated by Nernst equation (E_K=-82mV). The conductance results would then be normalized to their maximum (G/G_{max}) and the voltage-dependency of the current (G/G_{max} *vs.* V) would be described by the following Boltzmann equation:

$$G/G_{máx} = \frac{A_1 - A_2}{1 + e^{(V_{1/2} - V_m)/V_s}} + A_2$$

in which V_m is the pulse potential, $V_{1/2}$ is the potential necessary to activate half the channel population, V_S is the slope constant (which reflects the equivalent number of charges on the channel that move in the membrane voltage field to cause the channel opening (Standen et al., 1987)) and A_1 and A_2 are the curve's amplitude minimum and maximum, respectively.

3.2.5.3 Current density

Current density is a measure of the "amount" of current running through a normalized membrane at a given time.

The cell membrane acts as both a resistance and capacitor. The capacitance of a typical patch of membrane stays relatively unchanged by the molecules that form the membrane so it is often regarded as constant (Cm=1$\mu F/cm^2$) and hence proportional to the surface area of the cell (the larger the area, the larger the capacitance) (Sherman-Gold, 1993). Therefore, it is set that capacitance is a fair measure of membrane area.

Values of whole-cell capacitance were directly taken from the amplifier after current transients due to whole-cell capacitance were analogically compensated (Sherman-Gold, 1993).

Thus, the whole-cell current density was calculated by

$$J = \frac{I}{C}$$

where J is conductance (pA/pF), I is current (pA; elicited current from a +40mV depolarizing pulse) and C is capacitance (pF).

3.2.5.4 Margatoxin effect

Margatoxin (MgTx) is a selective Kv1.3 channel inhibitor, used in this project to isolate the Kv1.3 mediated current, which is insulin-modulated.

I_{fast} and I_{slow} were measured as described before (3.2.5.1 Exponential fitting) and plotted against time, creating 'time-course' graphics, where MgTx's time span of superfusion was noted. For the quantification of the effects of MgTx, current rundown was taken into account by analysing the behaviour of current throughout the experimental period. A concentration of 3nM

was used taking into consideration previous studies (Mondragão, 2010), as it would reach almost maximal reduction while still being specific.

Representative currents presented in **Figure 18** were chosen for the criteria: inhibition percentage most similar to the mean one, for each study group.

3.2.5.5 Statistics

Statistical analysis was performed with GraphPad Prism (version 6.01 or Windows, GraphPad Software, San Diego California USA, www.graphpad.com). Mean integrated densities were compared with Mann-Whitney test (nonparametric test that compares the distributions of two unmatched groups), with the following levels of significance: not-significant (ns, $p > 0.05$), * $P \leq 0.05$, ** $p \leq 0.01$, *** $p \leq 0.001$ and **** $p \leq 0.0001$. Presented results are described as mean±S.E.M (standard error of the mean) for n samples.

3.3 IMUNOHISTOCHEMISTRY

The aim of this protocol was to assess the presence of Kv1.3 channel in rats' dorsal and ventral hippocampus under two conditions – fasting and fed. As previous results from the group show (Lima P.A. (1), 2012), the insulin receptor's expression varies under these two conditions in the CA1 pyramidal cells, thus it was used as a positive control.

3.3.1 Animals

Animals were anaesthetized with pentobarbital (0,1mL/g; intraperitoneal injection of *Pentothal* or *Eutasil*). In total, four animals under the condition "fed" and four animals under the condition "fasting" were used. Gender, age and time of sacrifice (relative to light/dark cycle) variables were evenly distributed between groups, ensuring a case-control type of study.

3.3.2 Fixation

After assuring general anaesthesia, the rats were laid on their back and the chest was to be exposed, allowing us to determine the position of the sternum. The chest was opened to make the thoracic cavity fully accessible throughout the consequent procedure.

The pericardium was then eliminated and a needle was inserted in the left ventricle at the same time that the perfusion was turned on and a hole was done in the right atrium. By then, the perfusion system was filled with saline solution (**Table 7**; at 4°C) and ran at a steady rate, enabling the drainage of the animal's blood through its own circulatory circuit onto the thoracic cavity, where it was collected to an appropriate container.

By the time the system was considered clean (about 200 mL of solution were necessary to achieve a transparent drained fluid), the perfused solution was swapped to PFA 4% (**Table 7**; at 4°C) until the animal was rigid (approximately 500 mL of solution were necessary).

After decapitation, the base of the spinal cord was removed with a scalpel and tweezers were used to open the skull, exposing the brain. Carefully, the brain meninges were then removed and the brain was taken out. Post-fixation with the same PFA solution was performed overnight at 4°C (in a 50 mL falcon). The next day, the brains were stored in a saccharose 15% solution. was and kept at 4°C so that the brain would move down in the containing 'falcon tube' towards its base as it soaked in the solution (the process lasted for about 24h). When reach the bottom, the brain was transferred to a saccharose 30% solution at 4°C, and the method was repeated until the brain reached the bottom of the new container (again, the process lasted for about 24h). Once it did, the brain was impregnated with a gelatinous solution (**Table 7**) for 1h at 37°C.

Each brain was then placed on an already solid layer of the same gelatinous solution, in an appropriate container. The brain's heat (37°C) allowed it to fit into the mentioned layer and posterior maintenance of the brain's position. A sufficient amount of gelatinous solution to cover the brains was then placed over them. The solution cooled of and solidified at room temperature (20 - 22°C) and a new, thin, layer was then placed over it, ensuring the total coverage of the brains with gelatine. This layer solidified at room temperature (20 - 22°C) before the container was stored in the fridge (4°C) overnight.

Blocks of gelatine were then cut, so that each brain would be in the best possible position to the latter cut in slices. The blocks were identified and frozen using isopentane at -70°C (submerged in liquid nitrogen) and stored at 80°C.

3.3.3 Antibodies and detection

30μm thick hippocampal slices (from both the dorsal and ventral hippocampus) were obtained, according to the coronal (n=3 fasting animals, n=3 fed animals; male and female subjects for each condition) and sagittal planes (n=1 fasting animals, n=1 fed animals; both male), and laid on blades. The cryostat Leica CM-3050 was used to perform this. Slices were laid out so that a slice from a "fasting animal" and a slice from a "fed animal" would be in the same blade. The slices were then stored at -20°C until the procedure was resumed.

Afterwards, they were washed with PBS, at 37°C for 10 minutes, in order to remove the gelatine; the quenching was done using glycine freshly made (20 minutes at RT; **Table 7**).

Hereafter, the permeabilization and blocking were performed for 1h at RT (or 24h at 4°C) at using 400-500 μL of blocking solution per slide (**Table 7**) (in a humidity controlled chamber). The slices were incubated for 48h at 4°C with a primary antiserum dilution (primary antibodies: pAb-anti-Kv1.3 (**Table 8**): incubating solution 1:50*or* pAb-anti-CD220 (directed

against the β chain of the insulin receptor; **Table 8**): incubating solution 1:500; 70-75 µL per slide), in a humidity controlled environment.

After this incubation, the slices were washed with PBS 1X (**Table 7**) four (or three) times, each lasting 15 minutes at RT.A new incubation was then performed, with the secondary antiserum dilution (secondary antibody for Kv1.3 slices: Ab-anti-rabbit – Alexa Fluor 488 (**Table 8**): incubation solution 1:500*or* secondary antibody for CD220 slices: Ab-anti-rabbit – Alexa Fluor 546 (**Table 8**): incubation solution, 1:500; 400-500 µL per slide) for 24hat 4°C (+ 1h at RT in the case of Kv1.3 marked slices, or 1h30 at RT in both cases), in a humidity controlled environment. Before marking the cell's nucleus, a wash was carried out four (or three) times using PBS, for 15 minutes each at RT.

Afterwards, the slices were incubated for 10 minutes at room temperature (20-22°) with the fluorescent marker Hoechst (6µg/mL in PBS; 100µL per slice), in a humidity-controlled chamber. Slices were washed for the last time for 15 min with PBS and then mounted using Moviol (n Poly(vinyl alcohol), Hoechst, Germany; 10 µL per slice) or Dako (Dako Fluorescence Mounting Medium containing an anti-fading agent and 0.015 mol/L sodium azide, Dako, Denmark; 10 µL per slice).

The preview of the slices was done using a confocal point-scanning microscope (Zeiss LSM 710; Carl Zeiss MicroImaging), with 10X, 20X and oil-immersing 40X lenses. Obtained images are average of two confocal scannings and not stacks.

Apart from the mentioned slices, the treatment was also performed on negative controls (same tissue, but without adding the primary antibody) and positive controls.
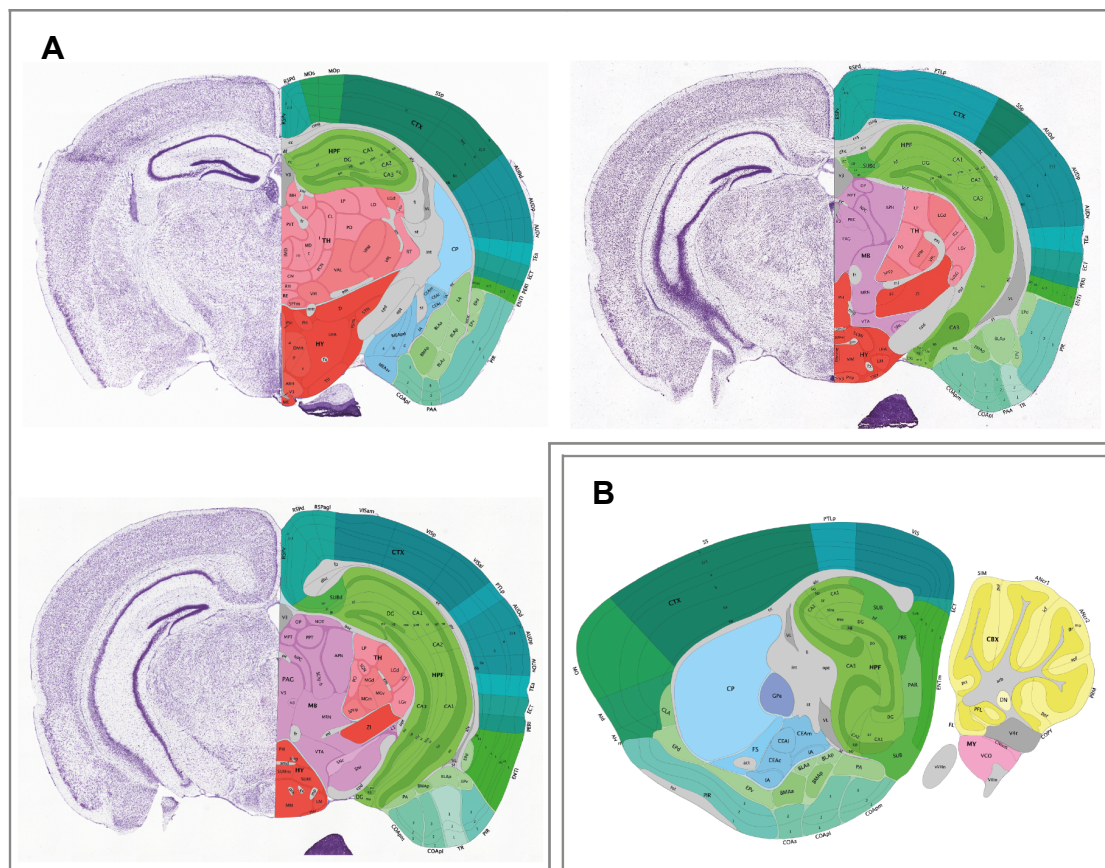
Figure 12: Examples of coronal (**A**) and sagittal (**B**) slices from P56 mouse brain, used as references when acquiring the experimental slices to this project. Adapted from Allen Mouse Brain Atlas(Lein et al., 2006) (Website: ©2012 Allen Institute for Brain Science. Allen Human Brain Atlas [Internet]. Available from: human.brain-map.org)

Table 7: Solutions used in 3.3Imunohistochemistry

Solutions	Constitution
PBS 10X	PBS 10X pH 7,4 with phosphate 0,2M and NaCl 1,5M
PBS 1X	PBS 1X pH 7,4 with phosphate 0,2M and NaCl 1,5M
Saline solution	NaCl 0,15 M
PFA 4%	Paraformaldehyde 4% in PBS 1X
Gelatinous solution	Gelatine 7,5% and saccharose 15% in PBS 1X
Glycine	Glycine 0,1M in PBS 1X (to be used freshly made)
Blocking solution	FBS 10% (v/v) and Triton X-100 0,3% (w/v) in PBS 1X
Incubating solution	FBS 4% (v/v) and Triton X-100 0,02% (w/v) in PBS 1X

Table 8: Antibodies used in 3.3Imunohistochemistry

Antibodies	Constitution
pAb-anti-Kv1.3	Rabbit polyclonal antibody anti-Kv1.3 (APC-002, Alomone Labs, Jerusalem, Israel)
Ab-anti-rabbit – Alexa Fluor 488	Secondary goat antibody anti-rabbit, conjugated with Alexa Fluor 488, 2 mg/ml (Invitrogen, Grand Island, NY, USA)
pAb-anti-CD220	Rabbit polyclonal antibody anti-CD220 (611277, BD, Le pont de Claix, France)
Ab-anti-rabbit – Alexa Fluor 546	Secondary goat antibody anti-rabbit, conjugated with Alexa Fluor 568, 2 mg/ml (Invitrogen, Grand Island, NY, USA)

3.3.4 Data analysis and statistics

A qualitative analysis was carried out by direct observation of the obtained images. This gave important information about the subcellular localization of the protein and allowed further conclusions regarding its distribution in the hippocampus.

Semi-quantitative image analysis was performed using ImageJ (National Institutes of Health, Bethesda, MD)(Schneider et al., 2012). Images were segmented, using the threshold tool in the software, so that fluorescence in the pyramidal cell layer would be isolated from the background (threshold min 60-221, threshold max 255). To further narrow down possible false positives, regions of interest (ROI's) were selected in the pyramidal cell layer (3 per image). Integrated density (Area*Mean grey density) was measured limited to threshold. Minimum, maximum, mean, modal and median and area fraction were also accessed (the ROI area was the same in almost every caption). This process is represented in **Figure 13**. Integrated density was then normalized to the maximum ROI integrated density, for each set of images that had been captured under the same conditions at the confocal microscopy (paired images). Mean integrated densities were then established for dorsal/ventral portions and fasting/fed conditions and plotted using Microsoft Excel (Mac 2011, v.14.3.8).

Illustrative images were sometimes refined using processing tools of ImageJ, for illustrative purposes only (parameter stated for each image in 4.2.2 Kv1.3 expression in CA1 hippocampal region). Analysis was performed onto raw images.

Statistical analysis was performed with GraphPad Prism (version 6.01 or Windows, GraphPad Software, San Diego California USA, www.graphpad.com). Mean integrated densities were compared with Mann-Whitney test (nonparametric test that compares the distributions of two unmatched groups), with the following levels of significance: not-significant (ns, $p > 0.05$), * $P \leq 0.05$, ** $p \leq 0.01$, *** $p \leq 0.001$ and **** $p \leq 0.0001$. Presented results are described as mean±S.E.M (standard error of the mean) for n samples.

Adobe Illustrator (CS5, v.15.0.2) was used to compose final images and graphics, with great care for not distorting them.
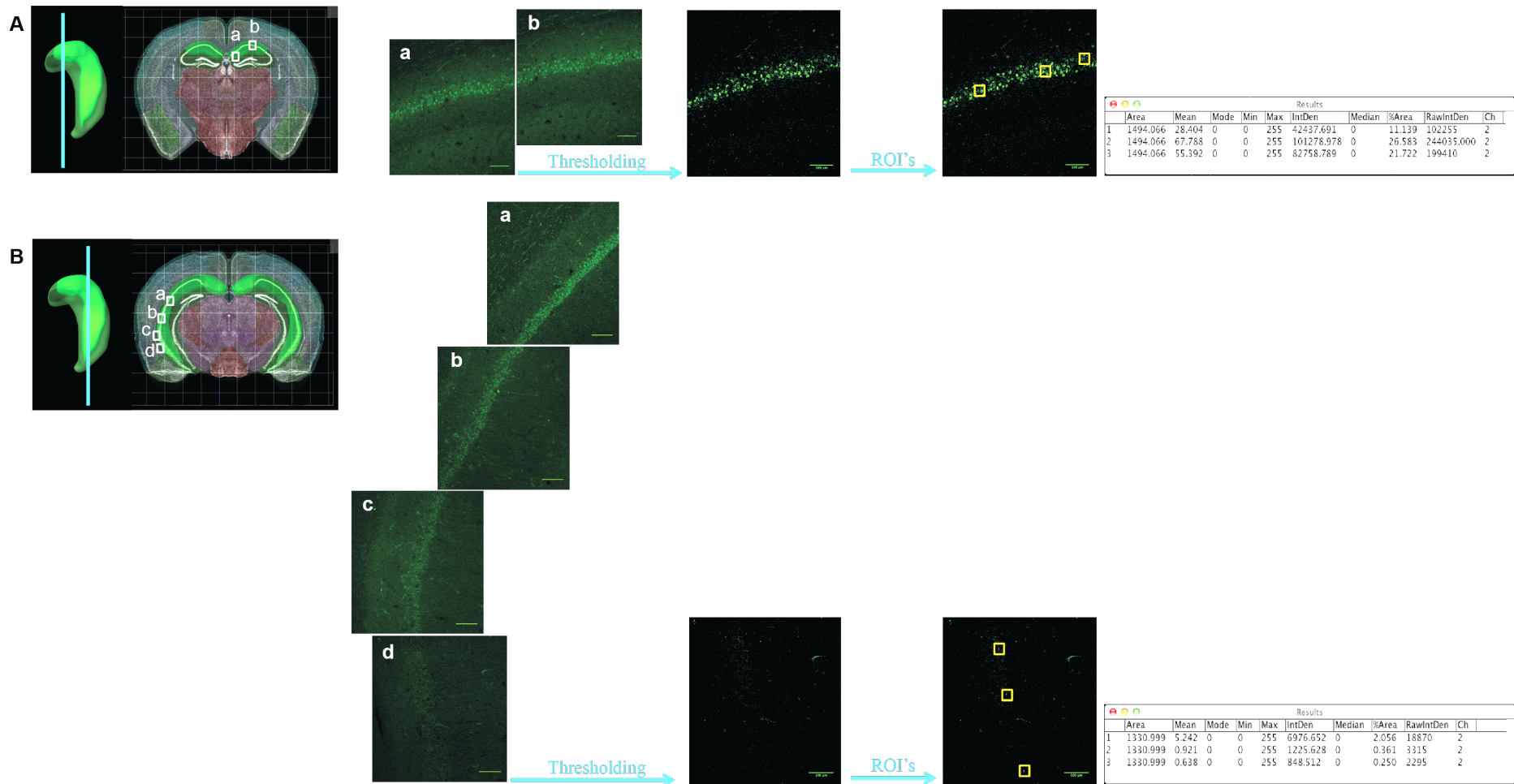
Figure 13: Technical approach to measure pyramidal cell layer Kv1.3 fluorescence illustrated by an example. Arrows indicate processes. Both panels illustrate coronal slices derived images, but panel **B** assumes a more caudal position than panel **A**. Confocal images from CA1 region were obtained from coronal (and sagittal – not illustrated) brain slices as an average of two confocal scannings, with 20X amplification. Images were then segmented (by thresholding) so that fluorescence in the pyramidal cell layer would be isolated. To further narrow down possible false positives, regions of interest (ROI's) were selected in the pyramidal cell layer (3 per image). Integrated density (Area*Mean grey density) was measured limited to threshold. Minimum, maximum, mean, modal and median and area fraction were also accessed (the ROI area was the same in almost every caption). Integrated density was then normalized to the maximum ROI integrated density for each set of images that had been captured under the same conditions at the confocal microscopy. Mean integrated densities were then established for dorsal/ventral portions and fasting/fed conditions.

This page was intentionally left blank.

4   RESULTS

Potassium (K^+) currents are of utmost importance in the cellular membrane potential maintenance and repolarization after an action potential. For the present context, Kv1.3 underlies the insulin sensitive K^+ current that has been shown to depend on the metabolic state (see 1.4.2.3.2 Insulin as a neuromodulator). Considering the key role of the hippocampus in cognition, it is of major interest to understand K^+ currents dynamics during metabolic states – fasting and fed – and within the hippocampus – dorsal and ventral portions – CA1 pyramidal neurons (see 1.8 Framework of the Project). Furthermore, Kv1.3 expression in the same groups was evaluated.

4.1 WHOLE-CELL K^+ CURRENTS IN CA1 PYRAMIDAL NEURONS

4.1.1 Currents features (kinetics)

Each coloured line-trace in **Figure 14A** is a K^+ current evoked by a +40mV depolarizing pulse (preceded by a -120mV prepulse).

Whole-cell K^+ currents of CA1 neurons are composed by a fast activation phase followed by a slow decay (inactivation phase) and a stable (steady-state) component. Our study focused on the decay phase and the stable component. A thorough exposition on this matter can be found in (Standen et al., 1987)

Whole-cell K^+ current decay could be described as a summation of exponential functions (**Figure 14A** top right inset; see 3.2.5.1Exponential fitting), and therefore was said to be composed by a sum of current components. Each component is the result of ion conductance through a set of Kv populations with similar biophysical profiles. In CA1 pyramidal neurons, currents were definable by two components:

- the fast component (I_{fast}), which is a result of *A-like-currents*, and
- the slow component (I_{slow}), which includes I_{DR} *current* and the one inhibited by MgTx.

A third component was also present, commonly referred as steady-state current (I_{ss}), which expresses non-inactivating currents.

We have analysed the decay phase of K^+ currents recorded from CA1 pyramidal cells (dorsal and ventral hippocampus of fasting and fed rats; **Figure 14**), by fitting a sum of exponential functions (see3.2.5.1Exponential fitting). I_{fast} and I_{slow} time constants (τ) are presented in **Figure 14B** – the upper panel refers to τ_{fast} and the lower panel to τ_{slow}.

4.1.1.1 Currents kinetics in CA1 pyramidal neurons from dorsal and ventral hippocampus

As to the hippocampal dorsal-ventral axis (compare light *vs.* dark blue bars and light *vs.* dark red bars in $\tau_{\mathbf{fast}}$ of **Figure 14B** and the respective currents in **Figure 14A**), results showed that I_{fast} is slower in ventral hippocampus (τ_{fast}=65,55±10,91ms) than in the dorsal counterpart (τ_{fast}=41,10±2,91ms). In other words, in the dorsal hippocampus, I_{fast} has a faster kinetics than in ventral hippocampus.

One should however note that τ_{fast} values cannot be directly read from **A**'s time axis, as they are obtained by a fitting of an exponential function onto the current's profiles (see3.2.5.1Exponential fitting). Furthermore, in the example, a striking difference between fasting condition dorsal hippocampus and ventral hippocampus currents is also noticed – this is due to the specific cells particularities and does not translate the average case.

Regarding current kinetics, no significant differences were observed in the slow component's kinetics, as translated in τ_{slow} (compare light *vs.* dark blue bars and light *vs.* dark red bars in $\tau_{\mathbf{slow}}$ of **Figure 14B** and the respective currents in in **Figure 14A**). However, like in regard to I_{fast}, a tendency of slower kinetics of I_{slow} could be noted in dorsal cells in comparison to those in ventral ones, although not reaching significance (**Figure 14B**).

4.1.1.2 Currents kinetics in CA1 pyramidal neurons from fasting and fed rats

Differences between the fasting/fed rats' derived K^+ currents were under scrutiny, within each of the hippocampal portion of the hippocampus.

Fed rats dorsal neurons have a slower I_{fast} kinetics than the fasting ones (compare light blue *vs.* light red bars in $\tau_{\mathbf{fast}}$ of **Figure 14B** and the respective currents in in **Figure 14A**). In ventral hippocampus the difference is not significant, but absolute values and observation of the currents suggest the same trend (compare dark blue *vs.* dark red bars in **Figure 14B** $\tau_{\mathbf{fast}}$ and the respective currents in in **Figure 14A**).

Again, I_{slow} kinetics did not differ significantly between fasting/fed conditions (compare light blue *vs.* red bars and dark blue *vs.* red bars in $\tau_{\mathbf{slow}}$ **Figure 14B** and the respective currents in **Figure 14A**).
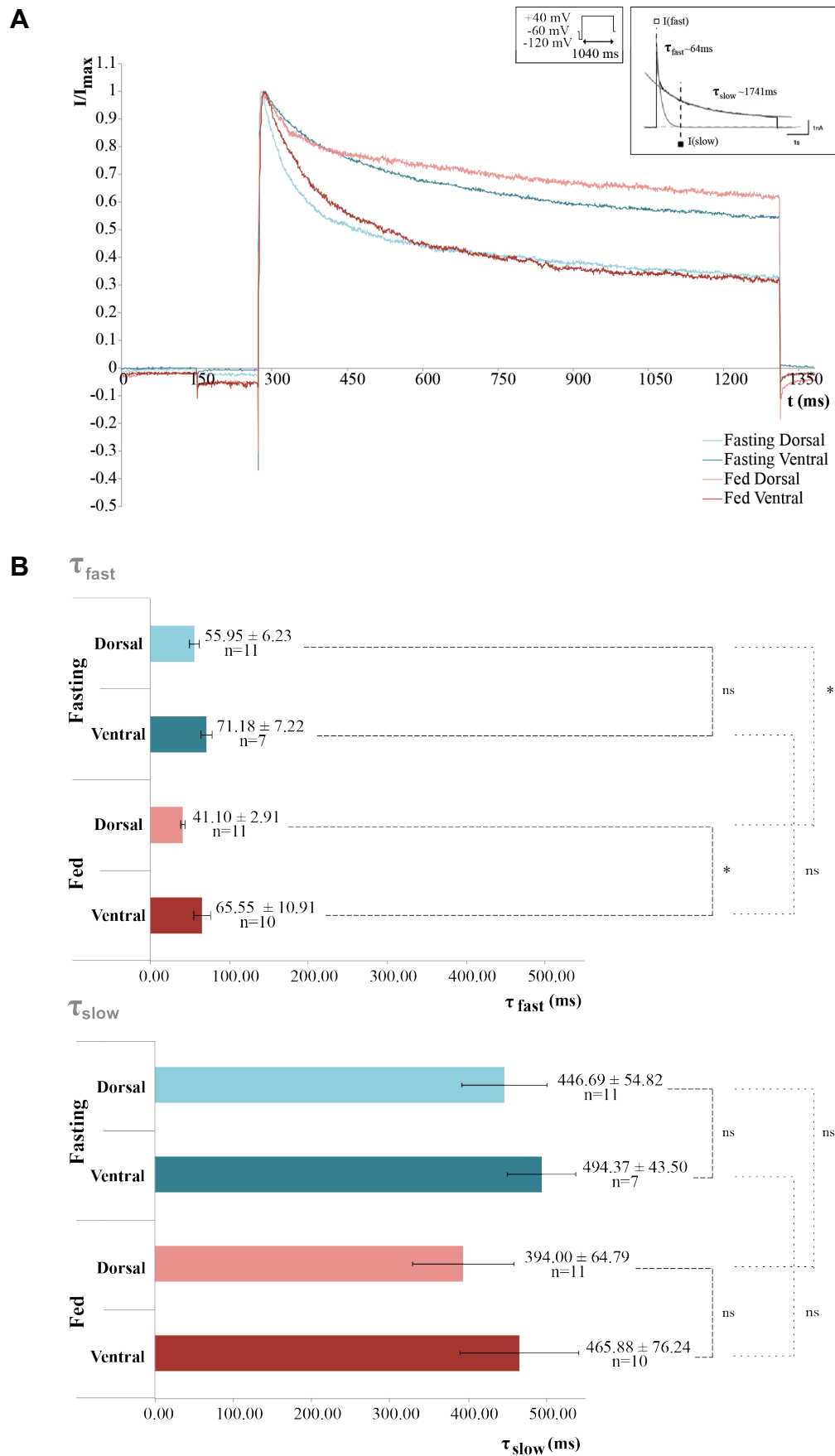
Figure 14: Time-course of K$^+$ currents (kinetics). These were evoked by a depolarizing pulse (+40 mV) applied from a holding potential of -60mV, preceded by a pre-pulse of -120mV (as shown in top inset). The presented whole-cell currents (**A**) Representative traces for each condition. (**B**) Pool data from n

cells. The significant differences between the two hippocampal portions (dorsal and ventral) of the fed individuals and between the two metabolic conditions (fasting and fed) in dorsal hippocampus τ_{fast} values (further described in **B)**, can be observed in the illustrative currents (**A**). τ_{fast} and τ_{slow} refer to the fitted exponential function time constants (top right corner inset; see3.2.5.1Exponential fitting), and as such cannot be directly read from the representative currents time courses (**A**'s time axis). τ_{fast}'s and τ_{slow}'s differences are characterized in **B**. Bars are mean±S.E.M.; ns, $p > 0.05$; *, $p \leq 0.05$; Mann Whitney test; n's are stated for each condition.

4.1.2 Current voltage-dependence

The decay phase of Kv current is voltage-dependent. Still, we have observed that the hippocampus is not homogenous regarding the voltage-dependences of I_{fast} and I_{slow} (activation profiles), and that these depend on the metabolic condition of the subject.

The activation profiles of K^+ currents in CA1 pyramidal neurons of both dorsal and ventral hippocampus from fasting and fed rats were assessed, by application of an activation protocol that complies incremental depolarizing pulses (as described in 3.2.4Voltage protocols). Resulting whole-cell currents were recorded. K^+ currents were then dissected into the previously described components as summarily illustrated in **Figure 15**. Each component's activation profile was outlined, by fitting Boltzmann functions, and dissimilarities between study groups were analysed (**Figure 16**). Generally, I_{slow} currents were elicited from around -60mV, following a sigmoidal increase until stabilizing around +20mV. I_{fast} was activated around -50mV and stabilized at around +30mV. Two parameters were in focus – voltage of half activation ($V_{1/2}$), which reflects the relative stability between open and closed states of Kv channels, and slope, which reflects the voltage-sensitivity (voltage difference necessary to elicit a *e*-fold increase in current/conductance) (Shih and Goldin, 1997, Costa, 1996).
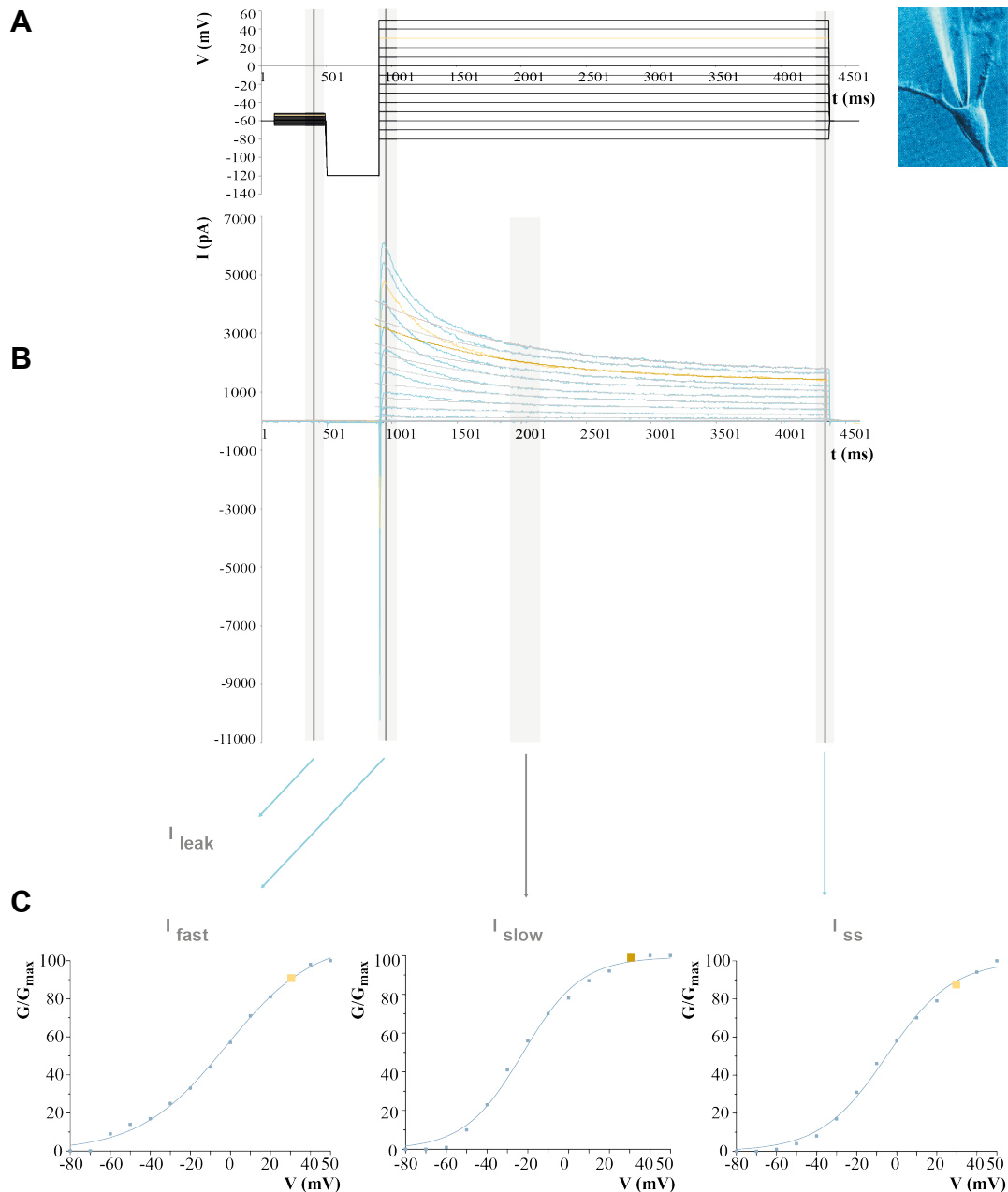
Figure 15: Voltage-dependence of activation of K$^+$ current components acquisition procedure, illustrated by example from a fasting rats' dorsal hippocampal neuron. The following activation protocol (**A**) applied to whole-cell voltage-clamped CA1 pyramidal neurons (top right corner inset): a series of depolarizing pulses (-80 to +50mV, in 10mV steps, lasting for 1040ms), proceeded by a -120mV pre-pulse, from a *holding potential* of -60mV. The elicited voltage-gated currents (I; **B**) were analysed and four current values were measured (at times signed by the vertical grey strips): the current in the pre-pre-pulse allowed for an estimation of I$_{leak}$ (which would be subtracted to the other components current values), the current peak was attributed to I$_{fast}$, an extrapolation of the I$_{slow}$ component's first order exponential function (grey exponential fittings in **B**) allowed for I$_{slow}$ determination at the same time of I$_{fast}$, and finally I$_{ss}$ was measured in the last ms of the command pulse. G/G$_{max}$ values were plotted against the pulses' voltages and a Boltzmann function was adequately fitted to the arising scatter (**C**). A single voltage pulse, its respective elicited current, I$_{slow}$ fitted exponential function and components' G/G$_{max}$ in the activation profiles are highlighted in yellow. This process is extensively described in 3.2.5.2 Voltage dependence of activation – "Activation profiles.

4.1.2.1 Current voltage-dependence in CA1 pyramidal neurons from fasting and fed rats

Results revealed that fasting rats' neurons showed more depolarized activation profiles than those from fed rats' neurons, for both current components (compare blue *vs.* red lines plotted in **Figure 16Aa** - I_{fast}, **Figure 16Ba** - I_{slow}, and **Figure 16Ca** - I_{ss}). Indeed, fasting rats' neurons had more positive voltages of half-activation values ($V_{1/2}$) than those from fed rats', but no differences were observed in the profiles' slopes (compare blue *vs.* red bars in **Figure 16Ab, Bb and Cb** and dx values in **Table 9**).

This means that fed rats neurons express currents that are sensitive to more negative transmembrane potentials. Therefore, a smaller depolarization is sufficient to activate the subjacent Kv channels in such neurons. In other perspective, at a given transmembrane potential (within the potential range of activation, for example V= -10mV), there are more active K^+ channels in the fed rats' neuron than in the fasting one.

4.1.2.2 Current voltage-dependence in CA1 pyramidal neurons from dorsal and ventral hippocampus

Although no significant differences were noticed between the voltage-profile values obtained from hippocampal portions, the discrepancies between fasting and fed conditions on the activation profiles were more compelling in the dorsal than in the ventral hippocampus (compare light blue *vs.* dark blue and light red *vs.* dark red lines/bars plotted in **Figure 16A** - I_{fast}, **Figure 16B** - I_{slow}, and **Figure 16C** - I_{ss} and values in **Table 9**). This raises the possibility that the hippocampus might not be homogeneous with regard to the pyramidal cell's K^+ voltage-dependence.

Indeed, no significant changes were detected in the parameters $V_{1/2}$ and slopes, with one exception - a minimally significant difference (*, $p \leq 0.05$) prevailed between I_{ss} activation profiles' slopes recorded in dorsal and ventral hippocampal neurons from fasting rat neurons.

Table 9: K^+ current components activation profiles parameters for each study group. Currents were obtained in CA1 pyramidal cells from the dorsal and ventral hippocampus of fasting and fed rats. I_{fast}, fast current component; I_{slow}, slow current component; I_{ss}, steady-state current component; $V_{1/2}$, voltage of half-activation slope refers to Boltzmann function slope. Values are means of n cells and respective errors are s.e.m..

Study group		n	I_{fast}		I_{slow}		I_{ss}	
			$V_{1/2}$ (mV)	slope (mV•e^{-1})	$V_{1/2}$ (mV)	slope (mV•e^{-1})	$V_{1/2}$ (mV)	slope (mV•e^{-1})
Fasting	Dorsal	11	-0,89 ± 1,78	16,04 ± 1,07	-4,24 ± 2,28	18,56 ± 1,54	-3,13 ± 1,71	20,67 ± 1,63
Fasting	Ventral	7	-3,24 ± 2,44	17,84 ± 0,78	-7,05 ± 1,16	15,55 ± 1,21	-8,90 ± 1,75	15,64 ± 1,07
Fed	Dorsal	11	-10,56 ± 1,67	17,62 ± 0,66	-17,22 ± 1,24	19,50 ± 0,98	-13,02 ± 1,91	24,02 ± 1,65
Fed	Ventral	10	-9,92 ± 3,40	18,06 ± 0,74	-16,73 ± 2,53	17,83 ± 1,36	-15,35 ± 3,36	19,00 ± 1,63
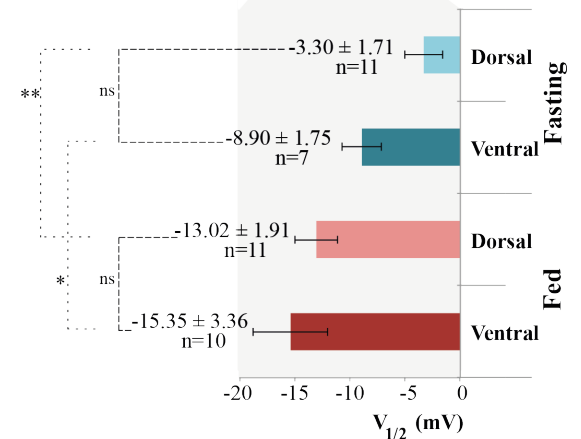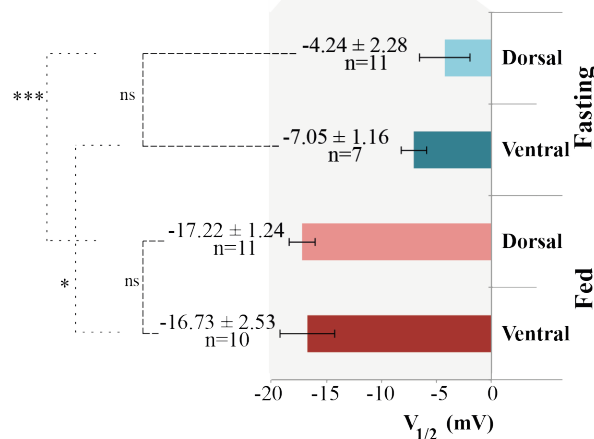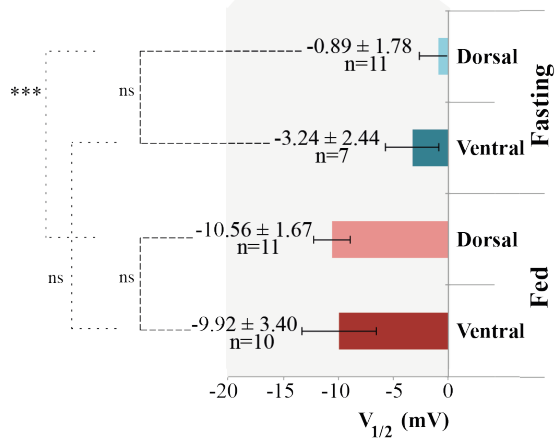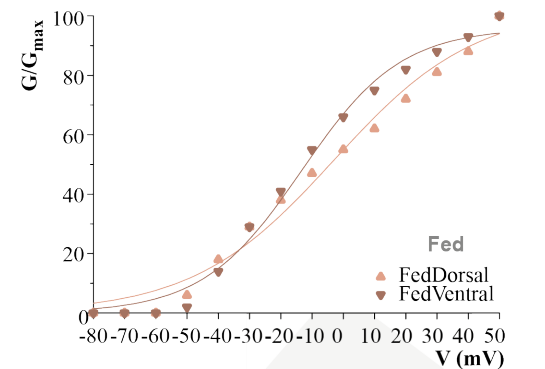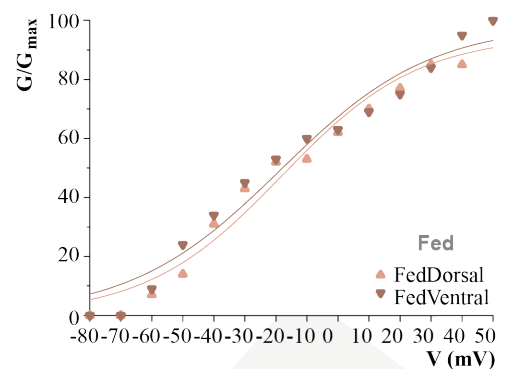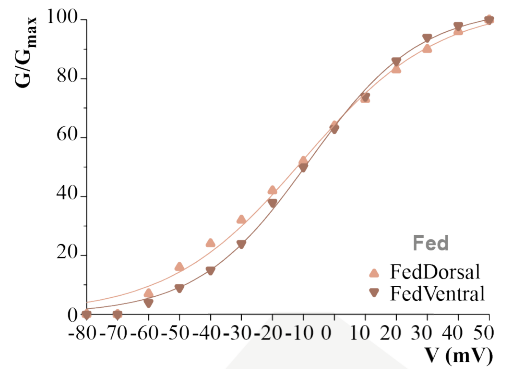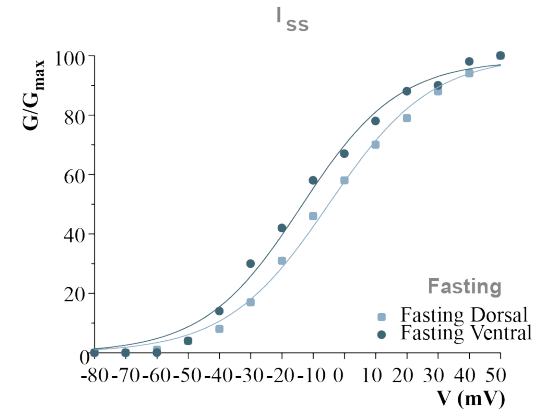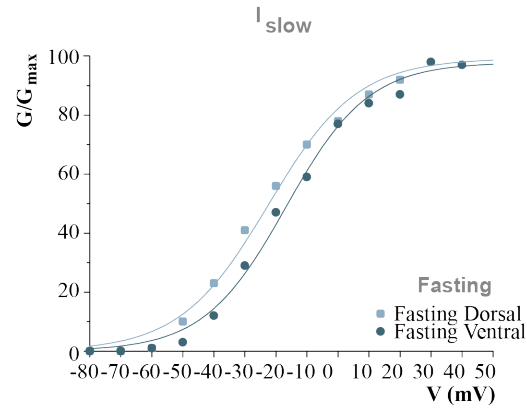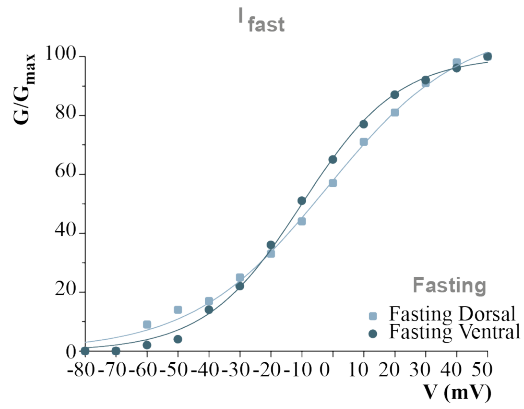
Figure 16: K$^+$ current components activation profiles. Briefly, the voltage protocol used was composed by a series of depolarizing pulses (-80 to +50mV, in 10mV steps, lasting for 1040ms) that were preceded by a -120mV pre-pulse 120mV (*holding potential*: -60mV) – it is extensively described in3.2.4Voltage protocols. I$_{fast}$ (**A**), I$_{slow}$ (**B**) and I$_{ss}$ (**C**) activation profiles are represented in the upper panels (**Aa, Ba, Ca**), representing the normalized conductance as a Boltzmann fitted function of the voltage. The presented profiles are not averages, but instead derivate from real recordings; these were selected for this illustration according to the criteria of closest V$_{1/2}$ to the mean V$_{1/2}$ for each particular condition. V$_{1/2}$ differences are characterized in the lower panels (**Ab, Bb, Cb**). Bars are mean±S.E.M.; ns, $p > 0.05$; *, $p \leq 0.05$; **, $p \leq 0.01$; ***, $p \leq 0.001$; Mann Whitney test; n's are stated for each condition.

4.1.3 Current density

Current density is a measure of the amount of current running through a normalized membrane, at a given time. It was evaluated by the current/capacitance ratio (pA/pF) as membrane capacitance is proportional to membrane surface area. As distinct populations of Kv channels underline Ifast, Islow and Iss, current's densities were studied for each current component (**Figure 17A** - I_{fast}, **Figure 17B** - I_{slow}, and **Figure 17C** - I_{ss}).

4.1.3.1 Current density in CA1 pyramidal neurons from dorsal and ventral hippocampus

Dorsal hippocampal neuron's current density values were significantly larger than those of ventral hippocampal neurons. This was true for all current components, in fed rats (compare light red *vs.* dark red bars in **Figure 17A, B and C**) but not in fasting animals.

4.1.3.2 Current density in CA1 pyramidal neurons from fasting and fed rats

No significant differences were observed between current density of fasting and fed rats' neurons. However, the above-mentioned differences between dorsal and ventral hippocampus were only true in fed rats' neurons, and not in fasting rats' ones (compare light *vs.* dark blue bars in **Figure 17A, B and C**). This suggests that current conductance may also be dependent on the feeding cycle.

Steady-state current density in fed rats' cells also showed to be significantly larger than in fasting rats' neurons, in the dorsal hippocampus (compare light blue *vs.* light red bars in **Figure 17C**). However, this discrepancy may be due to leak current contamination, which would be influencing the whole-cell capacitance in the fast records.
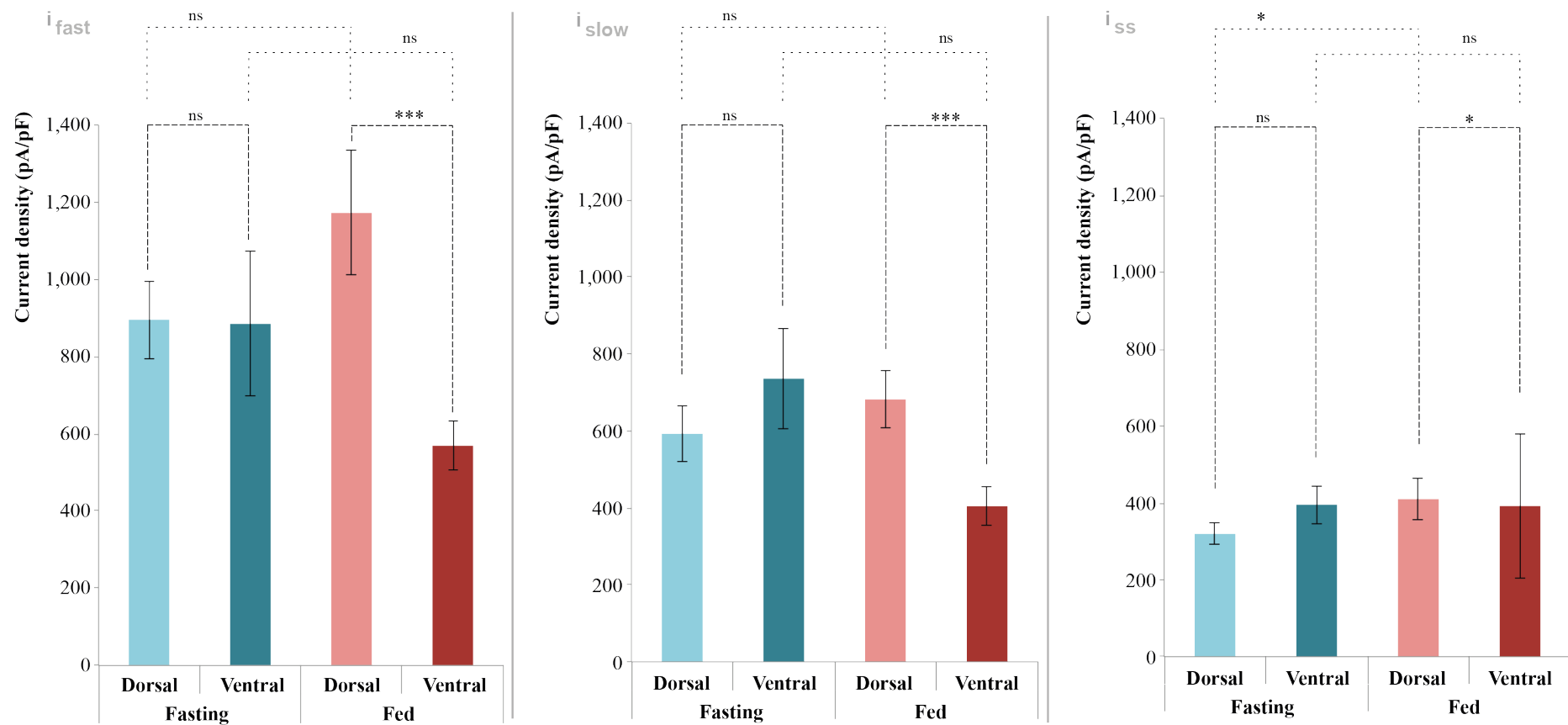
Figure 17: K$^+$ current components current density. Briefly, a depolarizing pulse (+40 mV) was applied (from a holding potential of -60mV, preceded by a pre-pulse of -120mV); an exponential function was fitted to the elicited current decay; capacitance was registered; I_{fast}, I_{slow} and I_{ss} currents were measured and corresponding current density were calculated (see 3.2.5.3Current density and plotted (**A**, **B** and **C**, respectively). Bars are mean±S.E.M.; ns, $p > 0.05$; *, $p \leq 0.05$; ***, $p \leq 0.001$; Mann Whitney test; Fasting Dorsal n=11, Fasting Ventral n=7, Fed Dorsal n=11, Fed Ventral n=10.

4.1.4 Margatoxin-sensitive K$^+$ currents

It has been shown that insulin receptor (InsR)-mediated currents are altered by the metabolic condition, namely during the feeding cycle. This insulin sensitive current mediated by the K$^+$ channel - Kv1.3 - is selectively inhibited by margatoxin (MgTx) (Mondragão, 2010). Therefore, it is reasonable to question if MgTx-sensitive currents are altered by the metabolic condition (without insulin modulation). Moreover, as it has been suggested so far in this project, the hippocampus may not be homogeneous regarding K$^+$ currents, so experiments were conducted to assess whether MgTx sensitive current varies throughout the dorsal-ventral axis.

MgTx 3nM was added to the superfusing solution while consecutive depolarizing pulses to +40mV were applied to whole-cell voltage-clamped CA1 pyramidal cells (from fasting or fed wistar rats), in 30 to 60s intervals. I_{slow} was the only current component analysed because(1) MgTx is a Kv1.3 selective blocker; (2) Kv1.3 currents are slow (τ_{activ}=3-20ms, $\tau_{inactiv}$=250-600ms), in the range of the time constants of I_{slow}; and (3) MgTx sensitive currents (see subtracted traces in **Figure 18**) were fitted by a single exponential with a time course similar to published Kv1.3 currents (see 1.6.3.2Kv1.3's electrophysiological and pharmacological properties).

Figure 18 illustrates MgTx effect in the currents recorded from the four studied groups' neurons (**A** – Fasting rats' dorsal hippocampus, **B** – Fed rats' dorsal hippocampus, **C** – Fasting rats' ventral hippocampus, **D** – Fed rats' ventral hippocampus). The voltage protocol used in all cases is represented in the left-side inset. Whenever MgTx inhibited voltage-dependent K$^+$ currents, an I_{slow} specific decrease in current is observed. In each panel, before (Control, black) and after (MgTx 3nM, grey) illustrative currents are presented, as well as their subtraction (Control-MgTx, black). A 1st order exponential function was then adequately fitted to the subtracted current's decay (Fit, in colour, respective τ_{slow} indicated, mean time constants in **Table 10**), further substantiating a solely inhibition of I_{slow}.

Table 10: Margatoxin (MgTx, 3nM) sensitive currents' time constants (τ_{slow}). Time-constant values of single-exponentials fitted to current subtractions (control – MgTx), obtained from CA1 pyramidal cells (dorsal and ventral hippocampus of fasting and fed rats). Values are means of n cells and respective errors are s.e.m..

Study group		n	τ_{slow} (ms)
Fasting	Dorsal	11	1784,10± 1170,60
	Ventral	7	1143,55± 924,42
Fed	Dorsal	11	447,79± 171,40
	Ventral	10	1150,14± 738,65

Moreover, there was no recovery of the MgTx-sensitive currents upon wash with MgTx-free solution (data not shown, n=10 distributed throughout all study groups). This comes in accordance with previous studies showing the same irreversible effect (Bednarczyk et al., 2010, Mondragão, 2010).

In order to inquire about the mode of action of MgTx and to access if the different effects of MgTx (in the different conditioned neurons), its effect on the voltage dependence of current-activation were investigated. Voltage activation protocols (such as the ones described in 4.1.2 Current voltage-dependence), were applied before and during the treatment with MgTx, in two concentrations (3nM, 30nM). In none of the study groups where statistical analysis could be applied, has a significant voltage-dependence alteration been observed (**Table 11**). The tendency is a slight depolarizing shift of $V_{1/2}$ when MgTx is superfused.

Table 11: Margatoxin (MgTx) effect upon I_{slow} current voltage dependence (assessed by activation profiles parameters), for each study group. Currents were elicited in CA1 pyramidal cells from the dorsal and ventral hippocampus of fast and fed rats, before and after MgTx (3nM or 30nM) was superfusing. I_{slow}, slow current component; $V_{1/2}$, voltage of half-activation; slope refers to the Boltzmann suction slope. Values are means of n cells and respective errors are s.e.m..

Study group					I_{slow}						
		MgTx free solution			MgTx 3nM			MgTx 30nM			
		n	$V_{1/2}$ (mV)	slope (mV^{-1})	n	$V_{1/2}$ (mV)	slope (mV^{-1})	n	$V_{1/2}$ (mV)	slope (mV^{-1})	
Fasting	Dorsal	11	-4,24 ± 2,28	18,56 ± 1,54	1	-2,80	15,59	2	-2,10 ± 4,22	21,96 ± 4,13	
	Ventral	7	-7,05 ± 1,16	15,55 ± 1,21	0	---	---	0	---	---	
Fed	Dorsal	11	-17,22 ± 1,24	19,50 ± 0,98	2	-20,61 ± 12,06	-16,37 ± 0,06	2	-18,59 ± 4,70	22,68 ± 3,55	
	Ventral	10	-16,73 ± 2,53	17,83 ± 1,36	1	-9,15	-16,15	2	14,97 ± 5,01	16,51 ±,83	

4.1.4.1 MgTx-sensitive currents in CA1 pyramidal neurons from dorsal and ventral hippocampus

I_{slow} currents from dorsal hippocampal neurons were significantly reduced by 3nM MgTx. Representative current traces (**Figure 19**) show that such reduction was more noticeable in the dorsal hippocampus than in ventral neurons' currents, in fed rats (compare light red *vs.* dark red bars in **Figure 19**). The MgTx-sensitive currents (subtracted current) were fit with a 1st order exponential function with time-constant values ranging from 400 to 1200 ms.

Most importantly, when analysing the pooled data from **Figure 19**, one can note that the MgTx induced inhibition was clearly more effective in experiments conducted in dorsal neurons. Indeed for fed rats, inhibition of I_{slow} by MgTx, in neurons from the dorsal hippocampus was 22,46±4,12%. This strongly contrast with 3,52±4,12% I_{slow} inhibition, when the same concentration of MgTx was applied to similar neurons from ventral hippocampus.

4.1.4.2 MgTx-sensitive currents in CA1 pyramidal neurons from fasting and fed rats

Striking results revealed that fed rats' neurons have more MgTx-sensitive currents than fasting ones. Representative current traces in **Figure 18** show larger MgTx-sensitive currents in neurons obtained from fed rats when compared with those deriving from fasting animals (dorsal hippocampus in particular) (compare light blue *vs.* light red traces in **Figure 18**). Current inhibition percentages from pooled data further emphasize these observations (**Figure 19** – fasting rats' dorsal neuron I_{slow} was inhibited by 1,52±0,86% and fed rats' dorsal neuron I_{slow} inhibition was 22,46±4,12%; ***, $p \leq 0.001$; Mann Whitney test). In other words, fasting rats' neurons are far less sensitive to MgTx. This difference was less noticeable in ventral hippocampal neurons, where the difference between MgTx-sensitive currents of fasting and fed rats was not significant (compare dark blue *vs.* dark red bars in **Figure 19**; fasting rats' ventral neuron 0,44±0,41% I_{slow} inhibition; fed rats' ventral neuron 3,52±2,59% I_{slow} inhibition).

Additionally, an indirect analysis can be done, comparing MgTx-sensitive currents of the two hippocampal portions. Differences observed between the referred currents of dorsal and ventral hippocampus from fed animals were not observed in fasting rats' hippocampus (compare light blue *vs.* dark blue bars in **Figure 19**; fasting rats' dorsal neuron 1,52±0,86% I_{slow} inhibition; fed rats' ventral neuron 0,44±0,41% I_{slow} inhibition). Also, comparing MgTx-sensitive currents kinetics (subtracted current mean τ_{slow}) from the two hippocampal portions, remarkably different values in fed rats' cells were not observed in fasting animals (Fasting rats' dorsal neuron Mean (τ_{slow}) = 1784,10±657,85 ms; n=3 /Fasting rats' ventral neuron Mean (τ_{slow}) = 1143,55±533,71 ms; n=7),
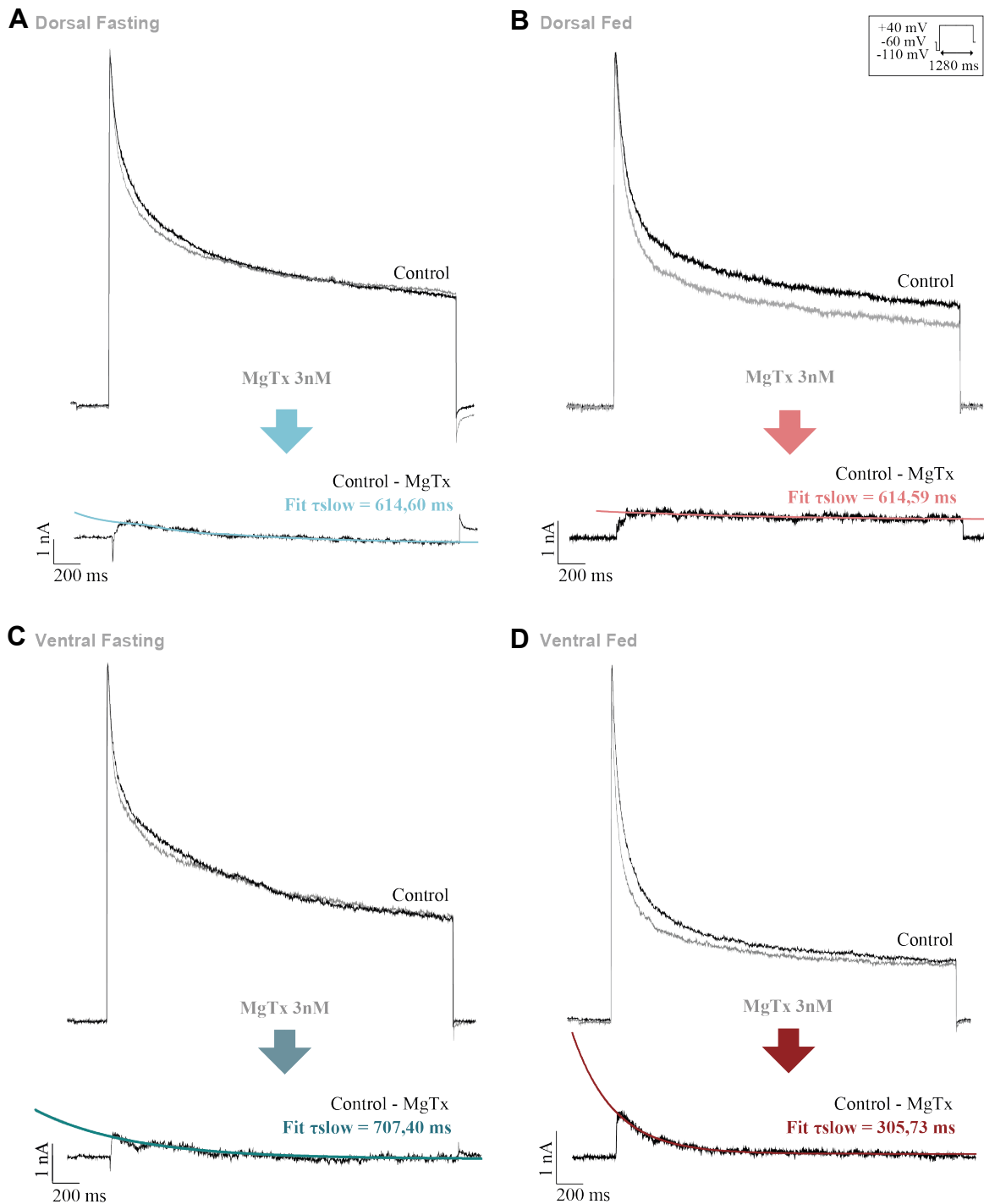
Figure 18: Margatoxin (3nM) effect upon (voltage-clamped) whole-cell K^+ currents from CA1 pyramidal cells. The voltage protocol shown in the top right corner inset was applied every 30-60ms (briefly, a depolarizing pulse (+40 mV) was applied from a holding potential of -60mV, preceded by a pre-pulse of -120mV). A sample current from before (Control, black) and after (MgTx 3nM, grey) were chosen to evaluate the current sensitivity towards MgTx – the ones chosen for these illustrative cases are marked in the respective time-courses. The subtracted current (Control-MgTx, black, shown in the lower part of each panel) was fitted with a 1st order exponential function (Fit, coloured line overlapping the subtracted current; the respective τ_{slow} is indicated). Each panel refers to a study condition (**A** Fasting rats' neuron from dorsal hippocampus; **B** Fed rats' neuron from dorsal hippocampus; **C** Fasting rats' neuron from ventral hippocampus; **D** Fed rats' neuron from the ventral hippocampus). Currents and time-courses are illustrative and do not represent the mean of all the recordings – these are real cases, chosen by the following criteria: inhibition percentage most similar to the mean one, for each condition.
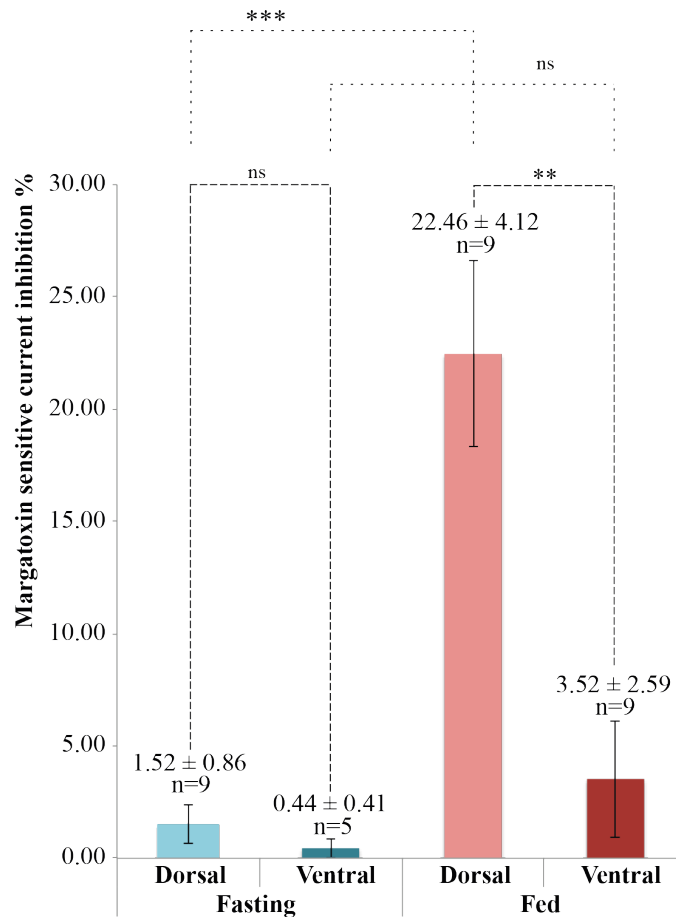
Figure 19: I_{slow} inhibition (in percentage) by 3nM margatoxin (MgTx). Briefly, whole-cell currents were elicited by consecutive +40mV pulses from a holding potential of -60mV (preceded by a -120mV prepulse); a 2nd order exponential function was fitted to the recorded currents and I_{slow} was measured at t > $5*\tau_{fast}$ (ms); inhibition percentage was calculated based on the difference of I_{slow} before and during the MgTx superfusion. Bars are mean±S.E.M.; ns, $p > 0.05$; *, $p \leq 0.05$; **, $p \leq 0.01$; ***, $p \leq 0.001$; Mann Whitney test; n's are stated for each condition.

4.2 KV1.3 PROTEIN EXPRESSION IN CA1 PYRAMIDAL NEURONS

Given the differences found in the electrophysiology/pharmacology part of these work, Kv1.3 channel protein expression was investigated. For this purpose, immunohistochemistry was carried out in hippocampal slices, using an anti-Kv1.3 primary antibody (as described in3.3Imunohistochemistry).

4.2.1 Subcellular distribution in CA1 region (pyramidal cells)

In **Figure 20**,one can observe that the fluorescence signal is almost completely confined to the somatic region. Very little labelling (Kv1.3 in green; cell nucleus in blue) was observed in the dendritic layer, which demonstrates a somatic distribution of the Kv1.3 protein.

A somatic but not dendritic expression patterns was observed throughout the hippocampus. Indeed, while **A** corresponds to coronal slice's confocal images (schematically referred to in **Aa** and **Ab**), **B** shows images from sagittal slices (schematically referred to in **Ba** and **Bb**). Kv1.3, marked in green, is present in the *stratum pyramidale*, where the pyramidal cells' somas are comprised, and not in *stratum oriens* nor in *stratum radium*, where dendrites are located (**Ac** and **Bc**). Higher magnification images (20X to 40X; **Ad**, **Bd** and **Be**) further evidence the somatic distribution of the protein, as the antibody marks round-like pyramidal cell bodies without any projection (as signed by arrows in **Ad**). Notably, some cells display a likely membranar tagging, as there seems to be a higher green intensity in the cell border than in the inside, (arrows in **Bd** and **Be**).

Notwithstanding, a couple of cells outside the pyramidal cell layer are tagged – these do not look like pyramidal cells, and correspond to false positives, which have higher levels of autofluorescence as they are also observable in negative controls (without the primary anti-Kv1.3 antibody, **data not shown**).
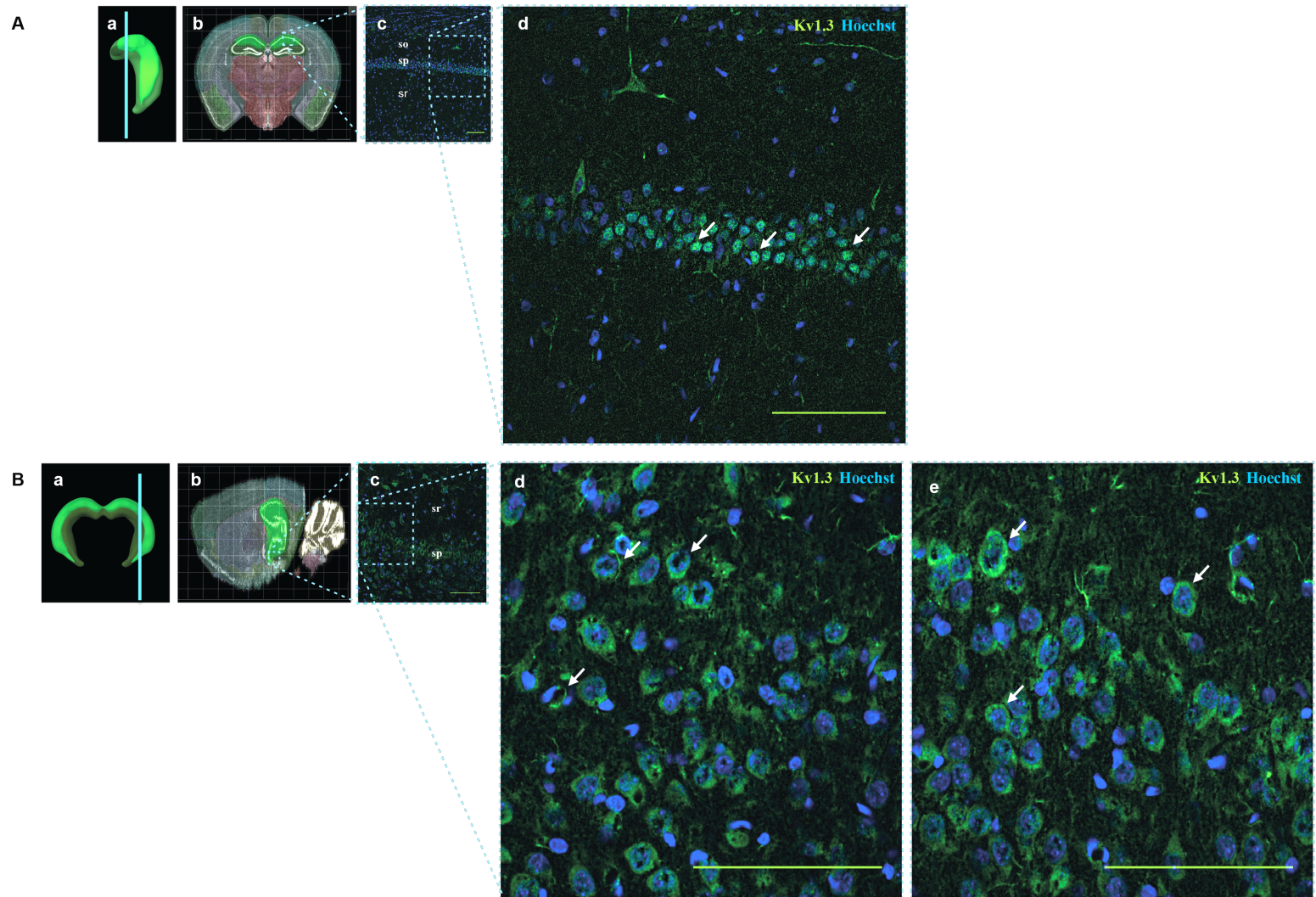
Figure 20: Immunohistochemical localization of Kv1.3 channel in rat hippocampal CA1 pyramidal cells. Nucleuses are marked blue whereas Kv1.3 is marked green. In panel **A**, a detail (**Ad**; 40X magnification) of the dorsal CA1 pyramidal layer (**Ac**; 20X magnification) from a coronal slice is emphasized, whereas in panel B, a couple of details

(**Bd** and **Be**; 40X magnification) of the ventral CA1 pyramidal layer (**Bc**; 20X magnification) from a sagittal slice are shown. Illustrative hippocampus and hippocampal slices (first 2 insets in both panels: **Aa, Ab, Ba, Bb**) are presented, adapted from Brain Explorer 2 (© 2006-2013 Allen Institute for Brain Science). In **Ad**, arrows point out some examples of pyramidal cell bodies with a clear somatic tagging and absent dendritic tagging. In **Bd** and **Be** arrows point out a likely membranar tagging. sp, *stratum pyramidale*. so, *stratum oriens*. sr, *stratum radium*. Scale bars, 100μm.For illustrative purposes only, images were processed as follows (ImageJ software): **Ac** and **Ad** - background was subtracted by rolling ball (16.0 pixels radius with sliding paraboloid), noise outliers (up to 2 pixel radius at a 85 threshold) were removed, a Gaussian filter (0.5 radius) was applied and the first two actions were repeated; **Bc**, **Bd** and **Be** - background was subtracted by rolling ball (70.0 pixels radius with sliding paraboloid), noise outliers (up to 2 pixel radius at a 50 threshold) were removed, a Gaussian filter (0.7 radius) was applied and the and the first two actions were repeated.

4.2.2 Kv1.3 expression in CA1 hippocampal region

Four fasting rats and other 4 fed rats were used to determine the relative localization of Kv1.3 within the hippocampus and compare its expression between metabolic conditions (**Figure 23**, **Figure 21** and **Figure 24**).

Kv1.3 expression was evaluated by immunohistochemistry performed in brain slices from three cutting planes: two coronal ones, one more caudal than the other (only the more caudal one included ventral hippocampus; both n=6), and one sagittal (n=2).

Alongside the direct observation of the microscopy images, semiquantitative analysis was performed, by measuring the pyramidal cell layer's fluorescence integrated density in sets of images and normalizing them to their inner maximum to be able to compare them (see **3.3.4**Data analysis and statistics).

4.2.2.1 Kv1.3 expression in CA1 region from dorsal and ventral hippocampus

Observation of coronal and sagittal images revealed that Kv1.3 expression varies throughout the hippocampus. **Figure 21** is an illustrative example of the observations, its images were obtained from two fed rats (one for the coronal slices, and another for the sagittal one). In each panel, a schematic representation of the slice's localization in the rostral-caudal (left image in **A, B**) or the inner-outer (left image in **C**) axis of the hippocampus is presented, as well as a schematic representation of each image's localization (middle column of **A**, **B** and **C**). Images are shown in a composed manner respecting the approximate relative localization in the CA1 region.

Coronal sections cut from a more caudal position (**Figure 21B**) include almost the whole dorsal-ventral axis of CA1 region. Its set of images (**Figure 21Ba-d**) clearly displays a heterogeneous expression of Kv1.3 – the fluorescence signal in the pyramidal cell layer is more intense in the most dorsal image (**Figure 21Ba**) than in the more ventral ones (namely **Figure 21Bd**).

Additionally, images obtained from the more rostral coronal brain slice (**Figure 21A**) had fluorescent intensities similar to those observed in the most dorsal images of the previously described caudal coronal slice (**Figure 21Ba**).

Regarding the sagittal brain slice, CA1 region is clearly divided in the dorsal and ventral CA1 portions. Again, a more intense labelling was observed in dorsal CA1 pyramidal cells (**Figure 21Ca-b**) than in ventral CA1 pyramidal cells (**Figure 21Cc-d**).

This relative decrease in the expression levels already mentioned is consistent with the semi-quantitative analysis, showing a significant greater fluorescent density in the dorsal than in the ventral hippocampus (****, $p \leq 0.0001$ Mann Whitney test, **Figure 23**).
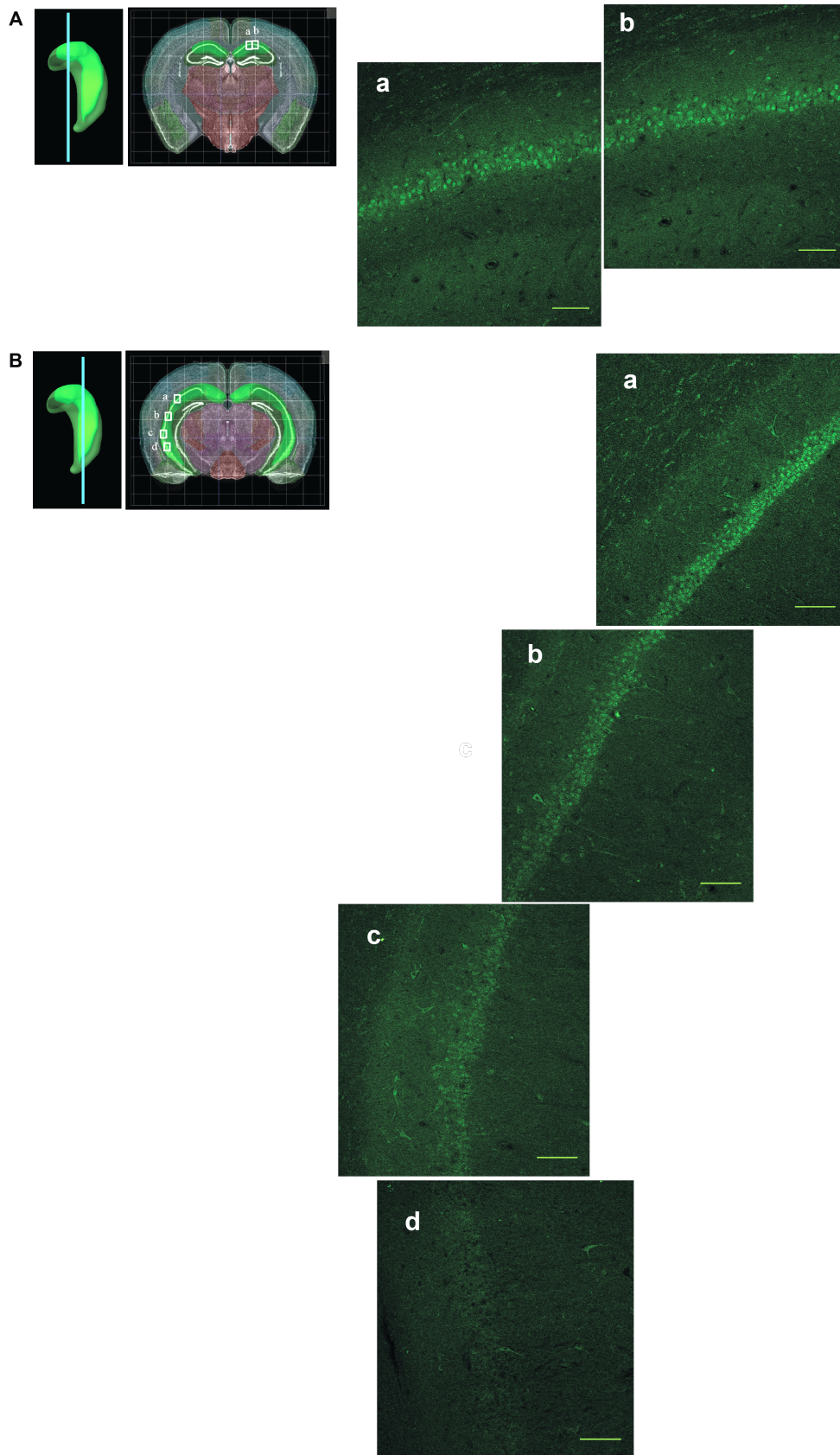
Figure 21:: Immunohistochemical localization of Kv1.3 channel in CA1 region from hippocampal coronal (rostral and caudal) slices. Illustrative hippocampus and hippocampal slices (first two insets in all panels) are presented, adapted from Brain Explorer 2 (© 2006-2013 Allen Institute for Brain Science). **Aa-Bd** approximate localizations are represented in the respective slice hippocampal slice, whereas each slice's approximate localization is referred to in the respective hippocampus (blue line). Coronal rostral

and caudal slices were from the same rat, whereas the sagittal one had its provenance in another subject.Kv1.3 (green tagging) is not evenly distributed throughout the dorsal-ventral axis. As to coronal slices, both the rostral (**Aa-b**) and the first image of the caudal set (**Ba**) have more intense staining than the more ventral captions from the caudal set (**Bb-d**). In fact, a seemingly gradient can be observed in the caudal set of images (**Ba-d**). Confocal images were obtained by an average of two confocal scannings, with 20X amplification. Scale bars, 100µm.For illustrative purposes only, images were processed as follows (ImageJ software): **Aa-b** and **Ba-d** - not processed.
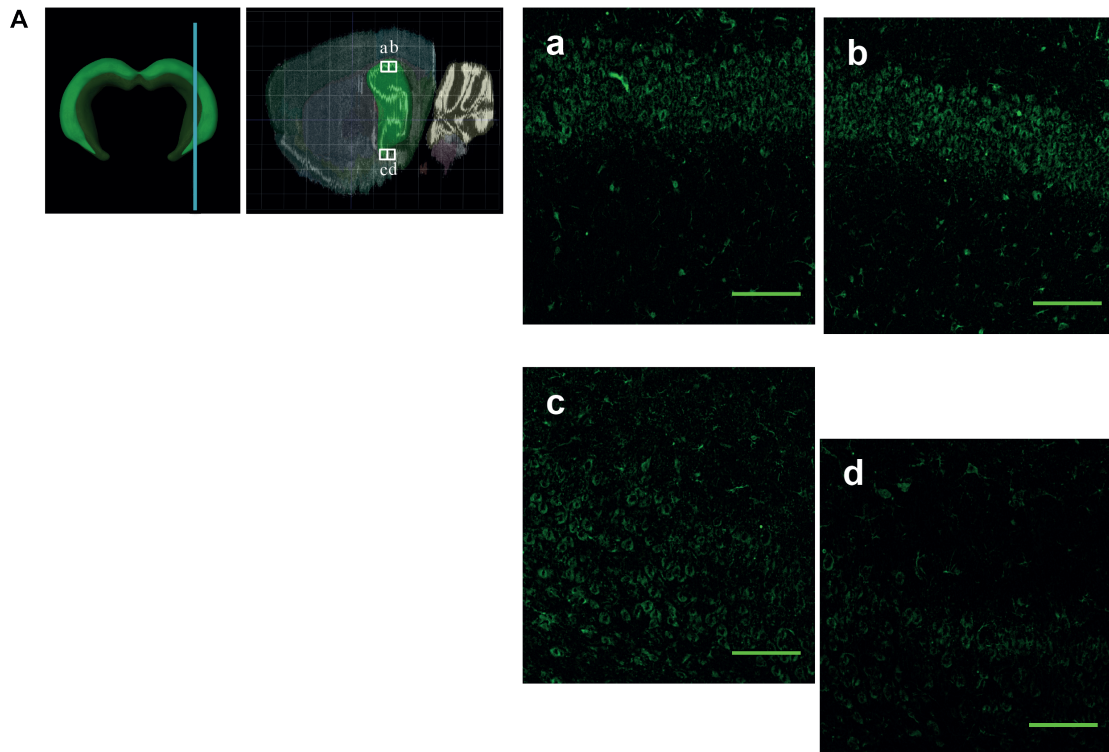
Figure 22:: Immunohistochemical localization of Kv1.3 channel in CA1 region from hippocampal sagittal slices. Illustrative hippocampus and hippocampal slices (first two insets in all panels) are presented, adapted from Brain Explorer 2 (© 2006-2013 Allen Institute for Brain Science). **Aa-d** approximate localizations are represented in the respective slice hippocampal slice, whereas each slice's approximate localization is referred to in the respective hippocampus (blue line). In sagittal slices, the dorsal hippocampus reveals a more intense labelling, when compared to its ventral counterpart (dorsal hippocampus – **Aa-b**; ventral hippocampus – **Ac-d**).Confocal images were obtained by an average of two confocal scannings, with 20X amplification. Scale bars, 100µm.For illustrative purposes only, images were processed as follows (ImageJ software): **Aa-d** -background was subtracted by rolling ball (16.0 pixels radius with sliding paraboloid), noise outliers (up to 2 pixel radius at a 40 threshold) were removed, a Gaussian filter (0.5 radius) was applied and the first two actions were repeated.
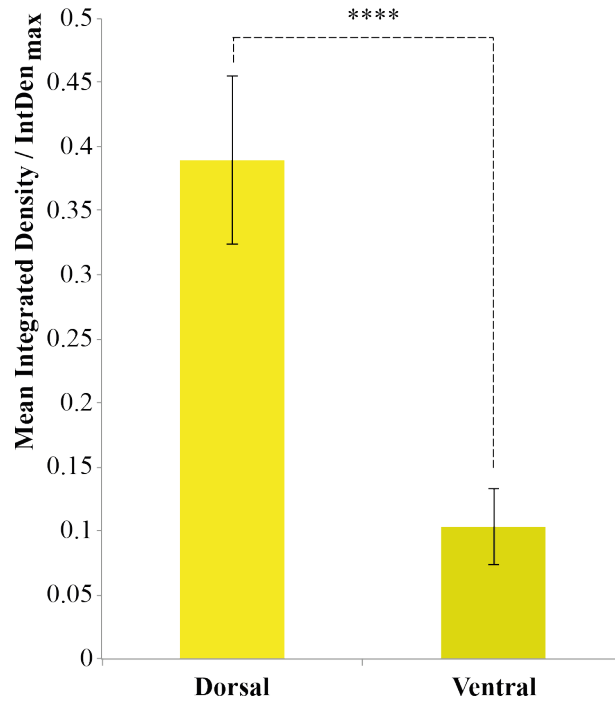
Figure 23: Dorsal and ventral Kv1.3 distribution, assessed by integrated fluorescence density. Pyramidal cell layer Kv1.3 tagging was measured (see 3.3.4 Data analysis and statistics) from the most dorsal and ventral images of each subject's set of images. Means shown in the graph were built upon these selected images alone. However, if all dorsal/ventral ROIs were covered, a significant (***, $p \leq 0.001$, n= 24 from 8 rats) difference would still be in place. Bars are mean±S.E.M.; ****, $p \leq 0.0001$ Mann Whitney test; both dorsal and ventral n=8 ROIs (from 8 rats).

4.2.2.2 Kv1.3 expression in CA1 region from fasting and fed rats

No significant difference could be assessed between fasting and fed conditioned rats' slices (**Figure 24**).
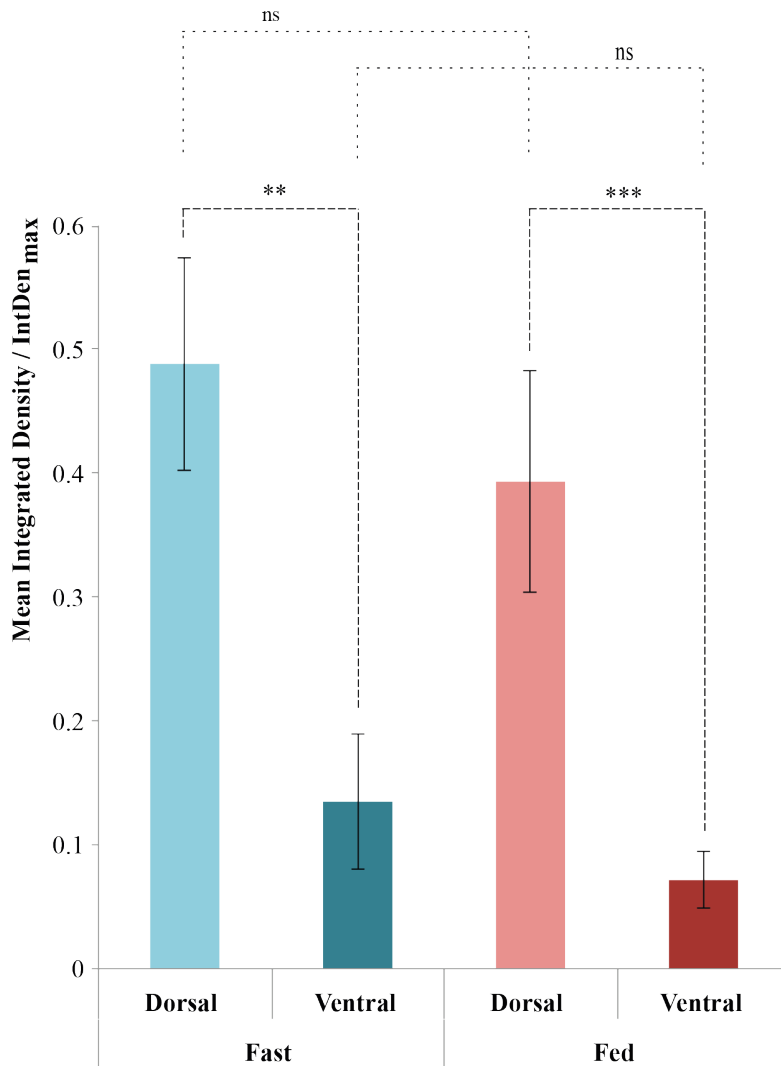
Figure 24: Dorsal and ventral Kv1.3 distribution, assessed by integrated fluorescence density. Pyramidal cell layer Kv1.3 tagging was measured (see 3.3.4 Data analysis and statistics) from the most dorsal and ventral images of each subject. Means shown in the graph were built upon these selected images alone. However, if all fasting/fed rat ROIs were covered, no significant differences between fasting and fed dorsal or ventral hippocampus would be observed either (ns, $p > 0.05$, n=12 from 4 rats). Bars are mean±S.E.M.; ns, $p > 0.05$; **, $p \leq 0.01$; ***, $p \leq 0.001$; Mann Whitney test; in all 4 conditions n=4 ROIs (from 4 rats).

This page was intentionally left blank.

5 DISCUSSION

In the present thesis evidences are provided showing that (1) in central neurons – pyramidal neurons from the CA1 region of the hippocampus – there are ionic features responsible for the control of excitability that are not constant, in their performance and expression, throughout the feeding cycle. Indeed, K^+ channels (particularly Kv1.3, which underlies an ionic current sensitive to insulin) reveal underlying currents with different biophysical and pharmacological properties, as well as diverse protein expression levels/patterns. At the same hand, it is showed that (2) there are also differences in the referred ionic currents and in the protein expression patterns among different regions of the hippocampus, namely throughout the dorsal-ventral axis of the hippocampus. Such differences are discussed here.

5.1.1 Is the Kv1.3 expression and whole-cell current in CA1 pyramidal cells dependent on the rat's feeding cycle?

Results here presented showed that K^+ currents of fed and fast rats' neurons had significantly different voltage-dependence of activation. Particularly, fed rats' neurons had a more hyperpolarised half-activation potential ($V_{1/2}$) than fasting rats' cells. As described, Kv1.3 currents are not equally expressed within the feeding cycle and 'fed $V_{1/2}$' is closer to what is described for $V_{1/2}$ recorded in expressed Kv1.3 ($V_{1/2}$=-30mV (Coetzee et al., 1999). This is indicative that this channel has a larger contribution in the whole-cell K^+ currents in fed animals' cells rather than in fasting animal's neurons. Indeed, margatoxin, a selective Kv1.3 inhibitor, caused an impressively larger current inhibition in fed rats' neurons than in fasting animals' cells. Moreover, when rats were fasting, their neurons had slower kinetics (I_{fast}) than fed rats neurons, further suggesting a biophysical modification of the currents.

All in all, evidence from this project suggest that the feeding cycle is associated with an alteration in Kv1.3 channel population that affect CA1 pyramidal cells biophysical and pharmacological properties.

Still, one should not disregard that Kv1.3 altered expression may not account for all the biophysical differences observed in fasted and fed neurons. As all K^+ current components (and not only I_{slow}, the one directly related to Kv1.3) showed voltage-dependence altered by the feeding cycle a more complex explanation should be considered:

Two hypothesis are outlined considering the different voltage profiles found in neurons of fed or fasting animals:

1. A Kv channel population is differentially expressed in the neural membrane throughout the feeding cycle (*access* hypothesis).
2. Kv's currents' voltage-sensitivity (brought by channel-gating phenomena) is being modified throughout the feeding cycle (*gating* hypothesis).

The "access hypothesis" could be explained by a metabolic regulation resulting in altered protein expression and/or recruitment to the membrane, whereas the "gating hypothesis" could happen as a consequence of metabolic modifications in the voltage-sensors, as would happen in the case of a variation in the constitutive phosphorylation for example.

The major point that corroborates the "access hypothesis" is larger margatoxin-sensitive currents in fed animal cells than in fasting ones. These striking results are evidence *per si* of metabolic modifications in the CA1 hippocampal region and, as such, have been carefully investigated.

Margatoxin-sensitive currents are indicative of Kv1.3 presence in neurons and have been evaluated through K^+ currents inhibition (in percentage). Results show smaller percentage values than previously described (31,69% in fed animal's neurons, and 18,17% in fasting rats' neurons (Mondragão, 2010)) but were indicative of the same trend. Differences may account for the fact that Mondragão (2010) did not separate dorsal from ventral neurons.

Still regarding MgTx-sensitive currents, the toxin's mode of action was investigated, as direct effect on voltage-dependence of activation was assessed. No significant differences were observed in CA1 pyramidal neurons. Still, this may not mean that margatoxin's action is not materialised in a change in voltage-dependence, since one has to look at the experimental procedure used. An experimental artefact described in (Vicente et al., 2010) has to be accounted for. It states that under whole-cell configuration, a hyperpolarizing shift of both activation and inactivation curves occurs through time - for the first 30 to 45 minutes after whole-cell configuration was achieved the shift occurs at a fast rate, and after that, it lasts all the way through the recording, at a slower rate, never stabilizing (monitored through K^+ currents evoked by depolarization pulses to 0mV). In this project, whenever a voltage-dependent process was under scrutiny, recording were not necessarily achieved after the fast-rate phase of the artefact to minimize its influence on the results, so the unchanged $V_{1/2}$ may be translating a MgTx-induced depolarizing shift concealed by the artefact. This would come in accordance with previous results describing an approximate +10mV depolarizing shift by application of 1nM of this toxin in CA1 pyramidal cells.

To further support the "access hypothesis", Kv1.3 expression in CA1 pyramidal cells was assessed by immunohistochemistry. Results reveal a tendency for higher levels of Kv1.3 channel expression in fed animals, consistent with MgTx-sensitive currents bias, but did not reach significance. The method applied did not prove to be fit to adequately compare between individuals as it does not accommodate substantial inter-subject variability. Western blot

analysis was also carried through to compare the channel's expression in the two metabolic conditions. Results were inconclusive though, due to poor quality of the antibody. Previous data with western blot in our laboratory however, suggested higher levels of the protein in fed animals (Mondragão, 2010).

Expression of proteins is a dynamic process that reflects a continual turnover between synthesis and degradation. Ionic channels are no exception, as they are synthesised by selective activation of the respective genes, transported to the membrane through a system of vesicles, where they suffer modifications, move in the membrane or are stabilized in particular areas, and then internalized, the respective vesicles become incorporated into lysosomes and are hydrolysed to amino acids. Rapid changes in channel populations have been described during development and neuronal differentiation.

On the other hand, biophysical changes give reason to the "gating hypothesis", since Kv1.3 only underlies Islow, and modifications seem to be transversal to other current components, therefore other channels.

Literature reveals that almost all voltage-gated channels' gating is affected by altered external divalent ions (namely Ca^{2+} and Mg^{2+}, probably due to association with negative charges in the voltage-sensor), pH, some external and internal monovalent ions (ionic strength) and a few other molecules. Noteworthy, K+ channels activation and inactivation is shifted toward more positive potentials as a result of ATP-induced phosphorylation of the channel that corresponds to a situation of added internal negative charge (Perozo and Bezanilla, 1990; described in (Hille, 1992)).

Hence, it possible that, alongside modifications in, at least, the Kv1.3 population, metabolic alterations may be in place, promoting constitutive phosphorylation of Kv channels in fed animals. Kv1.3 itself may be affected, since it has phosphorylation sites prone to modulate its voltage dependence (Fadool et al., 2000) and results suggest a depolarizing shift of MgTx-sensitive current's voltage-dependence.

Such a regulatory loop would be adequate for the studied Kv channels, since, as Bertil Hille (Hille, 1992) draws attention to, K^+ channel open probability is likely to be regulated by other cellular signals because of their importance in regulation of excitability and firing patterns. In fact, examples of similar regulatory loops can be found in the hippocampus: second messengers and protein kinases that are found in the heart when it needs to accelerate can be found depressing intermediate conductance Ca^{2+}-sensitive currents in the hippocampus, where they eliminate hippocampal spike-frequency adaptation, broaden presynaptic spikes and potentiate sensory neurotransmission during arousal. Besides, voltage-gated K^+ channels are also known to interact with various proteins and to heteromultimerize to form pharmacologically and biophysically distinct features. An association of Kv1 channels with

scaffolding proteins impacting the channel's localization, turnover and function has been described before (Schulte et al., 2006).

Given the collected data, we propose that both hypotheses are in place. Further investigation should address if it would be plausible that a regulatory loop, modulated by the feeding cycle, could affect channels populations' expression in the membrane (by either increasing the respective gene transcription or by translocation from internal vesicles to the membrane) and could affect the voltage-dependence.

5.1.2 Is the Kv1.3 expression and whole-cell current even throughout dorsal-ventral axis of hippocampal CA1 pyramidal cell layer?

Surprisingly, results reveal that CA1 pyramidal cells biophysical and pharmacological properties are not uniform throughout the hippocampus.

Results showed that CA1 pyramidal neurons from dorsal hippocampus had a slower I_{fast} kinetics than those from ventral hippocampus, translated by a longer time-constant of the fast component of the current's decay. But more striking are the results showing that dorsal hippocampus cells have a far greater whole-cell K^+ current density than the ones from ventral hippocampus. The difference is very significant (*** $p \leq 0,001$ for I_{fast} and I_{slow}, * $p \leq 0,05$ for I_{ss}, Mann-Whitman t-test) and reflects a biophysical change in the cell's membrane.

Still, a clear asymmetry within the dorsal-ventral axis of the hippocampus was found, regarding Kv1.3. Not only the MgTx-sensitive current component of the whole-cell K^+ current is larger in CA1 pyramidal neurons isolated from the dorsal part of the rat hippocampus when compared with those of the ventral part, but also the expression levels of Kv1.3, which in the CA1 region of the hippocampus is solely somatic. Such expression is unequal throughout the hippocampus – the dorsal portion shows higher levels of expression when compared with the ventral portion, as assessed by immunohistochemistry. The fact that the expression in solely somatic is unusual for a Kv1 channel, which customarily have a axonal neuronal staining pattern throughout the brain (Gribkoff and Kaczmarek, 2008), but comes in accordance with previous results, namely immunostaining in the molecular layer (Veh et al., 1995) and MgTx-binding experiments (Koch et al., 1997).

Summing up, results indicate that not only the protein expression pattern (namely, Kv1.3 channel) and consequent pharmacological properties of the cell current (MgTx-sensitive current) seem to be variant in dorsal and ventral cells, but also the biophysical properties may be uneven throughout the dorsal-ventral hippocampal axis, as shown by modified kinetic features (I_{fast}) and in the current density of various current components (I_{fast}, I_{slow} and I_{ss}).

These differences arose when the animal was fed. Otherwise (in fasting conditions), no difference was significant besides the expression pattern of the Kv1.3 protein between the

dorsal and ventral hippocampus, disclosed by immunohistochemistry. Even in fasting conditions, Kv1.3 associated fluorescence was still higher in the dorsal than in the ventral hippocampus, but the difference was less significant than the one found when comparing dorsal and ventral hippocampus of a fed rat. Perhaps, this is so because during fasting, the expression of Kv1.3 decreases in all the Kv1.3 expressing neurons, to a level that enables an adequate resolution to detect further differences, in this case, of regional nature. Alternatively, other considerations can be considered as following.

5.1.3 Are CA1 pyramidal cells from the dorsal and ventral hippocampus evenly dependent on the rat's feeding cycle?

Evidence points toward a different role of dorsal and ventral hippocampus in the metabolic processes regulated by the fasting/fed cycle.

In fact, most of the differences described before (see 5.1.1Is the Kv1.3 expression and whole-cell current in CA1 pyramidal cells dependent on the rat's feeding cycle?) are true only in neurons deriving from the dorsal portion of the hippocampus. In ventral hippocampus, only a minimally significant voltage-dependence shift was observed in I_{slow} and I_{ss} (*, $p \le 0,05$). The remaining differences (faster kinetics when fed; depolarized voltage-dependence of activation for all current components when fasting; greater MgTx-sensitive currents when fed) were not significantly different in ventral hippocampus. Hence, it is the dorsal hippocampus that is most affected by feeding cycle.

The fact that the two portions of the hippocampus may play different roles in the metabolic process is not unexpected, and evidence comes along with results that reveal that the different hippocampal portions may have distinct functions and connectivity patterns.

Extensive studies on the dorsal and ventral hippocampus contributions to spatial memory have been carried out. It has been shown that dorsal lesions have a more striking effect on behaviour than ventral lesions (Hughes, 1965, Nadel, 1968, Stevens and Cowey, 1973, Sinnamon et al., 1978, Volpe et al., 1992, Olsen et al., 1994), and that the impairment is proportional to the dorsal lesion extent. This comes in accordance to the premise that visual sensory information is channelled to the dorsal, but not the ventral, hippocampus and gives raise to the assumption that this partition of the information is maintained within the hippocampus and, therefore, the hippocampus can be regarded as a sectioned structure (Moser and Moser, 1998). Furthermore, the dorsal hippocampus has a higher resolution regarding place localization, as place fields get progressively larger, and the probability of observing a field in a given environment gets progressively smaller towards the ventral hippocampus (probably non-linearly) (Tanaka et al., 2012). The ventral hippocampus may also have a neuronal backing for forgetting/erasing (by perturbation of the cellular events that induce and/or stabilize LTP through adenosine receptor A1), giving a new depth to what are the hippocampal classical

functions in memory (Colgin et al., 2004b, Colgin et al., 2004a).Notwithstanding, several studies refer that the ventral hippocampus is concerned of regulation of behaviour (Felice et al., 2012, Fanselow and Dong, 2010), namely (un)conditioned fear-related (Kjelstrup et al., 2002). There is reason to believe, however, that this ventral hippocampus circuitry is more concerned of anxiety-related behaviour rather than fear itself, which is comprised in the amygdala (Bannerman Dm Fau - Rawlins et al.). The intermediate hippocampus is thought to have an integrative function in this regard (Bast et al., 2009), namely in translating cognitive and spatial knowledge into motivation and action. It is thought to control behavioural performance requiring rapid place learning which is critical for survival (Bast et al., 2009, Fanselow and Dong, 2010).

Moreover, the afferent and efferent connections of the hippocampus are not uniform along the hippocampus. On the caudal side, the connections seem to respect previous partitions on the information flow from and to the entorhinal cortex (which is divided in 3 layers), as projections from each layer reach distinct portions of the hippocampus longitudinally and reciprocally (Ruth et al., 1982, Dolorfo and Amaral, 1998a, Dolorfo and Amaral, 1998b, Deacon et al., 1983, Naber et al., 1997, Burwell and Amaral, 1998a, Burwell and Amaral, 1998b, Köhler, 1985, Van Groen and Wyss, 1990, Moser and Moser, 1998, Sugar et al., 2011). This way, the visual, auditory and somatosensory information is conveyed to the dorsal, but not the ventral, portion of the hippocampus. As to the rostral side of the hippocampus, the connections from dorsal/ventral portions project to cytoarchitectonically different sectors of, for example, the lateral septum or the amygdala (Swanson and Cowan, 1977, Van Groen and Wyss, 1990, Risold and Swanson, 1996, Risold and Swanson, 1997). As the hippocampus inputs and outputs are diverse throughout the dorsal-ventral axis, different functions and constitutions can be implied (Moser and Moser, 1998). According to (Bannerman Dm Fau - Rawlins et al.) the dorsal subregion, defined as 50% of hippocampal volume starting at the septal pole, and sometimes referred to as posterior hippocampus in primates (or septal hippocampus, although it is not exactly the same), has a preferential role in spatial learning and memory, and the ventral subregion, defined as 50% of hippocampal volume starting at the temporal pole, and sometimes referred to as anterior hippocampus in primates (or temporal hippocampus, although it is not exactly the same), may have a preferential role in anxiety-related behaviours as a consequence.

K^+ currents differences observed in this project between the two portions of the hippocampus may reflect diverse CA1 pyramidal cells roles in the respective hippocampal portion functions. As seen previously, the dorsal portion of the hippocampus is involved in memory formation more than the ventral counterpart. The reinforcement of long-term synaptic plasticity requires excitability fluctuations and therefor may benefit from cyclic changes in K^+

currents, as those provided by the feeding cycle. This may contribute to the understanding of the intuitive notion that the feeding cycle affects the way one learns.

5.2 CONCLUSIVE REMARKS

The major conclusions of the project answer the goals as follows:

- *K^+ whole-cell currents are affected by metabolic condition (feeding cycle), in their biophysical as well as pharmacological properties;*
- *The hippocampus is not homogenous regarding K^+ biophysical and pharmacological properties, nor in Kv1.3 protein expression pattern;*
- *Kv1.3 may be responsible for heterogeneous K^+ currents profiles within the dorsoventral axis of the hippocampus but a more complex system is in place according to the metabolic condition.*

Overall, results strongly suggest that marked differences denote that there are important differences in CA1 pyramidal pyramidal neurons from fasting and fed rats and from dorsal and ventral regions of the hippocampus.

Hence, results presented in this project challenge the idea of the brain as a sealed entity, unchanged by the peripheral variations in the metabolic condition. It also further challenges the classical idea of CA1 pyramidal cells as a homogenous population dedicated to consolidation of memories neuronal circuits.

Although the physiological relevance of the results is not clear in the context of the current state of the art, one put forward the hypothesis that they are involved in neuroexcitability modulation. As K^+ channels are repolarizing channels rather than depolarizing ones, their connection with increased neuroexcitability is not direct. Their participation in such neuronal performance modulation is usually by more rapidly restoring the resting membrane potential, enabling a shorter interspike interval. Moreover, the dynamic regulation of excitability can modify neuron's behaviour, neuronal signalling and consequentially plasticity. Aberrant expression, localization and function of ion channels are the basis for ionic channels-based pathophysiologies, also known as channelopathies. (Cannon, 2006, Gribkoff and Kaczmarek, 2008). Kv1 regulation failures (on expression, localization or function) can lead to hyperexcitability-derived pathologies, namely epilepsy and ataxia (Gribkoff and Kaczmarek, 2008). Kv1.3 has been recently reported as a potential pharmacological target for diabetes in the periphery (Choi and Hahn, 2010). Hence, current clamp recordings should be done in the future to assess the real physiological implications of these findings.

Finally, one can only speculate on the physiological relevance of those different neuroexcitability profiles (according to the feeding cycle). They may be associated with primary

instincts such as survivor behaviour, lowering the brain functions to a minimum and using spatial memories to find prey, in fasting conditions. Also, they may have to do with memory formation itself, in fed conditions, as K^+ repolarization is essential for consolidation of plasticity events.

5.3 FUTURE PERSPECTIVES

The challenged idea of a "sealed brain", shown by the variations of a single protein expression and function (translated into currents), opens up a lot of possibilities regarding future work. Also, the neuroexcitability CA1 pyramidal cell's features will have to be further studied, for example, by current clamp recordings with brain slices or, even, by *in vivo* recordings. Current clamp would refine the study of cell excitability, and extracellular recording (in dorsal hippocampal slices) would open up the study to the repercussions of the observed neuroexcitability modifications onto synaptic performance.

Regarding the pathways involved in metabolic conditioning of the hippocampal cells, a study should be focused on dorsal hippocampal neurons alone. That said, it could also be advantageous to study more time periods (fed, short-term fasting, as well as the long-term one), as the general picture could become clearer in terms of the time-course of the modifications. Diabetic and obese models (ZDF, OZR, with the respective control – LZR rats) could be studied in tandem with fasting and fed rats to further elaborate Kv1.3/InsR interconnections.

To have a more comprehensive frame on K^+ currents modifications, inactivation profiles, using a two pulse experiment should be conducted. (Standen et al., 1987). The voltage dependence of steady state of inactivation should be suited in the context of the feeding cycle and the different anatomical regions now detected.

In order to evaluate the Kv1.3 expression levels, quantitative PCR analysis, combined with western blot would be ideal, especially if it could accommodate the study of post-translationally modified forms. The only known post-translational modifications described for Kv1 channels are asparagine N-linked glycosylation and phosphorylation of α subunits and phosphorylation of β subunits (Gribkoff and Kaczmarek, 2008). Both have been described for Kv1.3 – while N-glycosylation promotes the cell surface expression of Kv1.3 potassium channels(Zhu et al., 2012), tyrosine phosphorylation of Kv1.3's α subunits impacts it's function in the membrane (Holmes et al., 1996).This would be a resourceful approach, as it could give information about altered protein expression and it's subcellular localization (through a subcellular fractionation protocol).

In a longer future, a ground breaking procedure would be to study the synaptic performance of hippocampal slices' neurons of Kv1.3$^{+/-}$,or even Kv1.3$^{-/-}$, mice (described in (Fadool et al., 2004)).

Noteworthy, regarding the dorsal-ventral axis of the hippocampus, it would be useful to further study the cell's capacitance and modifications in other ion channels (mainly Na^+ and Ca^{2+}).

This page was intentionally left blank.

REFERENCES

ÅBERG, M. A., ÅBERG, N. D., HEDBÄCKER, H., OSCARSSON, J. & ERIKSSON, P. S. 2000. Peripheral infusion of IGF-I selectively induces neurogenesis in the adult rat hippocampus. *The Journal of Neuroscience,* 20**,** 2896-2903.

ALSHUAIB, W., HASAN, S., CHERIAN, S., MATHEW, M., HASAN, M. & FAHIM, M. 2001. Reduced potassium currents in old rat CA1 hippocampal neurons. *Journal of neuroscience research,* 63**,** 176-184.

ALVARADO, M. C., WRIGHT, A. A. & BACHEVALIER, J. 2002. Object and spatial relational memory in adult rhesus monkeys is impaired by neonatal lesions of the hippocampal formation but not the amygdaloid complex. *Hippocampus,* 12**,** 421-433.

ANDERSON, P., BLISS, T. & SKREDE, K. 1971. Lamellar organization of hippocampal pathways. *Experimental brain research. Experimentelle Hirnforschung. Experimentation cerebrale,* 13**,** 222.

APLAND, J. P., FIGUEIREDO, T. H., QASHU, F., ARONIADOU-ANDERJASKA, V., SOUZA, A. P. & BRAGA, M. F. 2010. Higher susceptibility of the ventral versus the dorsal hippocampus and the posteroventral versus anterodorsal amygdala to soman-induced neuropathology. *Neurotoxicology,* 31**,** 485-492.

BANKS, W. A. 2004. The source of cerebral insulin. *European journal of pharmacology,* 490**,** 5-12.

BANKS, W. A., OWEN, J. B. & ERICKSON, M. A. 2012. Insulin in the brain: There and back again. *Pharmacology & Therapeutics*.

BANNERMAN DM FAU - RAWLINS, J. N. P., RAWLINS JN FAU - MCHUGH, S. B., MCHUGH SB FAU - DEACON, R. M. J., DEACON RM FAU - YEE, B. K., YEE BK FAU - BAST, T., BAST T FAU - ZHANG, W. N., ZHANG WN FAU - POTHUIZEN, H. H. J., POTHUIZEN HH FAU - FELDON, J. & FELDON, J. Regional dissociations within the hippocampus--memory and anxiety.

BAST, T., WILSON, I. A., WITTER, M. P. & MORRIS, R. G. 2009. From rapid place learning to behavioral performance: a key role for the intermediate hippocampus. *PLoS biology,* 7**,** e1000089.

BAYASCAS, J. R. 2008. Dissecting the role of the 3-phosphoinositide-dependent protein kinase-1 (PDK1) signalling pathways. *Cell Cycle,* 7**,** 2978-2982.

BEDNARCZYK, P., KOWALCZYK, J. E., BERESEWICZ, M., DOLOWY, K., SZEWCZYK, A. & ZABLOCKA, B. 2010. Identification of a voltage-gated potassium channel in gerbil hippocampal mitochondria. *Biochem Biophys Res Commun,* 397**,** 614-20.

BEETON, C., PENNINGTON, M. W., WULFF, H., SINGH, S., NUGENT, D., CROSSLEY, G., KHAYTIN, I., CALABRESI, P. A., CHEN, C.-Y. & GUTMAN, G. A. 2005. Targeting effector memory T cells with a selective peptide inhibitor of Kv1. 3 channels for therapy of autoimmune diseases. *Molecular pharmacology,* 67**,** 1369-1381.

BEETON, C., WULFF, H., STANDIFER, N. E., AZAM, P., MULLEN, K. M., PENNINGTON, M. W., KOLSKI-ANDREACO, A., WEI, E., GRINO, A. & COUNTS, D. R. 2006. Kv1. 3 channels are a therapeutic target for T cell-mediated autoimmune diseases. *Proceedings of the National Academy of Sciences,* 103**,** 17414-17419.

BERGMAN, R. N., ADER, M., HUECKING, K. & VAN CITTERS, G. 2002. Accurate assessment of β-cell function the hyperbolic correction. *Diabetes,* 51**,** S212-S220.

BLASCO‐IBÁÑEZ, J. & FREUND, T. 1997. Distribution, ultrastructure, and connectivity of calretinin‐immunoreactive mossy cells of the mouse dentate gyrus. *Hippocampus,* 7**,** 307-320.

BRAMMAR, W. J. 1998. *Ion Channel Factsbook: Voltage-Gated Channels*, Access Online via Elsevier.

BUNSEY, M. & EICHENBAUM, H. 1995. Selective damage to the hippocampal region blocks long‐term retention of a natural and nonspatial stimulus‐stimulus association. *Hippocampus,* 5**,** 546-556.

BURWELL, R. D. & AMARAL, D. G. 1998a. Cortical afferents of the perirhinal, postrhinal, and entorhinal cortices of the rat. *The Journal of comparative neurology,* 398**,** 179-205.

BURWELL, R. D. & AMARAL, D. G. 1998b. Perirhinal and postrhinal cortices of the rat: interconnectivity and connections with the entorhinal cortex. *Journal of Comparative Neurology,* 391**,** 293-321.

BYRNE, J. H. & ROBERTS, J. L. 2009. *From molecules to networks: an introduction to cellular and molecular neuroscience*, Access Online via Elsevier.

CAHALAN, M. D. & CHANDY, K. G. 1997. Ion channels in the immune system as targets for immunosuppression. *Current opinion in biotechnology,* 8**,** 749-756.

CANNON, S. C. 2006. Pathomechanisms in channelopathies of skeletal muscle and brain. *Annu. Rev. Neurosci.,* 29**,** 387-415.

CARRO, E., TREJO, J. L., BUSIGUINA, S. & TORRES-ALEMAN, I. 2001. Circulating insulin-like growth factor I mediates the protective effects of physical exercise against brain insults of different etiology and anatomy. *The Journal of Neuroscience,* 21**,** 5678-5684.

CHANG, X., JØRGENSEN, A. M. M., BARDRUM, P. & LED, J. J. 1997. Solution structures of the R6 human insulin hexamer. *Biochemistry,* 36**,** 9409-9422.

CHEATHAM, B., VLAHOS, C. J., CHEATHAM, L., WANG, L., BLENIS, J. & KAHN, C. R. 1994. Phosphatidylinositol 3-kinase activation is required for insulin stimulation of pp70 S6 kinase, DNA synthesis, and glucose transporter translocation. *Molecular and cellular biology,* 14**,** 4902-4911.

CHEUNG, T. H. & CARDINAL, R. N. 2005. Hippocampal lesions facilitate instrumental learning with delayed reinforcement but induce impulsive choice in rats. *BMC neuroscience,* 6**,** 36.

CHIH, C.-P., LIPTON, P. & ROBERTS JR, E. L. 2001. Do active cerebral neurons really use lactate rather than glucose? *Trends in neurosciences,* 24**,** 573-578.

CHOI, B. H. & HAHN, S. J. 2010. Kv1. 3: a potential pharmacological target for diabetes. *Acta Pharmacologica Sinica,* 31**,** 1031-1035.

CLARKE, D. D. & SOKOLOFF, L. 1999. Circulation and energy metabolism of the brain. *Basic neurochemistry: molecular, cellular and medical aspects,* 6.

COETZEE, W. A., AMARILLO, Y., CHIU, J., CHOW, A., LAU, D., MCCORMACK, T., MORENA, H., NADAL, M. S., OZAITA, A. & POUNTNEY, D. 1999. Molecular diversity of K+ channels. *Annals of the New York Academy of Sciences,* 868**,** 233-255.

COLGIN, L. L., KUBOTA, D., BRUCHER, F. A., JIA, Y., BRANYAN, E., GALL, C. M. & LYNCH, G. 2004a. Spontaneous waves in the dentate gyrus of slices from the ventral hippocampus. *Journal of neurophysiology,* 92**,** 3385-3398.

COLGIN, L. L., KUBOTA, D., JIA, Y., REX, C. S. & LYNCH, G. 2004b. Long-term potentiation is impaired in rat hippocampal slices that produce spontaneous sharp waves. *The Journal of physiology,* 558**,** 953-961.

COSTA, P., SANTOS, A. & RIBEIRO, M. 1994. Potassium currents in acutely isolated maturing rat hippocampal CA1 neurones. *Brain research. Developmental brain research,* 83, 216.

COSTA, P. F. 1996. The kinetic parameters of sodium currents in maturing acutely isolated rat hippocampal CA1 neurones. *Developmental brain research,* 91**,** 29-40.

CRAFT, S. 2007. Insulin Resistance and Alzheimers Disease Pathogenesis: Potential Mechanisms and Implications for Treatment. *Current Alzheimer Research,* 4**,** 147-152.

CRAFT, S., ASTHANA, S., COOK, D. G., BAKER, L. D., CHERRIER, M., PURGANAN, K., WAIT, C., PETROVA, A., LATENDRESSE, S. & WATSON, G. 2003. Insulin dose–response effects on memory and plasma amyloid precursor protein in Alzheimer's disease: interactions with apolipoprotein E genotype. *Psychoneuroendocrinology,* 28**,** 809-822.

CRAFT, S., ASTHANA, S., NEWCOMER, J. W., WILKINSON, C. W., MATOS, I. T., BAKER, L. D., CHERRIER, M., LOFGREEN, C., LATENDRESSE, S. & PETROVA, A. 1999. Enhancement of memory in Alzheimer disease with insulin and somatostatin, but not glucose. *Archives of general psychiatry,* 56**,** 1135.

CRAFT, S., NEWCOMER, J., KANNE, S., DAGOGO-JACK, S., CRYER, P., SHELINE, Y., LUBY, J., DAGOGO-JACK, A. & ALDERSON, A. 1996. Memory improvement following induced hyperinsulinemia in Alzheimer's disease. *Neurobiology of aging,* 17**,** 123-130.

CRAFT, S. & STENNIS WATSON, G. 2004. Insulin and neurodegenerative disease: shared and specific mechanisms. *The lancet neurology,* 3**,** 169-178.

D. GRANT, L. & JARRARD, L. E. 1968. Functional dissociation within hippocampus. *Brain Research,* 10**,** 392-401.

DAS, P., PARSONS, A., SCARBOROUGH, J., HOFFMAN, J., WILSON, J., THOMPSON, R., OVERTON, J. & FADOOL, D. 2005. Electrophysiological and behavioral phenotype of insulin receptor defective mice. *Physiology & behavior,* 86**,** 287-296.

DAVIDSON, T. L. & JARRARD, L. E. 1993. A role for hippocampus in the utilization of hunger signals. *Behavioral and neural biology,* 59**,** 167-171.

DE LA MONTE, S. M., NEUSNER, A., CHU, J. & LAWTON, M. 2009. Epidemiological trends strongly suggest exposures as etiologic agents in the pathogenesis of sporadic Alzheimer's disease, diabetes mellitus, and non-alcoholic steatohepatitis. *Journal of Alzheimer's Disease,* 17**,** 519-529.

DE LA MONTE, S. M., TONG, M., LESTER-COLL, N., PLATER, J., MICHAEL & WANDS, J. R. 2006. Therapeutic rescue of neurodegeneration in experimental type 3 diabetes: relevance to Alzheimer's disease. *Journal of Alzheimer's Disease,* 10**,** 89-109.

DE LA MONTE, S. M. & WANDS, J. R. 2005. Review of insulin and insulin-like growth factor expression, signaling, and malfunction in the central nervous system: relevance to Alzheimer's disease. *Journal of Alzheimer's Disease,* 7**,** 45-61.

DE MEYTS, P. 2004. Insulin and its receptor: structure, function and evolution. *Bioessays,* 26**,** 1351-1362.

DE MEYTS, P. & WHITTAKER, J. 2002. Structural biology of insulin and IGF1 receptors: implications for drug design. *Nature Reviews Drug Discovery,* 1**,** 769-783.

DEACON, T. W., EICHENBAUM, H., ROSENBERG, P. & ECKMANN, K. W. 1983. Afferent connections of the perirhinal cortex in the rat. *Journal of Comparative Neurology,* 220**,** 168-190.

DOLORFO, C. L. & AMARAL, D. G. 1998a. Entorhinal cortex of the rat: organization of intrinsic connections. *Journal of Comparative Neurology,* 398**,** 49-82.

DOLORFO, C. L. & AMARAL, D. G. 1998b. Entorhinal cortex of the rat: topographic organization of the cells of origin of the perforant path projection to the dentate gyrus. *Journal of Comparative Neurology,* 398**,** 25-48.

DONG, H. W., SWANSON, L. W., CHEN, L., FANSELOW, M. S. & TOGA, A. W. 2009. Genomic-anatomic evidence for distinct functional domains in hippocampal field CA1. *Proc Natl Acad Sci U S A,* 106**,** 11794-9.

DOUGHERTY, K. A., ISLAM, T. & JOHNSTON, D. 2012. Intrinsic Excitability of CA1 Pyramidal Neurones from the Rat Dorsal and Ventral Hippocampus. *The Journal of Physiology.*

DOUGHERTY, K. A., NICHOLSON, D. A., DIAZ, L. M., BUSS, E. W., NEUMAN, K. M., CHETKOVICH, D. M. & JOHNSTON, D. 2013. Differential Expression of HCN Subunits Alters Voltage-Dependent Gating of h-channels in CA1 Pyramidal Neurons from the Dorsal and Ventral Hippocampus. *J Neurophysiol*.

DOYLE, D. A., CABRAL, J. M., PFUETZNER, R. A., KUO, A., GULBIS, J. M., COHEN, S. L., CHAIT, B. T. & MACKINNON, R. 1998. The structure of the potassium channel: molecular basis of K+ conduction and selectivity. *science,* 280**,** 69-77.

DUARTE, A. I., SANTOS, P., OLIVEIRA, C. R., SANTOS, M. S. & REGO, A. C. 2008. Insulin neuroprotection against oxidative stress is mediated by Akt and GSK-3 β signaling pathways and changes in protein expression. *Biochimica et Biophysica Acta (BBA)-Molecular Cell Research,* 1783**,** 994-1002.

DUFF, K., KNIGHT, H., REFOLO, L., SANDERS, S., YU, X., PICCIANO, M., MALESTER, B., HUTTON, M., ADAMSON, J. & GOEDERT, M. 2000. Characterization of pathology in transgenic mice over-expressing human genomic and cDNA tau transgenes. *Neurobiology of disease,* 7**,** 87-98.

DUNN, M. F. 2005. Zinc–ligand interactions modulate assembly and stability of the insulin hexamer–a review. *Biometals,* 18**,** 295-303.

EDINGER, H., SIEGEL, A. & TROIANO, R. 1973. Single unit analysis of the hippocampal projections to the septum in the cat. *Experimental Neurology,* 41**,** 569-583.

EICHENBAUM, H. 1996. Is the rodent hippocampus just for 'place'? *Current Opinion in Neurobiology,* 6**,** 187-195.

EICHENBAUM, H. 2004. Hippocampus: cognitive processes and neural representations that underlie declarative memory. *Neuron,* 44**,** 109-120.

ELSAYED, A. M. 2012. Oral Delivery of Insulin: Novel Approaches.

ELUL, R. 1964. Regional differences in the hippocampus of the cat. *Electroencephalography and Clinical Neurophysiology,* 16**,** 470-488.

FADOOL, D., TUCKER, K., PERKINS, R., FASCIANI, G., THOMPSON, R., PARSONS, A., OVERTON, J., KONI, P., FLAVELL, R. & KACZMAREK, L. 2004. Kv1. 3 channel gene-targeted deletion produces "Super-Smeller Mice" with altered glomeruli, interacting scaffolding proteins, and biophysics. *Neuron,* 41**,** 389-404.

FADOOL, D., TUCKER, K., PHILLIPS, J. & SIMMEN, J. 2000. Brain insulin receptor causes activity-dependent current suppression in the olfactory bulb through multiple phosphorylation of Kv1. 3. *Journal of neurophysiology,* 83**,** 2332-2348.

FANSELOW, M. S. & DONG, H. W. 2010. Are the dorsal and ventral hippocampus functionally distinct structures? *Neuron,* 65**,** 7-19.

FEHM, H. L., PERRAS, B., SMOLNIK, R., KERN, W. & BORN, J. 2000. Manipulating neuropeptidergic pathways in humans: a novel approach to neuropharmacology? *European journal of pharmacology,* 405**,** 43-54.

FELICE, D., O'LEARY, O. F., PIZZO, R. C. & CRYAN, J. F. 2012. Blockade of the GABA< sub> B</sub> receptor increases neurogenesis in the ventral but not dorsal adult hippocampus: Relevance to antidepressant action. *Neuropharmacology*.

FERNÁNDEZ, G., WEYERTS, H., SCHRADER-BÖLSCHE, M., TENDOLKAR, I., SMID, H. G., TEMPELMANN, C., HINRICHS, H., SCHEICH, H., ELGER, C. E. & MANGUN, G. R. 1998. Successful verbal encoding into episodic memory engages the posterior hippocampus: a parametrically analyzed functional magnetic resonance imaging study. *The Journal of Neuroscience,* 18**,** 1841-1847.

FRÖLICH, L., BLUM-DEGEN, D., BERNSTEIN, H.-G., ENGELSBERGER, S., HUMRICH, J., LAUFER, S., MUSCHNER, D., THALHEIMER, A., TÜRK, A. & HOYER, S. 1998. Brain insulin and insulin receptors in aging and sporadic Alzheimer's disease. *Journal of neural transmission,* 105**,** 423-438.

FULKS, R. M., LI, J. B. & GOLDBERG, A. L. 1975. Effects of insulin, glucose, and amino acids on protein turnover in rat diaphragm. *Journal of Biological Chemistry,* 250**,** 290-298.

FUSTER-MATANZO, A., LLORENS-MARTÍN, M., DE BARREDA, E. G., ÁVILA, J. & HERNÁNDEZ, F. 2011. Different Susceptibility to Neurodegeneration of Dorsal and Ventral Hippocampal Dentate Gyrus: A Study with Transgenic Mice Overexpressing GSK3 β. *PloS one,* 6**,** e27262.

GAGE, F. H. & THOMPSON, R. G. 1980. Differential distribution of norepinephrine and serotonin along the dorsal-ventral axis of the hippocampal formation. *Brain Res Bull,* 5**,** 771-3.

GAGE, F. H., THOMPSON, R. G. & VALDES, J. J. 1978. Endogenous norepinephrine and serotonin within the hippocampal formation during the development and recovery from septal hyperactivity. *Pharmacology Biochemistry and Behavior,* 9**,** 359-367.

GARCIA-CALVO, M., LEONARD, R., NOVICK, J., STEVENS, S., SCHMALHOFER, W., KACZOROWSKI, G. & GARCIA, M. 1993. Purification, characterization, and biosynthesis of margatoxin, a component of Centruroides margaritatus venom that selectively inhibits voltage-dependent potassium channels. *Journal of Biological Chemistry,* 268**,** 18866-18874.

GASPARINI, L., NETZER, W. J., GREENGARD, P. & XU, H. 2002. Does insulin dysfunction play a role in Alzheimer's disease? *Trends in pharmacological sciences,* 23**,** 288-293.

GILBERT, M., RACINE, R. & SMITH, G. 1985. Epileptiform burst responses in ventral vs dorsal hippocampal slices. *Brain research,* 361**,** 389-391.

GRIBKOFF, V. K. & KACZMAREK, L. K. 2008. *Structure, function and modulation of neuronal voltage-gated ion channels*, Wiley. com.

GRIGORYAN, G., KORKOTIAN, E. & SEGAL, M. 2012. Selective facilitation of LTP in the ventral hippocampus by calcium stores. *Hippocampus,* 22**,** 1635-1644.

GROSSE, G., DRAGUHN, A., HÖHNE, L., TAPP, R., VEH, R. W. & AHNERT-HILGER, G. 2000. Expression of Kv1 potassium channels in mouse hippocampal primary cultures: development and activity-dependent regulation. *The Journal of Neuroscience,* 20**,** 1869-1882.

GU, C., JAN, Y. N. & JAN, L. Y. 2003. A conserved domain in axonal targeting of Kv1 (Shaker) voltage-gated potassium channels. *Science,* 301**,** 646-649.

GUAL, P., GRÉMEAUX, T., GONZALEZ, T., BARRÈS, R. & TANTI, J. 2003. Fatty acid-induced insulin resistance: role of insulin receptor substrate 1 serine phosphorylation in the retroregulation of insulin signalling. *Biochemical Society Transactions,* 31**,** 1152-1156.

GUNGOR, N., BACHA, F., SAAD, R., JANOSKY, J. & ARSLANIAN, S. 2005. Youth Type 2 Diabetes Insulin resistance, β-cell failure, or both? *Diabetes Care,* 28**,** 638-644.

GUTMAN, G. A., CHANDY, K. G., GRISSMER, S., LAZDUNSKI, M., MCKINNON, D., PARDO, L. A., ROBERTSON, G. A., RUDY, B., SANGUINETTI, M. C. & STÜHMER, W. 2005. International Union of Pharmacology. LIII. Nomenclature and molecular relationships of voltage-gated potassium channels. *Pharmacological reviews,* 57**,** 473-508.

HAWLEY, D. F., MORCH, K., CHRISTIE, B. R. & LEASURE, J. L. 2012. Differential Response of Hippocampal Subregions to Stress and Learning. *PLoS ONE,* 7**,** e53126.

HEGINBOTHAM, L., LU, Z., ABRAMSON, T. & MACKINNON, R. 1994. Mutations in the K+ channel signature sequence. *Biophysical Journal,* 66**,** 1061-1067.

HENQUIN, J.-C. 2000. Triggering and amplifying pathways of regulation of insulin secretion by glucose. *Diabetes,* 49**,** 1751-1760.

HEUSSER, K. & SCHWAPPACH, B. 2005. Trafficking of potassium channels. *Current opinion in neurobiology,* 15**,** 364-369.

HILLE, B. 1992. *Ion channels of excitable membranes*.

HOLMES, T. C., FADOOL, D. A. & LEVITAN, I. B. 1996. Tyrosine phosphorylation of the Kv1. 3 potassium channel. *The Journal of neuroscience,* 16**,** 1581-1590.

HOYER, S. 2002. The aging brain. Changes in the neuronal insulin/insulin receptor signal transduction cascade trigger late-onset sporadic Alzheimer disease (SAD). A mini-review. *Journal of neural transmission,* 109**,** 991-1002.

HOYER, S. & LANNERT, H. 1999. Inhibition of the Neuronal Insulin Receptor Causes Alzheimer‐like Disturbances in Oxidative/Energy Brain Metabolism and in Behavior in Adult Rats. *Annals of the New York Academy of Sciences,* 893**,** 301-303.

HOYER, S. & NITSCH, R. 1989. Cerebral excess release of neurotransmitter amino acids subsequent to reduced cerebral glucose metabolism in early-onset dementia of Alzheimer type. *Journal of neural transmission,* 75**,** 227-232.

HU, Y. & WILSON, G. S. 1997. A temporary local energy pool coupled to neuronal activity: Fluctuations of extracellular lactate levels in rat brain monitored with rapid‐response enzyme‐based sensor. *Journal of neurochemistry,* 69**,** 1484-1490.

HUGHES, K. R. 1965. Dorsal and ventral hippocampus lesions and maze learning: influence of preoperative environment. *Canadian journal of psychology,* 19**,** 325.

JARRARD, L. E. 1978. Selective hippocampal lesions: Differential effects on performance by rats of a spatial task with preoperative versus postoperative training. *Journal of comparative and physiological psychology,* 92**,** 1119.

JARRARD, L. E. 1991. On the neural bases of the spatial mapping system: Hippocampus vs. hippocampal formation. *Hippocampus,* 1**,** 236-239.

JARRARD, L. E., LUU, L. P. & DAVIDSON, T. L. 2012. A study of hippocampal structure‐function relations along the septo‐temporal axis. *Hippocampus,* 22**,** 680-692.

JOHNSON, C. T., OLTON, D. S., GAGE, F. H. & JENKO, P. G. 1977. Damage to hippocampus and hippocampal connections: effects on DRL and spontaneous alternation. *Journal of comparative and physiological psychology,* 91**,** 508-522.

JOOST, H. G. & THORENS, B. 2001. The extended GLUT-family of sugar/polyol transport facilitators: nomenclature, sequence characteristics, and potential function of its novel members (review). *Mol Membr Biol,* 18**,** 247-56.

KAHN, C. R. & WHITE, M. 1988. The insulin receptor and the molecular mechanism of insulin action. *Journal of Clinical Investigation,* 82**,** 1151.

KAHN, S. 2003. The relative contributions of insulin resistance and beta-cell dysfunction to the pathophysiology of type 2 diabetes. *Diabetologia,* 46**,** 3-19.

KAZARIAN, A. L., HEKIMIAN, A. A., HARUTIUNIAN-KOZAK, B. A. & GRIGORIAN, G. G. 1995. Responses of cat's dorsal hippocampal neurones to moving visual stimuli. *Acta Neurobiologiae Experimentalis*.

KIM, D. S., KIM, J. E., KWAK, S. E., WON, M. H. & KANG, T. C. 2007. Seizure activity affects neuroglial Kv1 channel immunoreactivities in the gerbil hippocampus. *Brain Res,* 1151**,** 172-87.

KJELSTRUP, K. G., TUVNES, F. A., STEFFENACH, H.-A., MURISON, R., MOSER, E. I. & MOSER, M.-B. 2002. Reduced fear expression after lesions of the ventral hippocampus. *Proceedings of the National Academy of Sciences,* 99**,** 10825-10830.

KLEIN, W. L. 2002. A β toxicity in Alzheimer's disease: globular oligomers (ADDLs) as new vaccine and drug targets. *Neurochemistry international,* 41**,** 345-352.

KOCH, R. O., WANNER, S. G., KOSCHAK, A., HANNER, M., SCHWARZER, C., KACZOROWSKI, G. J., SLAUGHTER, R. S., GARCIA, M. L. & KNAUS, H.-G. 1997. Complex subunit assembly of neuronal voltage-gated K+ channels basis for high-affinity toxin interactions and pharmacology. *Journal of Biological Chemistry,* 272**,** 27577-27581.

KÖHLER, C. 1985. Intrinsic projections of the retrohippocampal region in the rat brain. I. The subicular complex. *Journal of Comparative Neurology,* 236**,** 504-522.

KOSOLAPOV, A. & DEUTSCH, C. 2003. Folding of the voltage-gated K+ channel T1 recognition domain. *Journal of Biological Chemistry,* 278**,** 4305-4313.

KOURRICH, S., MANRIQUE, C., SALIN, P. & MOURRE, C. 2005. Transient hippocampal down-regulation of Kv1.1 subunit mRNA during associative learning in rats. *Learn Mem,* 12**,** 511-9.

KUPPER, J., PRINZ, A. A. & FROMHERZ, P. 2002. Recombinant Kv1.3 potassium channels stabilize tonic firing of cultured rat hippocampal neurons. *Pflugers Arch,* 443**,** 541-7.

LANDRETH, G. 2007. Therapeutic Use of Agonists of the Nuclear Receptor PPAR in Alzheimers Disease. *Current Alzheimer Research,* 4**,** 159-164.

LEIN, E. S., HAWRYLYCZ, M. J., AO, N., AYRES, M., BENSINGER, A., BERNARD, A., BOE, A. F., BOGUSKI, M. S., BROCKWAY, K. S. & BYRNES, E. J. 2006. Genome-wide atlas of gene expression in the adult mouse brain. *Nature,* 445**,** 168-176.

LESTER-COLL, N., RIVERA, E. J., SOSCIA, S. J., DOIRON, K., WANDS, J. R. & DE LA MONTE, S. M. 2006. Intracerebral streptozotocin model of type 3 diabetes: relevance to sporadic Alzheimer's disease. *Journal of Alzheimer's Disease,* 9**,** 13-33.

LEWIS, R. S. & CAHALAN, M. D. 1995. Potassium and calcium channels in lymphocytes. *Annual review of immunology,* 13**,** 623-653.

LEYBAERT, L. 2005. Neurobarrier coupling in the brain: a partner of neurovascular and neurometabolic coupling? *J Cereb Blood Flow Metab,* 25**,** 2-16.

LEYBAERT, L., DE BOCK, M., VAN MOORHEM, M., DECROCK, E. & DE VUYST, E. 2007. Neurobarrier coupling in the brain: adjusting glucose entry with demand. *J Neurosci Res,* 85**,** 3213-20.

LIMA P.A. (1), C. P. C., MONDRAGÃO M. (1), ALVES F.M. (1), COSTA G. (1), HARDY D. (3), JALIL A. (3), DAVID O. (3) & AUGER C. (3) 2012. Metabolic states induced by feeding/fasting influence insulin-induced excitability and levels of insulin receptor in hippocampal but not cerebellar neurons. *Conference: 8th FENS Forum of Neuroscience Abstract book,* Abstract: A-471-0031-03243.

LIMA, P. A., VICENTE, M. I., ALVES, F. M., DIONISIO, J. C. & COSTA, P. F. 2008. Insulin increases excitability via a dose-dependent dual inhibition of voltage-activated K+ currents in differentiated N1E-115 neuroblastoma cells. *Eur J Neurosci,* 27**,** 2019-32.

MAGGIO, N. & SEGAL, M. 2007. Striking variations in corticosteroid modulation of long-term potentiation along the septotemporal axis of the hippocampus. *J Neurosci,* 27**,** 5757-65.

MAGISTRETTI, P. J. & PELLERIN, L. 1999. Cellular mechanisms of brain energy metabolism and their relevance to functional brain imaging. *Philos Trans R Soc Lond B Biol Sci,* 354**,** 1155-63.

MAGUIRE, E. A., BURGESS, N., DONNETT, J. G., FRACKOWIAK, R. S., FRITH, C. D. & O'KEEFE, J. 1998. Knowing where and getting there: a human navigation network. *Science,* 280**,** 921-924.

MAGUIRE, E. A., FRACKOWIAK, R. S. & FRITH, C. D. 1997. Recalling routes around London: Activation of the right hippocampus in taxi drivers. *The Journal of Neuroscience,* 17**,** 7103-7110.

MARCELIN, B., LUGO, J. N., BREWSTER, A. L., LIU, Z., LEWIS, A. S., MCCLELLAND, S., CHETKOVICH, D. M., BARAM, T. Z., ANDERSON, A. E., BECKER, A., ESCLAPEZ, M. & BERNARD, C. 2012. Differential dorso-ventral distributions of Kv4.2 and HCN proteins confer distinct integrative properties to hippocampal CA1 pyramidal cell distal dendrites. *J Biol Chem,* 287**,** 17656-61.

MARCHETTI, P., DOTTA, F., LAURO, D. & PURRELLO, F. 2008. An overview of pancreatic beta-cell defects in human type 2 diabetes: implications for treatment. *Regulatory peptides,* 146**,** 4-11.

MARINO-BUSLJE, C., MARTIN-MARTINEZ, M., MIZUGUCHI, K., SIDDLE, K. & BLUNDELL, T. 1999. The insulin receptor: from protein sequence to structure. *Biochemical Society Transactions,* 27**,** 715-726.

MARUKI, K., IZAKI, Y., NOMURA, M. & YAMAUCHI, T. 2001. Differences in paired‐pulse facilitation and long‐term potentiation between dorsal and ventral CA1 regions in anesthetized rats. *Hippocampus,* 11**,** 655-661.

MAURER, A. P., VANRHOADS, S. R., SUTHERLAND, G. R., LIPA, P. & MCNAUGHTON, B. L. 2005. Self‐motion and the origin of differential spatial scaling along the septo‐temporal axis of the hippocampus. *Hippocampus,* 15**,** 841-852.

MAYER, J. P., ZHANG, F. & DIMARCHI, R. D. 2007. Insulin structure and function. *Peptide Science,* 88**,** 687-713.

MCEWEN, B. S. & REAGAN, L. P. 2004. Glucose transporter expression in the central nervous system: relationship to synaptic function. *Eur J Pharmacol,* 490**,** 13-24.

MCNAY, E. C. & GOLD, P. E. 1999. Extracellular Glucose Concentrations in the Rat Hippocampus Measured by Zero‑Net‑Flux. *Journal of neurochemistry,* 72**,** 785-790.

MILNER, B., SQUIRE, L. R. & KANDEL, E. R. 1998. Cognitive Neuroscience Review and the Study of Memory. *Neuron,* 20**,** 445-468.

MONDRAGÃO, M. A. S. 2010. Aspectos fisiológicos da insulina e seu receptor em neurónios do hipocampo.

MOREIRA, P. I., SANTOS, M. S., SENA, C., SEIÇA, R. & OLIVEIRA, C. R. 2005. Insulin protects against amyloid β-peptide toxicity in brain mitochondria of diabetic rats. *Neurobiology of disease,* 18**,** 628-637.

MORRIS, R., GARRUD, P., RAWLINS, J. & O'KEEFE, J. 1982. Place navigation impaired in rats with hippocampal lesions. *Nature,* 297**,** 681-683.

MORRIS, R., SCHENK, F., TWEEDIE, F. & JARRARD, L. 1990. Ibotenate lesions of hippocampus and/or subiculum: dissociating components of allocentric spatial learning. *European Journal of Neuroscience,* 2**,** 1016-1028.

MOSER, E., MOSER, M.-B. & ANDERSEN, P. 1993. Spatial learning impairment parallels the magnitude of dorsal hippocampal lesions, but is hardly present following ventral lesions. *The Journal of neuroscience,* 13**,** 3916-3925.

MOSER, M.-B., MOSER, E. I., FORREST, E., ANDERSEN, P. & MORRIS, R. 1995. Spatial learning with a minislab in the dorsal hippocampus. *Proceedings of the National Academy of Sciences,* 92**,** 9697-9701.

MOSER, M. B. & MOSER, E. I. 1998. Functional differentiation in the hippocampus. *Hippocampus,* 8**,** 608-19.

MULLER, R. 1996. A quarter of a century of place cells. *Neuron,* 17**,** 813.

NABER, P. A., CABALLERO-BLEDA, M., JORRITSMA-BYHAM, B. & WITTER, M. P. 1997. Parallel input to the hippocampal memory system through peri-and postrhinal cortices. *Neuroreport,* 8**,** 2617-2621.

NADEL, L. 1968. Dorsal and ventral hippocampal lesions and behavior. *Physiology & Behavior,* 3**,** 891-900.

NADEL, L. 1991. The hippocampus and space revisited. *Hippocampus,* 1**,** 221-229.

NASCIMENTO, A. M. S. D. 2009. Estudo do papel neuroprotector da insulina a agressões celulares: amilóides, oxidativas e de membrana.

NELSON, T. J., SUN, M.-K., HONGPAISAN, J. & ALKON, D. L. 2008. Insulin, PKC signaling pathways and synaptic remodeling during memory storage and neuronal repair. *European journal of pharmacology,* 585**,** 76-87.

NICOLLS, M. R. 2004. The clinical and biological relationship between type II diabetes mellitus and Alzheimers disease. *Current Alzheimer Research,* 1**,** 47-54.

NYBERG, L., MCLNTOSH, A., HOULE, S., NILSSON, L.-G. & TULVING, E. 1996. Activation of medial temporal structures during episodic memory retrieval. *Nature,* 380**,** 715-717.

O'KEEFE, J. & DOSTROVSKY, J. 1971. The hippocampus as a spatial map: Preliminary evidence from unit activity in the freely-moving rat. *Brain research*.

O'KEEFE, J. & NADEL, L. 1978. *The hippocampus as a cognitive map*, Clarendon Press Oxford.

O'KEEFE, J. & SPEAKMAN, A. 1987. Single unit activity in the rat hippocampus during a spatial memory task. *Experimental Brain Research,* 68**,** 1-27.

O'MALLEY, D. & HARVEY, J. 2004. Insulin activates native and recombinant large conductance Ca2+-activated potassium channels via a mitogen-activated protein kinase-dependent process. *Molecular pharmacology,* 65**,** 1352-1363.

O'MALLEY, D., SHANLEY, L. J. & HARVEY, J. 2003. Insulin inhibits rat hippocampal neurones via activation of ATP-sensitive K< sup>+</sup> and large conductance Ca< sup> 2+</sup>-activated K< sup>+</sup> channels. *Neuropharmacology,* 44**,** 855-863.

OLSEN, G. M., SCHEEL-KRÜGER, J., MØLLER, A. & JENSEN, L. H. 1994. Relation of spatial learning of rats in the Morris water maze task to the number of viable CA1 neurons following four-vessel occlusion. *Behavioral neuroscience,* 108**,** 681.

OLSON, A. L. & PESSIN, J. E. 1996. Structure, function, and regulation of the mammalian facilitative glucose transporter gene family. *Annu Rev Nutr,* 16**,** 235-56.

OLSON, T., BAMBERGER, M. & LANE, M. 1988. Post-translational changes in tertiary and quaternary structure of the insulin proreceptor. Correlation with acquisition of function. *Journal of Biological Chemistry,* 263**,** 7342-7351.

OLTON, D. S., WALKER, J. A. & GAGE, F. H. 1978. Hippocampal connections and spatial discrimination. *Brain research,* 139**,** 295-308.

PAPAZIAN, D. M., SCHWARZ, T. L., TEMPEL, B. L., JAN, Y. N. & JAN, L. Y. 1987. Cloning of genomic and complementary DNA from Shaker, a putative potassium channel gene from Drosophila. *Science,* 237**,** 749-753.

PARK, K. H., CHUNG, Y. H., SHIN, C., KIM, M. J., LEE, B. K., CHO, S. S. & CHA, C. I. 2001. Immunohistochemical study on the distribution of the voltage-gated potassium channels in the gerbil hippocampus. *Neurosci Lett,* 298**,** 29-32.

PASQUIER, D. A. & REINOSO-SUAREZ, F. 1977. Differential efferent connections of the brain stem to the hippocampus in the cat. *Brain Research,* 120**,** 540-548.

PASQUIER, F., BOULOGNE, A., LEYS, D. & FONTAINE, P. 2006. Diabetes mellitus and dementia. *Diabetes & metabolism,* 32**,** 403-414.

PLUM, L., SCHUBERT, M. & BRÜNING, J. C. 2005. The role of insulin receptor signaling in the brain. *Trends in Endocrinology & Metabolism,* 16**,** 59-65.

POPPENK, J., EVENSMOEN, H. R., MOSCOVITCH, M. & NADEL, L. 2013. Long-axis specialization of the human hippocampus. *Trends in cognitive sciences*.

POTHUIZEN, H. H., ZHANG, W. N., JONGEN‐RÊLO, A. L., FELDON, J. & YEE, B. K. 2004. Dissociation of function between the dorsal and the ventral hippocampus in spatial learning abilities of the rat: a within‐subject, within‐task comparison of reference and working spatial memory. *European Journal of Neuroscience,* 19**,** 705-712.

PRUSS, H., GROSSE, G., BRUNK, I., VEH, R. W. & AHNERT-HILGER, G. 2010. Age-dependent axonal expression of potassium channel proteins during development in mouse hippocampus. *Histochem Cell Biol,* 133**,** 301-12.

RACINE, R., ROSE, P. & BURNHAM, W. 1977. Afterdischarge thresholds and kindling rates in dorsal and ventral hippocampus and dentate gyrus. *The Canadian journal of neurological sciences. Le journal canadien des sciences neurologiques,* 4**,** 273.

RAWLINS, J. 1985. Associations across time: The hippocampus as a temporary memory store. *Behav Brain Sci,* 8**,** 479-496.

REGER, M., WATSON, G., GREEN, P., WILKINSON, C., BAKER, L., CHOLERTON, B., FISHEL, M., PLYMATE, S., BREITNER, J. & DEGROODT, W. 2008. Intranasal insulin improves cognition and modulates β-amyloid in early AD. *Neurology,* 70**,** 440-448.

REMPEL-CLOWER, N. L., ZOLA, S. M., SQUIRE, L. R. & AMARAL, D. G. 1996. Three cases of enduring memory impairment after bilateral damage limited to the hippocampal formation. *The Journal of Neuroscience,* 16**,** 5233-5255.

RISOLD, P. & SWANSON, L. 1996. Structural evidence for functional domains in the rat hippocampus. *Science,* 272**,** 1484-1486.

RISOLD, P. & SWANSON, L. 1997. Connections of the rat lateral septal complex. *Brain research reviews,* 24**,** 115-195.

RIVERA, E. J., GOLDIN, A., FULMER, N., TAVARES, R., WANDS, J. R. & DE LA MONTE, S. M. 2005. Insulin and insulin-like growth factor expression and function deteriorate with progression of Alzheimer's disease: link to brain reductions in acetylcholine. *Journal of Alzheimer's Disease,* 8**,** 247-268.

ROBBINS, J. 2001. KCNQ potassium channels: physiology, pathophysiology, and pharmacology. *Pharmacology & therapeutics,* 90**,** 1-19.

ROMBOUTS, S. A., MACHIELSEN, W., WITTER, M. P., BARKHOF, F., LINDEBOOM, J. & SCHELTENS, P. 1997. Visual association encoding activates the medial temporal lobe: a functional magnetic resonance imaging study. *Hippocampus,* 7**,** 594-601.

ROPIREDDY, D., BACHUS, S. E. & ASCOLI, G. A. 2012. Non-homogeneous stereological properties of the rat hippocampus from high-resolution 3D serial reconstruction of thin histological sections. *Neuroscience,* 205**,** 91-111.

RUDY, J. W. & SUTHERLAND, R. J. 1995. Configural association theory and the hippocampal formation: An appraisal and reconfiguration. *Hippocampus,* 5**,** 375-389.

RUS, H., PARDO, C. A., HU, L., DARRAH, E., CUDRICI, C., NICULESCU, T., NICULESCU, F., MULLEN, K. M., ALLIE, R., GUO, L., WULFF, H., BEETON, C., JUDGE, S. I. V., KERR, D. A., KNAUS, H.-G., CHANDY, K. G. & CALABRESI, P. A. 2005. The voltage-gated potassium channel Kv1.3 is highly expressed on inflammatory infiltrates in multiple sclerosis brain. *Proceedings of the National Academy of Sciences of the United States of America,* 102**,** 11094-11099.

RUTH, R. E., COLLIER, T. J. & ROUTTENBERG, A. 1982. Topography between the entorhinal cortex and the dentate septotemporal axis in rats: I. Medial and intermediate entorhinal projecting cells. *Journal of Comparative Neurology,* 209**,** 69-78.

SALTIEL, A. R. & KAHN, C. R. 2001. Insulin signalling and the regulation of glucose and lipid metabolism. *Nature,* 414**,** 799-806.

SCHNEIDER, C. A., RASBAND, W. S. & ELICEIRI, K. W. 2012. NIH Image to ImageJ: 25 years of image analysis. *Nat Methods,* 9**,** 671-675.

SCHUBERT, M., BRAZIL, D. P., BURKS, D. J., KUSHNER, J. A., YE, J., FLINT, C. L., FARHANG-FALLAH, J., DIKKES, P., WAROT, X. M. & RIO, C. 2003. Insulin receptor substrate-2 deficiency impairs brain growth and promotes tau phosphorylation. *The Journal of neuroscience,* 23**,** 7084-7092.

SCHULINGKAMP, R., PAGANO, T., HUNG, D. & RAFFA, R. 2000. Insulin receptors and insulin action in the brain: review and clinical implications. *Neuroscience & Biobehavioral Reviews,* 24**,** 855-872.

SCHULTE, U., THUMFART, J.-O., KLÖCKER, N., SAILER, C. A., BILDL, W., BINIOSSEK, M., DEHN, D., DELLER, T., EBLE, S. & ABBASS, K. 2006. The epilepsy-linked Lgi1 protein assembles into presynaptic Kv1 channels and inhibits inactivation by Kvβ1. *Neuron,* 49**,** 697-706.

SCHURR, A. 2005. Lactate: the ultimate cerebral oxidative energy substrate? *Journal of Cerebral Blood Flow & Metabolism,* 26**,** 142-152.

SCOVILLE, W. B. & MILNER, B. 1957. Loss of recent memory after bilateral hippocampal lesions. *Journal of neurology, neurosurgery, and psychiatry,* 20**,** 11.

SHEPHERD, T. M., ÖZARSLAN, E., KING, M. A., MARECI, T. H. & BLACKBAND, S. J. 2006. Structural insights from high-resolution diffusion tensor imaging and tractography of the isolated rat hippocampus. *Neuroimage,* 32**,** 1499-1509.

SHERMAN-GOLD, R. 1993. The Axon Guide for Electrophysiology & Biophysics Laboratory Techniques. Axon Instruments. *Inc., Foster City, CA,* 94404.

SHIEH, C.-C., COGHLAN, M., SULLIVAN, J. P. & GOPALAKRISHNAN, M. 2000. Potassium channels: molecular defects, diseases, and therapeutic opportunities. *Pharmacological reviews,* 52**,** 557-594.

SHIH, T. M. & GOLDIN, A. L. 1997. Topology of the Shaker potassium channel probed with hydrophilic epitope insertions. *The Journal of cell biology,* 136**,** 1037-1045.

SIEGEL, A. & FLYNN, J. P. 1968. Differential effects of electrical stimulation and lesions of the hippocampus and adjacent regions upon attack behavior in cats. *Brain Research,* 7**,** 252-267.

SIEGEL, A. & TASSONI, J. P. 1971. Differential Efferent Projections of the Lateral and Medial Septal Nuclei to the Hippocampus in the Cat. *Brain, Behavior and Evolution,* 4**,** 201-219.

SINNAMON, H., FRENIERE, S. & KOOTZ, J. 1978. Rat hippocampus and memory for places of changing significance. *Journal of comparative and physiological psychology,* 92**,** 142.

SPANSWICK, D., SMITH, M., MIRSHAMSI, S., ROUTH, V. & ASHFORD, M. 2000. Insulin activates ATP-sensitive K^+ channels in hypothalamic neurons of lean, but not obese rats. *Nature neuroscience,* 3**,** 757-758.

SPENCER, R. H., SOKOLOV, Y., LI, H., TAKENAKA, B., MILICI, A., AIYAR, J., NGUYEN, A., PARK, H., JAP, B. K. & HALL, J. E. 1997. Purification, visualization, and biophysical characterization of Kv1. 3 tetramers. *Journal of Biological Chemistry,* 272**,** 2389-2395.

SQUIRE, L. R. 1992. Memory and the hippocampus: a synthesis from findings with rats, monkeys, and humans. *Psychological review,* 99**,** 195.

STANDEN, N. B., GRAY, P. T. & WHITAKER, M. J. 1987. *Microelectrode techniques: the plymouth workshop handbook,* Company of Biologists Cambridge.

STEEN, E., TERRY, B. M., RIVERA, E. J., CANNON, J. L., NEELY, T. R., TAVARES, R., XU, X. J., WANDS, J. R. & DE LA MONTE, S. M. 2005. Impaired insulin and insulin-like growth factor expression and signaling mechanisms in Alzheimer's disease-is this type 3 diabetes? *Journal of Alzheimer's Disease,* 7**,** 63-80.

STERN, C. E., CORKIN, S., GONZÁLEZ, R. G., GUIMARAES, A. R., BAKER, J. R., JENNINGS, P. J., CARR, C. A., SUGIURA, R. M., VEDANTHAM, V. & ROSEN, B. R. 1996. The hippocampal formation participates in novel picture encoding: evidence from functional magnetic resonance imaging. *Proceedings of the National Academy of Sciences,* 93**,** 8660-8665.

STEVENS, R. & COWEY, A. 1973. Effects of dorsal and ventral hippocampal lesions on spontaneous alternation, learned alternation and probability learning in rats. *Brain research,* 52**,** 203-224.

SUGAR, J., WITTER, M. P., VAN STRIEN, N. & CAPPAERT, N. 2011. The retrosplenial cortex: intrinsic connectivity and connections with the (para)hippocampal region in the rat. An interactive connectome. *Frontiers in Neuroinformatics,* 5.

SUZANNE, M. & WANDS, J. R. 2008. Alzheimer's disease is type 3 diabetes–evidence reviewed. *Journal of diabetes science and technology (Online),* 2**,** 1101.

SWANSON, L. & COWAN, W. 1977. An autoradiographic study of the organization of the efferet connections of the hippocampal formation in the rat. *Journal of Comparative Neurology,* 172**,** 49-84.

TANAKA, K. F., SAMUELS, B. A. & HEN, R. 2012. Serotonin receptor expression along the dorsal-ventral axis of mouse hippocampus. *Philos Trans R Soc Lond B Biol Sci,* 367**,** 2395-401.

TANTI, A., RAINER, Q., MINIER, F., SURGET, A. & BELZUNG, C. 2012. Differential environmental regulation of neurogenesis along the septo-temporal axis of the hippocampus. *Neuropharmacology,* 63**,** 374-384.

THORENS, B. & MUECKLER, M. 2010. Glucose transporters in the 21st Century. *American Journal of Physiology-Endocrinology and Metabolism,* 298**,** E141-E145.

TRIVEDI, M. A. & COOVER, G. D. 2004. Lesions of the ventral hippocampus, but not the dorsal hippocampus, impair conditioned fear expression and inhibitory avoidance on the elevated T-maze. *Neurobiology of learning and memory,* 81**,** 172-184.

TU, L., SANTARELLI, V., SHENG, Z., SKACH, W., PAIN, D. & DEUTSCH, C. 1996. Voltage-gated K+ channels contain multiple intersubunit association sites. *Journal of Biological Chemistry,* 271**,** 18904-18911.

TURRIGIANO, G. G., MARDER, E. & ABBOTT, L. 1996. Cellular short-term memory from a slow potassium conductance. *Journal of neurophysiology,* 75**,** 963-966.

UNGER, J., MOSS, A. & LIVINGSTON, J. 1991. Immunohistochemical localization of insulin receptors and phosphotyrosine in the brainstem of the adult rat. *Neuroscience,* 42**,** 853-861.

UPADHYAY, S. K., ECKEL-MAHAN, K. L., MIRBOLOOKI, M. R., TJONG, I., GRIFFEY, S. M., SCHMUNK, G., KOEHNE, A., HALBOUT, B., IADONATO, S., PEDERSEN, B., BORRELLI, E., WANG, P. H., MUKHERJEE, J., SASSONE-CORSI, P. & CHANDY, K. G. 2013. Selective Kv1.3 channel blocker as therapeutic for obesity and insulin resistance. *Proceedings of the National Academy of Sciences,* 110**,** E2239-E2248.

VAN GROEN, T. & WYSS, J. M. 1990. Extrinsic projections from area CA1 of the rat hippocampus: olfactory, cortical, subcortical, and bilateral hippocampal formation projections. *Journal of comparative neurology,* 302**,** 515-528.

VAN STRIEN, N., CAPPAERT, N. & WITTER, M. 2009. The anatomy of memory: an interactive overview of the parahippocampal–hippocampal network. *Nature Reviews Neuroscience,* 10**,** 272-282.

VARGHA-KHADEM, F., GADIAN, D. G., WATKINS, K. E., CONNELLY, A., VAN PAESSCHEN, W. & MISHKIN, M. 1997. Differential effects of early hippocampal pathology on episodic and semantic memory. *Science,* 277**,** 376-380.

VEH, R. W., LICHTINGHAGEN, R., SEWING, S., WUNDER, F., GRUMBACH, I. M. & PONGS, O. 1995. Immunohistochemical Localization of Five Members of the KV1 Channel Subunits: Contrasting Subcellular Locations and Neuron-specific Co-localizations in Rat Brain. *European Journal of Neuroscience,* 7**,** 2189-2205.

VENTERS, H. D., BROUSSARD, S. R., ZHOU, J.-H., BLUTHÉ, R.-M., FREUND, G. G., JOHNSON, R. W., DANTZER, R. & KELLEY, K. W. 2001. Tumor necrosis factor α and insulin-like growth factor-I in the brain: Is the whole greater than the sum of its parts? *Journal of neuroimmunology,* 119**,** 151-165.

VERNEY, C., BAULAC, M., BERGER, B., ALVAREZ, C., VIGNY, A. & HELLE, K. 1985. Morphological evidence for a dopaminergic terminal field in the hippocampal formation of young and adult rat. *Neuroscience,* 14**,** 1039-1052.

VICENTE, M. I., COSTA, P. F. & LIMA, P. A. 2010. Galantamine inhibits slowly inactivating K+ currents with a dual dose-response relationship in differentiated N1E-115 cells and in CA1 neurones. *Eur J Pharmacol,* 634**,** 16-25.

VOLPE, B. T., DAVIS, H. P., TOWLE, A. & DUNLAP, W. P. 1992. Loss of hippocampal CA1 pyramidal neurons correlates with memory impairment in rats with ischemic or neurotoxin lesions. *Behavioral neuroscience,* 106**,** 457.

WALLENSTEIN, G. V., HASSELMO, M. E. & EICHENBAUM, H. 1998. The hippocampus as an associator of discontiguous events. *Trends in neurosciences,* 21**,** 317-323.

WANG, T., LEE, M. H., CHOI, E., PARDO-VILLAMIZAR, C. A., LEE, S. B., YANG, I. H., CALABRESI, P. A. & NATH, A. 2012. Granzyme B-induced neurotoxicity is mediated via activation of PAR-1 receptor and Kv1.3 channel. *PLoS One,* 7**,** e43950.

WATSON, G. & CRAFT, S. 2004. Modulation of memory by insulin and glucose: neuropsychological observations in Alzheimer's disease. *European journal of pharmacology,* 490**,** 97-113.

WINOCUR, G., GREENWOOD, C. E., PIROLI, G. G., GRILLO, C. A., REZNIKOV, L. R., REAGAN, L. P. & MCEWEN, B. S. 2005. Memory impairment in obese Zucker rats: an investigation of cognitive function in an animal model of insulin resistance and obesity. *Behavioral neuroscience,* 119**,** 1389.

WONG, R. & TRAUB, R. D. 1983. Synchronized burst discharge in disinhibited hippocampal slice. I. Initiation in CA2-CA3 region. *Journal of neurophysiology,* 49**,** 442-458.

WOOD, I. S. & TRAYHURN, P. 2003. Glucose transporters (GLUT and SGLT): expanded families of sugar transport proteins. *British Journal of Nutrition,* 89**,** 3-9.

WOODS, S. C., LOTTER, E. C., MCKAY, L. D. & PORTE, D. 1979. Chronic intracerebroventricular infusion of insulin reduces food intake and body weight of baboons.

WOODS, S. C., SEELEY, R. J., BASKIN, D. G. & SCHWARTZ, M. W. 2003. Insulin and the blood-brain barrier. *Current pharmaceutical design,* 9**,** 795-800.

WULFF, H., CALABRESI, P. A., ALLIE, R., YUN, S., PENNINGTON, M., BEETON, C. & CHANDY, K. G. 2003. The voltage-gated Kv1. 3 K+ channel in effector memory T cells as new target for MS. *The Journal of Clinical Investigation,* 111**,** 1703-1713.

WULFF, H. & PENNINGTON, M. 2007. Targeting effector memory T-cells with Kv1. 3 blockers. *Current Opinion in Drug Discovery and Development,* 10**,** 438.

XU, J., WANG, P., LI, Y., LI, G., KACZMAREK, L. K., WU, Y., KONI, P. A., FLAVELL, R. A. & DESIR, G. V. 2004. The voltage-gated potassium channel Kv1. 3 regulates peripheral insulin sensitivity. *PNAS,* 101.

YELLEN, G. 2002. The voltage-gated potassium channels and their relatives. *Nature,* 419**,** 35-42.

ZHAO, W., CHEN, H., XU, H., MOORE, E., MEIRI, N., QUON, M. J. & ALKON, D. L. 1999. Brain insulin receptors and spatial memory correlated changes in gene expression, tyrosine phosphorylation, and signaling molecules in the hippocampus of water maze trained rats. *Journal of Biological Chemistry,* 274**,** 34893-34902.

ZHAO, W.-Q. & ALKON, D. 2001. Role of insulin and insulin receptor in learning and memory. *Molecular and Cellular Endocrinology,* 177**,** 125-134.

ZHU, J., YAN, J. & THORNHILL, W. B. 2012. N‐glycosylation promotes the cell surface expression of Kv1. 3 potassium channels. *FEBS Journal,* 279**,** 2632-2644.

ZOLA-MORGAN, S., SQUIRE, L. R. & AMARAL, D. 1986. Human amnesia and the medial temporal region: enduring memory impairment following a bilateral lesion limited to field CA1 of the hippocampus. *The Journal of Neuroscience,* 6**,** 2950-2967.

This page was intentionally left blank.

6 SUPPLEMENTARY MATERIAL

6.1 DORSAL-VENTRAL ASYMMETRIES

Table 12: Main dorsal-ventral asymmetries described in the literature, classified according to generic subjects. References are provided. LTP long-term potentiation, n.a. not applicable, RT-PCR real time polymerase chain reaction, WB western blot, IHC immunohistochemistry.

Classification	Hippocampal areas/cells on focus	Animal model	Description	Ref.(s)
Cytoarchitecture	Dorsoventral axis of the hilus	Mice	The ventral hilus is 9 times more abundant in mossy cells than the dorsal hilus. Because the volume of the hilus is also larger in the ventral end, the absolute number of mossy cells should be more than an order of magnitude higher in the ventral hilus. The mossy cell's axon terminals are highly concentrated in the inner molecular layer This imbalance in the distribution of mossy cells is relevant since hilar mossy cells play a role in the generation of bilaterally synchronous electrical activity patterns in the dentate gyrus and in the development of hyperexcitability and consequently in seizure initiation and pathology. Hyperactivity occurring first in the ventral dentate gyrus might be amplified and spread via the bilaterally extensive mossy fibre projections to the dorsal ipsilateral and the whole contralateral dentate gyrus.	(Blasco−Ibáñez and Freund, 1997)
	Perirhinal and parahippocampal cortices, dorsal and ventral dentate gyrus	Rat	Afferents of the hippocampus are biased regarding dorsal and ventral hippocampus, and the perihinal intrinsic connections are also asymmetric. The entorhinal cortex projects powerfully and unidirectionally to the dentate gyrus (perforant pathway) in a lateral-to-medial topography that is related to the septotemporal level of the dentate gyrus that is innervated (''bandlike'' organization of the entorhinal-to-dentate- projecting neurons). Moreover, there appeared to be three segregated and perhaps functionally distinct components of the perforant path system. These studies set the ground for the possibility that some autonomy of function within different regions of the entorhinal cortex and at different septotemporal levels of the hippocampus and dentate gyrus might be in place.	(Burwell and Amaral, 1998a, Burwell and Amaral, 1998b, Dolorfo and Amaral, 1998a, Dolorfo and Amaral, 1998b)

	Entire longitudinal extent	Rat	DG, CA3, and CA1 occupy comparable volumes as whole structures, but are unevenly distributed throughout the hippocampus: CA1 makes up more than half of the dorsal portion, whereas CA3 and DG were more prominent in the ventral hippocampus. Also, the CA3/CA1 ratio increases septotemporally because of a specific change in stratum radiatum volume. Many pathological conditions and animal models are characterized by changes in hippocampus volumes as volumetric distributions can place considerable constraints on hippocampal function. The dendritic density is also unevenly distributed, as in CA1 dendritic occupancy is as much as >60% higher temporally than septally, CA3 values vary both across subfields and layers and is substantially lower in DG. This has implications in the volume available for axons and other components of the hippocampal matter and hence to neurogenesis and/or intrinsic and extrinsic connectivity patterns.	(Ropireddy et al., 2012)
	Dorsal and ventral CA1 pyramidal cells' distal dendrites	Rat	No obvious morphological differences in the dendritic arbour of neurons of dorsal and ventral CA1 pyramidal cells are visible.	(Marcelin et al., 2012)
	Dorsal and ventral CA1 pyramidal cells	Rat	Dorsal neurons present significantly more dendritic surface area than ventral neurons.	(Dougherty et al., 2012)
Molecular biology	Dorsal and ventral hippocampus	Rat	Kv1.1 mRNA is differentially regulated in the dorsal and ventral hippocampus during an odor-discrimination associative task: expression in the ventral portion decreases (when rats begin to learn odor-reward association) before it does in the dorsal hippocampus. Both alterations are transient throughout the learning process. The decrease in Kv1.1 mRNA expression suggests modifications of the synaptic excitability modulation during learning and memory processes, and that ventral hippocampus Kv1.1 is involved at the early learning stages.	(Kourrich et al., 2005)
	Longitudinal axis of CA1 (pyramidal cells)	Mouse	Genetic markers divide the hippocampus in diverse (sub) domains, including the CA1 pyramidal cells that likewise assume multiple subtypes, with characteristic laminar distributions. Moreover, efferent CA1 axons project to subcortical brain regions that are genetically distinct, suggesting that they can be genetically wired prior to distinct functional networks being established. Plus, dorsal and ventral hippocampi are genetically wired independently in a way that allows for different functional capabilities (the dorsal part	(Dong et al., 2009) (Fanselow and Dong, 2010)

			being related to learning and memory and the ventral portion being related to emotion and behaviour).	
Protein expression	Dorsal and ventral CA1 pyramidal cells' distal dendrites	Rat	Kv4.2 mRNA (RT-PCR), protein levels in total homogenates and synaptosomes (WB), as well as optical density (IHC) is larger in the dorsal hippocampus than in the ventral counterpart (by about 50%). HCN1 and HCN2 mRNA levels (RT-PCR) are not different in dorsal and ventral hippocampus, but protein expression, the synaptosome fraction of HCN1 protein (WB) and its optical density (IHC) is significantly larger in ventral hippocampus.	(Marcelin et al., 2012)
	Dorsal-ventral axis	Mice	Serotonin receptors Htr1a, Htr2a, Htr2c and Htr7 are differentially expressed along the dorsal-central axis. Except Htr1a (that changes along the CA1 region, being more expressed in the dorsal hippocampus), most serotonin receptors are more expressed in ventral hippocampal CA3 or DG. Thus, serotonin neurotransmission enriched ventral hippocampus assist to mood- and anxiety-related behaviours. This contributes to the understanding of the neuronal basis of serotonin reuptake inhibitors (SSRIs), a class of widely used antidepressants that function by increasing serotonin neurotransmission.	(Tanaka et al., 2012)
	Dorsal and ventral CA1 pyramidal cells	Rat	Larger HCN1/HCN2 subunits ratio for ventral hippocampal neurons than for dorsal ones (as it is associated with functional changes in I_h for ventral neurons, but not dorsal neurons, this may alter significantly the capacity for dendritic integration)	(Dougherty et al., 2013)
Membrane excitability and ionic currents	Extreme dorsal to the middle portion of the hippocampus, CA1 pyramidal cells and interneurons	Rat	The hippocampal activity (manner and rate) changes according to the animal's spatial location. This study reveals that this alteration is also dorsal/ventral dependent. A systematic variation from dorsal (high resolution) to ventral 96hippocampus (low resolution) takes place, as place fields get progressively larger, and the probability of observing a field in a given environment gets progressively smaller. Thus, the hippocampal spatial scale factor increases from dorsal to ventral 96hippocampus, as much as twice, accompanied by a proportional decrease in peak firing rate and a less than 10% change in the intrinsic frequency throughout the axis. Moreover, when the animal is running and not resting, both dorsal pyramidal cells and interneurons have higher mean rates and they increase as a function of speed more visibly in the dorsal hippocampus.	(Maurer et al., 2005)
	Dorsal and ventral CA1 pyramidal cells' distal	Rat	Distal dendrites from the ventral hippocampus are slightly more depolarized, have increased b-APs (I_h) amplitude (by 50%) without kinetics alterations, a lower input resistance, a decreased temporal summation, but stronger resonance and phase lead	(Marcelin et al., 2012)

	dendrites		than dendrites from the dorsal hippocampus. Enhanced backpropagation in ventral CA1 pyramidal cells is attributed to, at least in part, decreased expression levels of Kv4.2, involving transcriptional regulation, and increased ERK- dependent phosphorylation, while differences in resonance, phase response and temporal summation is attributed to different expression levels of HCN1/2.	
	Dorsal and ventral CA1 pyramidal cells	Rat	Ventral hippocampal neurons are intrinsically more excitable than dorsal neurons. Somatic current injections of equal magnitude elicit significantly more action potentials in ventral neurones than in dorsal ones. Additionally, ventral neurons have higher input resistance and more depolarized resting membrane potential (there is a significant depolarizing shift in the $V_{1/2}$ of activation for dendritic h-channels in ventral neurons but not in dorsal neurons) in the soma *and in* apical dendrite. Hence ventral neurons can be more prone to hyperexcitability, explaining why the ventral hippocampus is more sensitive to epileptogenic stimuli than dorsal counterpart, and seizures tend to originate in the ventral hippocampus before spreading to other brain regions.	(Dougherty et al., 2012)
Neurotransmission	Dorsal and ventral (crude synaptosomes)	Rat	There is a higher density of norepinephrine (NE) and serotonin (5-HT) terminals in the ventral hippocampus (higher uptake V_{max}) and a higher Km for 5-HT uptake in the dorsal hippocampus. This may be due to more terminals with low NE/5-HT concentration being present in the ventral hippocampus or due to dorsal's NE/5-HT receptors being more responsive.	(Gage and Thompson, 1980)
Synaptic plasticity (LTP and other types)	Dorsal and ventral CA1 region	Rat	The hippocampus has regional differences in short-term and long-term synaptic plasticity *in vivo* (anesthetised animals). PFF (a form of short-term synaptic plasticity) facilitation is weaker in the ventral than in the dorsal hippocampus, and the LTP (a form of long-term synaptic plasticity) degree is also lower in ventral than in dorsal hippocampus. The interaction of PFF and LTP also varied between the two regions. These asymmetries may derive from diverse transmitter release probabilities and other cellular mechanisms.	(Maruki et al., 2001)
	Septotemporal axis of CA1	Rat	Ventral hippocampus has impaired ability to express LTP compared with the rest of the hippocampus, and LTP is mediated by activation of a glucocorticoid receptor (which is not mediated by activation of the NMDA receptor but by enhancement of voltage-gated calcium channels). If subjected to acute stress, ventral hippocampus LTP ability is increased compared to	(Maggio and Segal, 2007)

		the rest of the hippocampus and is mediated by activation of a mineralocorticoid receptor. This may be due to activation of ventral hippocampus' exclusive efferent system.	
		On the other hand, ventral hippocampus non- NMDA receptor dependent LTP can be facilitated by activation of mGuRs or by stress hormones more than dorsal hippocampus (Maggio and Segal, 2007b), indicating that different mechanisms for generating LTP operate in dorsal and ventral sectors.	
Dorsal and ventral hippocampus	Rat	If subjected to chronic unpredictable stress (CUS) and evaluated by the radial arm water maze, a task that draws simultaneously on the established functions of both dorsal (spatial navigation) and ventral hippocampus (emotional responses), plasticity-associated proteins' expression is different in those areas (proBDNF is increased in dorsal hippocampus and decreased in ventral hippocampus, while PSD-95 was selectively unregulated in ventral hippocampus). CUS enhances spatial memory. Dorsal hippocampus is more stress-resistant and more prone to undergo adaptive plasticity, while ventral hippocampus is more severely impacted by stress (less neurogenesis). So, dorsal hippocampus is more likely to be involved in behavioral adaptations, such as escape from or neutralization of a stress factor, whereas the ventral portion may be more involved in emotional responses.	(Hawley et al., 2012)
Dorsal and ventral CA1 stratum radiatum	Rat	Ventral hippocampus is more sensitive to ryanodine receptors-dependent calcium stores operated mechanisms (ryanodine is able to convert short-term potentiation to LTP in VENTRAL HIPPOCAMPUS only, a postsynaptic effect that reflects a higher concentration of ryanodine receptors in ventral hippocampus). Caffeine produces a postsynaptic increase in the slope of population EPSPs in ventral hippocampus, and facilitated LTP in this region, as it is able to release store-associated calcium and change reactivity to afferent stimulation. Therefore, dorsal hippocampus is more precise but less tunable, and ventral hippocampus is more amenable to regulation, depending on hormonal ambient and neuromodulator actions, as calcium stores play a more dominant role in ventral hippocampus.	(Grigoryan et al., 2012)

Function	Afferent and efferent projections of the hippocampus		The hippocampus is functionally dissociated, as well as neuroanatomically and biochemically asymmetric. Eating, drinking and behavioural arousal were evaluated following chemical stimulation of specific cell fields (according to the afferent and efferent projections of the hippocampus) with specific neurohumoral substances. While in control of eating the hippocampus is functionally homogeneous, behavioural arousal was also found to be dissociated on a biochemical basis and control of drinking was dissociated both on a neuroanatomical and biochemical basis.	(D. Grant and Jarrard, 1968)
	Dorsal and ventral hippocampus	Rat	The dorsal hippocampus is required for learning, but only at mini slab of tissue is necessary. Rats can acquire spatial navigation abilities (with rate and precision deficits if a 20% threshold of the total hippocampal volume is surpassed) if small tissue blocks are spared from two-thirds of dorsal hippocampus, but equally large blocks at ventral hippocampus are not capable of supporting spatial learning. Moreover, the level of impairment is correlated with the lesion volume. These effects are not accompanied by alteration in electrophysiological responses, synaptic plasticity, or preserved acetylcholinesterase.	(Moser et al., 1993, Moser et al., 1995, Moser and Moser, 1998)
	Dorsal and ventral hippocampus	Rat	Dorsal and ventral hippocampus play different roles in working and non-working memory used in operant-type delayed alternation tasks (the dorsal part may be related to the performance of working memory and non-working memory components in the operant chamber, while the ventral hippocampus may be related to working memory performance in the radial arm maze, but not in the operant chamber).	(Maruki et al., 2001)
	Dorsal and ventral hippocampus	Rat	Ventral, and not dorsal, hippocampus is necessary for unconditioned fear (but not to contextual fear conditioning or spatial navigation), hence it may regulate only some types of defensive fear-related behaviour.	(Kjelstrup et al., 2002)
	Dorsal and mainly ventral CA1 and CA3 pyramidal cell layer	Rat	Slices prepared from the ventral hippocampus have spontaneous sharp wave activity whereas slices from the dorsal hippocampus do not. Moreover, LTP is significantly impaired in ventral hippocampus than in dorsal counterpart. This may be a possible reversion of LTP mediated by extracellular adenosine, which interferes with the induction and/or stabilization of LTP. Viewed as a neuronal support for forgetting, these results point to a new ventral hippocampus function in memory. Similar waves that are described in the dentate gyrus from ventral hippocampus slices ("dentate waves"), and seem to relay on the activity of the ascending cholinergic	(Colgin et al., 2004b) (Colgin et al., 2004a)

			projections, indicate that depending on the behavior of the animal the hippocampus might switch between processing, encoding, or erasing modes.	
	Dorsal and Ventral hippocampus	Rat	Selective lesions to dorsal and ventral effects on fear-conditioned (recent and remote) freezing, anxious behaviour (passive avoidance on the elevated T-maze (ETM) test of anxiety), and general activity levels were assessed. Freezing and anxiety behaviour are reduced in ventral hippocampus injured animals, but not in dorsal hippocampus injured animals, in a temporally stable manner. Since ventral hippocampus may be specifically involved in modulating goal-oriented, defensive fear-related behaviour through hypothalamic and amygdaloid connections, the reduced passive avoidance (anxiety behaviour) in ventral hippocampus lesioned rats may be due to damage to the amygdala–ventral hippocampus–hypothalamic circuit. Neither dorsal nor ventral lesions increased general activity.	(Trivedi and Coover, 2004)
	Dorsal and ventral hippocampus	Rat	Following dorsal or ventral hippocampus lesion, spatial reference and working memory impairments were assessed by a within-subject within-task comparison of four-baited/four-unbaited version of the eight-arm radial maze task results. The results built on those by Moser (watermaze) and Bannerman (T-maze), showing that the dorsal hippocampus is preferentially involved in spatial memory. Dorsal hippocampus lesion causes more severe impairment than ventral hippocampus lesion, as it is similar to the complete (conjoint dorsal and ventral) lesion. Additionally, working memory (learning to avoid re-entry to any arm of the maze) deficits observed in dorsal hippocampus (and complete hippocampus) lesioned rats tended to appear before reference memory (avoid the non-baited arms) deficits.	(Pothuizen et al., 2004)
	Dorsal, intermediate and ventral hippocampus	Rat	The intermediate hippocampus has integrative properties essential for translation of rapid place learning into efficient search behaviour. The proposed model is derived from a region specific lesion study *in vivo* (where performance was intact if the lesion spared the intermediate hippocampus, impaired if either dorsal or ventral hippocampus were lesioned but abolished if the intermediate hippocampus was affected*)* and goes as follows. Visual-spatial information is processed by the neocortex and transmitted to the dorsal hippocampus, which is responsible for quick learning (LTP, precise place-related firing, and rapid remapping), but is not capable of translating a rapidly acquired place representation into appropriate behaviour, by itself. Therefore, the information has to be channelled to the intermediate hippocampus, which has appropriate anatomical	(Bast et al., 2009)

			links to behavioural-control functions through ventral hippocampus to the prefrontal cortex and subcortical sites that control behaviour. This explains why the place fields increase from dorsal to ventral hippocampus (ability of hippocampal neurons to encode accurate place information declines) is inversely proportional to hippocampal connectivity to prefrontal and subcortical sites.	
	Dorsal and mainly ventral hippocampus	n.a.	While dorsal hippocampus is a neural substrate of the learning and memory, notably in spatial learning, VENTRAL HIPPOCAMPUS is a neural substrate of anxiety (and not fear, which is a distinct emotional entity even though highly interactive with anxiety, and is backed up by amygdala). Therefore, ventral hippocampus makes its own distinctive contribution to the control of behavior in certain anxiogenic situations. Moreover, the hippocampal memory system may provide the means for encoding both the spatial and temporal contexts (the 'where' and the 'when') associated with a particular event, thus capturing the key properties associated with episodic memory in humans.	(Bannerman Dm Fau - Rawlins et al.)
	Dorsal-ventral axis	Mouse	A GABA$_B$ receptor antagonist (CGP 52432) induces increased cell proliferation in ventral hippocampus but not in the dorsal counterpart. Since GABA$_B$ receptor antagonists have shown antidepressant-like properties, this topographical segregation supports the hypothesis that ventral hippocampus is primarily involved in the regulation of stress and emotionality.	(Felice et al., 2012)
Neurodegeneration	Dorsal and ventral dentate gyrus	Mice	The dorsal hippocampal dentate gyrus is more sensible to increased glycogen synthase kinase-3β than the ventral counterpart in neurodegeneration animal models. This is reflected in reactive astrocytosis indicating more tissue stress, a significant reduction in total cell number and significantly higher cell death. In the ventral hippocampus, the enzyme has a different regulatory system that inactivates it when in excess. Moreover, the mice have impaired navigation abilities but no anxiety-related disorder, meaning that the two areas behave differently faced with neurodegeneration.	(Fuster-Matanzo et al., 2011)
	Dorsal and ventral hippocampus (and posteroventral versus anterodorsal amygdala)	Rat	The hippocampus and the amygdala are particularly prone to seizure activity and consequently to pathological damage induced by seizurogenic insults. After status epilepticus induced by soman administration to rats, the ventral hippocampus (hilus, CA1, and CA3) and posteroventral amyglada reveal more neurodegeneration than the dorsal hippocampus and the anterodorsal amygdala one day after the injury, and not significant difference after 7 days. Comparing the whole	(Apland et al., 2010)

			structures, the amygdala is more severally impaired than the hippocampus. The granule cell layer of the DG seems to be spared from the neurodegeneration in both dorsal and ventral hippocampus but, in contrast, the hilus is the more affected subregion. The neuronal damage is probably caused by glutamate-mediated excitotoxicity. The non-uniform damage of these structures may itself facilitate epileptogenesis and generation of spontaneous seizures.	
Cell proliferation & Neurogenesis	Dorsal and ventral hippocampus	Mice	Unpredictable Chronic Mild Stress (UCMS), a murine model of depression, and fluoxetine, a chronic antidepressant treatment (which reverses UCMS-induced changes in cell proliferation/neurogenesis), modulate neurogenesis and cell proliferation preferentially in the VENTRAL HIPPOCAMPUS but environmental enrichment increases neurogenesis preferentially in the dorsal hippocampus.. This might suggest that the ventral hippocampus is more vulnerable to the effects of stress and that environmental enrichment (such as change of interests) might induce neurogenesis.	(Tanti et al., 2012)

6.2 RESULTS SUMMARY

Margatoxin-sensitive K^+ currents

- DH %inhibition > VH %inhibition, in fed rats (** p≤0.01, Mann Whitney t-test)

- DH %inhibition ≈ VH %inhibition, in fast rats (ns p>0.05, Mann Whitney t-test)

- Fast %inhibition < Fed %inhibition, in the DH (*** p≤0.001, Mann Whitney t-test)

- Fast %inhibition ≈ Fed %inhibition, in the VH (ns p>0.05, Mann Whitney t-test)

Kv1.3 protein expression in hippocampal CA1 region

- Kv1.3 protein expression differs between the DH and VH
  - DH mean integrated density (fluorescence) > VH mean integrated density (fluorescence), in fed rats (** p≤0.01, Mann Whitney t-test)
  - DH mean integrated density (fluorescence) ≈ VH mean integrated density (fluorescence), in fast rats (ns p>0.05, Mann Whitney t-test)

- Kv1.3 protein expression does not differ significantly according to metabolic condition
  - Fast mean integrated density (fluorescence) ≈ Fed mean integrated density (fluorescence), in the DH & VH (ns p>0.05, Mann Whitney t-test)